FINAL REPORT

HANDBOOK OF EXPLOSION-GENERATED WATER WAVES

TC-130

October, 1968

TETRA TECH, INC., 630 NO. ROSEMEAD BOULEVARD, PASADENA, CALIFORNIA 91107

FINAL REPORT

HANDBOOK OF EXPLOSION-GENERATED WATER WAVES
VOLUME I - STATE OF THE ART

Prepared for

Office of Naval Research
Washington, D. C., 20360

Prepared by

W. G. Van Dorn, Scripps Institution of Oceanography
B. LeMéhauté, Tetra Tech, Incorporated
Li-San Hwang, Tetra Tech, Incorporated

Tetra Tech Report No. TC-130

Contract No. N00014-68-C-0227

October, 1968

Tetra Tech, Incorporated
630 North Rosemead Boulevard
Pasadena, California 91107

PREFACE

Preparation of this handbook was begun in 1965 with ONR sponsorship [contract NONR 2216(20)] under the direction of Dr. William Van Dorn of Scripps Institution of Oceanography, University of California. The work was completed at the offices of Tetra Tech, Incorporated in Pasadena under the joint authorship of Dr. Van Dorn and Drs. B. LeMéhauté and Li-San Hwang because of the extensive experience and contributions of the Tetra Tech staff in the field of explosion-generated waves.

TABLE OF CONTENTS

LIST OF FIGURES

CHAPTER VI

CHAPTER VII

LIST OF NOTATIONS

A	wave amplitude (ft)
b	cavity height (ft)
B	dimensionless cavity height $B = b/h$
c	phase velocity (ft/sec)
E_t	total wave energy
f	friction factor
g	gravitational acceleration (ft/sec^2)
h	water depth (ft)
h_b	water depth at breaking (ft)
h_t	water depth below wave trough
H	wave height (ft)
H_i	initial wave height (ft)
H_o	deep water wave height (ft)
$\overline{H}_o$	initial surface deformation (ft)
H'_o	deep water wave height obtained from back shoaling (ft)
H_3	wave height calculated by use of third order wave theory (ft)
H_5	wave height calculated by use of fifth order wave theory (ft)
I_o	zero-order Hankel transform of $\overline{H}_o(R)$
J_0	Bessel function of first kind and zero order
J_3	Bessel function of first kind and third order
k	wave number (ft^{-1})
L	wave length (ft)
L_o	wave length in deep water (ft)
M_o	momentum (lb/sec)
p	exponent used in scaling law
P_a	atmospheric pressure head (ft)

q	exponent used in scaling law
Q	discharge (ft^3/sec), or source strength
r	radial distance (ft)
r_o	cavity radius (ft)
$\bar{r}$	distance between center of source point and observing point (ft)
R	dimensionless radial distance ($R = r/h$)
R_o	dimensionless cavity radius (ft)
$\bar{R}$	wave run-up (ft)
S	slope
$\bar{S}$	boundary
t	time (sec)
T	non-dimensional time ($T = t\sqrt{g/h}$)
u	horizontal velocity (ft/sec)
U_R	Ursell parameter
v	group velocity (ft/sec)
v_o	group velocity in deep water (ft/sec)
$\underline{v}$	vertical velocity (ft/sec)
V	normalized group velocity
$\overline{V}$	volume (ft^3)
W	perimeter (ft)
x, y, z	coordinate system (z positive upward from still water level)
Y	charge yield (lb, TNT equivalent)
Z	location of explosion above free surface (ft)
α	angle of the sloping beach
β	angle between incoming wave crest and shoreline

$\overline{\beta}$	normalized frequency
β'	saturation coefficient
δ	distance between wave orthogonals, or channel width (ft)
ζ	wave set-up (ft)
η	wave elevation (ft)
η_m	maximum wave amplitude of explosion wave train (ft)
θ	angle in the polar coordinate system
$\overline{\lambda}$	characteristic time
ρ	density of water (lb/sec^3)
σ	normalized wave number (= kh)
σ_m	normalized wave number at maximum wave height
τ	wave period (sec)
Υ	dimensionless wave period
Φ	velocity potential
φ	velocity potential kernel
$\overline{\varphi}$	phase angle
ω	angular wave frequency (rad/sec)
Ω	normalized wave frequency

FOREWORD

The problem of water waves generated by underwater explosions became of conceptual importance with the inception of atomic testing in a water environment. Initial interest in waves was primarily to appraise them as an adjunctive hazard to such testing. However, as large thermonuclear devices were developed, questions arose as to the tactical and/or strategic implications of the wave systems that were produced. Thus, even during current testing moratoria investigation of these problems has continued.

The first problem systematically attacked was that of coastal damage due to large explosion-generated waves, since, by analogy with the well-known phenomena of tsunami waves generated by earthquakes, it was initially hypothesized that the explosion of large atomic weapons at sea could result in considerable coastal damage by wave run-up and/or flooding.

Later, as theoretical and experimental studies revealed the relatively inefficient wave making potential of large explosions, and that in many cases most wave energy is dissipated by breaking on the continental shelf before reaching shore, concern over run-up per se was replaced by the realization that other more serious wave problems exist. Accordingly, recent emphasis has been directed towards assessing the nature of the breaking wave regime offshore and its implications on the vulnerability of ships and undersea structures to breaking waves in relatively deep water (100 feet). These studies, in turn, have indicated more refined secondary problems. These include harbor oscillations induced by cumulative wave action offshore, and anomalous wave-induced clogging or erosion of harbor entrance channels by sediment transport.

Most of these problems are amenable to analysis, and present techniques have been developed for gross wave predictions over fairly complicated topography that are in good agreement with experimental and field test results. But increasing prediction accuracy requires, unavoidably, increasing environmental detail and consequent complexity of treatment. It is to be emphasized that there is no cut-and-dried shortcut to accurate

prediction, and each case of importance must be considered as a separate problem.

This report seeks to present to the non-disciplinary educated scientist a procedure for wave predictions based upon the state-of-the-art in the field of explosion-generated waves. Rather than attempting to assemble all the advanced hydrodynamic theories related to the explosion-generated waves, which have been carried out during the past decade, careful selection has been made with the aim of presenting the minimum amount of information necessary to justify the conclusions reached without sacrificing logic. Second-order effects, even though sometimes thoroughly investigated elsewhere, have been neglected in this presentation when they do not significantly alter these conclusions.

A specific background in hydrodynamics and water waves would indeed be necessary for more exhaustive analysis than that presented here, and the reader who wishes to study the subject in depth is directed to the abundantly referenced material.

It is to be hoped that the accumulation in one report of widely scattered information will permit the reader a basic understanding of the state-of-the-art, and also permit efficient orientation of further research on unanswered questions which are of interest to the Department of Defense.

CHAPTER I - INTRODUCTION

GENERAL CHARACTERISTICS OF EXPLOSION-GENERATED WAVES

I-1 GENERATION HYDRODYNAMICS

Anyone who has witnessed a pebble being tossed into a large shallow pond is familiar with the type of wave system set up following its impact with the free surface. Rings of waves spread out over the surface, each propagating radially outward until the margins of the pond are reached, after which the individual crests are either reflected in a rather complicated manner or are absorbed by breaking and/or viscous dissipation on the sloping shore. Except for secondary details and an enormous difference in scale, this phenomenon is a perfect analog to the wave system produced by a large explosion in the sea. Indeed, the present best estimates of the waves and wave effects to be expected from very large nuclear explosions are obtained from observational data on the waves produced by explosions on a much smaller scale, together with a generalized hydrodynamic model to which the appropriate scaling factors can be applied.

Basically, the wave system is produced by the attempts of the free surface to restore itself to its original level under gravitational forces, following the deformations and velocities imparted to it by the explosion. While the wave system, once formed, can be considered to conserve energy during its subsequent development, the generation process appears to be extremely non-conservative, in that only a small fraction of the total available thermal energy of the explosion emerges in the form of organized wave motion. This fraction appears to increase slowly with the absolute energy of the explosion. It is sensibly negligible for explosions relatively high above or far beneath the surface, and reaches a maximum of a few percent for those in the immediate vicinity of the surface.

As much as 50% of the thermal energy available in a submerged (nuclear) explosion is lost as irreversible heating or shock in the water during the first bubble expansion. All of the remainder, (excepting that small fraction appearing as wave motion) appears as disorganized turbulent motion, and later is dissipated as heat. These phenomena are readily observable for an explosion at shallow depth by the successive appearances of the massive spray

dome, column, plume, and base surge as precursers to the issuance of waves from the central region. For very deep explosions the turbulence is generated within the violent toroidal circulation associated with successive bubble pulsations, and there may be very little surface manifestation.

For explosions above the surface, the percentage of energy effective in water wave generation is $<< 1\%$ and decreases with burst height. Attempts to explain wave generation from air bursts theoretically have been largely unsuccessful.

Fortunately, however, certain observable features of both chemical and nuclear explosions have been found to be scaleable in terms of power functions of the explosive energy release. It has also been found possible to express a linear theory for wave generation in terms of similar functions. This theory, when normalized to a given set of experimental data, adequately predicts the wave characteristics observed from other experiments on much larger scales, provided that geometric similitude is maintained. Enough experimental data for surface and subsurface chemical explosions (1/2 - 14,500 lbs, TNT equivalent) now exists to normalize the theory to a wide range of initial conditions. The extension to nuclear tests where wave measurements were conducted is, however, limited to two deeply submerged explosions in the kiloton range (Wigwam and Hardtack Wahoo), several megaton range surface shots within an atoll (Operation Redwing), and a number of high-altitude megaton-range shots over the open sea (Operation Dominic). Although the accuracy of the wave measurements for the deep tests was very poor, the best estimate of the maximum wave heights was well within the confidence limits for scaled chemical explosions, under similar geometries. This suggests that the wavemaking efficiencies of submerged nuclear and chemical explosions do not differ significantly. Although there is no comparable chemical data for the surface (atoll) and high-altitude tests, the effective surface loading (pressure-time history) is known to be very different in the two cases. Therefore, one suspects that the scaled-

up results from chemical explosions in the atmosphere would not be a reliable guide to nuclear effects in the same geometry. However, the largest previous air-bursts have produced surface displacements only of the order of inches directly below the shot point and a maximum of a foot or so at any shore location. Since it is known that air-impulse effects scale very well, no wave effects of critical civil or military importance are to be expected from air bursts as large as 100 megatons. For this reason, waves from air-bursts will not be considered further in this context.

The appropriate scaling for nuclear surface explosions is at the same time the most critical and the most uncertain. This is because of an anomalous high peak in the curves of reduced maximum wave height versus charge depth for chemical explosions at the surface - a phenomenon which currently has no sound physical explanation - together with the mixed boundary condition that chemical scaling apparently works in water but not in air. There appears to be no reliable guide to selecting the best scaling coefficient, since predictions for cratering by nuclear devices in solid materials suffer from precisely the same lack of experimental information. Therefore, pending further experiments, it will be assumed that surface nuclear explosions will produce effects identical with those from chemical explosions scaled in the conventional ratio of 1 kilo-calorie/gram TNT equivalent.

Despite the fact that extensive efforts have not provided a quantitative picture of surface and subsurface explosion hydrodynamics, enough information exists to put together a fairly consistent qualitative picture. Some discussion of the mechanism is appropriate here for completeness, even though no direct physical connection with the generation model, described later, can be defended.

To begin with, we neglect any consideration of hydroacoustic shock effects in wave formation, except to note that energy going into shock

is considered to be irreversibly lost and unavailable. The percentage of total available thermal energy lost to shock varies from a minimum of about 40% for a surface explosion to over 90% for a very deep one, wherein several bubble pulsations may have occurred (Kot, 1964).

Secondly, ignoring any intrinsic difference in the nature of the explosive, an explosion anywhere within the water column produces a cavity in the water. The shape and subsequent time-history of the cavity depends upon the absolute energy release, the depth of the detonation point beneath the free surface, and the proximity of the bottom. In the absence of boundaries, the explosion cavity tends to spherical symmetry. However, this symmetry is vertically more and more distorted the closer the proximity of the free surface, owing to the hydrostatic pressure differential across the cavity. If the cavity vents before reaching its maximum expansion, the resulting crater will be approximately parabolic in section at early times. Since this differential will be least for small explosions because of atmospheric pressure, the corresponding cavities will approach spherical symmetry at relatively shallower charge depths than those from large explosions. The characteristics of explosion cavities at reduced pressure have been modeled in detail on a small scale by Kaplan and Goodale (1962).

In contradistinction to explosion cavities in solid materials, where the ultimate cavity size is limited by the rigidity and compressibility of the medium, a water cavity can continue to expand under inertial forces alone, even after the internal pressure has dropped below the local hydrostatic pressure. As a result of the differential pressure across the cavity, the bottom of the cavity will reverse direction and begin to move inward (upward) in advance of the sides and top, respectively. Thus there is a general tendency for the cavity to turn inside out, or evert, during the ensuing collapse phase, leading to the formation of a jet that is strongly accelerated vertically upwards by the potential field of the collapsing cavity (Ash and Eichler, 1964).

The subsequent history of the jet appears to depend rather intimately on the initial charge depth, but for situations important from the point of

wave production, it penetrates through the surface, emerging as a dense vertical column of water, often enshrouded in a spray plume of explosion products and water thrown up directly by the initial cavity expansion. Upon falling back under gravity, the column degenerates into a turbulent and unstable mound of water which, at some undefined point, might be considered as the mathematical precursor to the formation of water waves. As might be expected, either displacement of the charge to great depth or the introduction of a rigid bottom in close proximity beneath the charge acts to inhibit the formation of a substantial water column, and hence, the formation of large waves. However, the resulting wave spectrum will be quite different in the two cases cited.

Students of this complicated subject will recognize the considerable over-simplification of the true state of affairs in the above description. However, most of these phenomena are readily observable in small-scale laboratory experiments, wherein hemispherical charges are detonated against a glass plate, which acts as a transparent half-space, through which the ensuing cavity history can be recorded with high-speed photography (see Fig. II-2).

I-2 EXPLOSION WAVE CHARACTERISTICS

For a discussion of the wave system produced by an explosion, we refer again to the analogy of the pebble tossed into a pond. This also exhibits, sequentially, a cavity, an everted jet that collapses into a mound, followed by rings of waves spreading over the surface. In the mathematical sense, all of these waves originate within the same central mound (or depression) and are simultaneously released to propagate radially outward in their characteristic and familiar pattern. If the water depth is everywhere uniform, or relatively very deep, the pattern will be perfectly circular, and consists of concentric rings of crests and troughs, bounded at the outside by an intangible "front", that expands outward at the limiting velocity $c_o = \sqrt{gh}$ for free gravity waves in water of depth h (g = gravity). All subsequent waves travel more slowly. At any instant of time the radial separation between successive crests (wavelength) is largest near the front and progressively smaller towards the center. All individual waves of the system retain their identity, although the total number of waves present increases with time, as if they were being pulled like an accordion bellows out of a black box that comprises the source region.

In general, no two waves of the system are of the same size, nor does the amplitude of any wave remain the same from place to place and time to time. Within this everchanging pattern the energy distribution among waves is manifested by amplitude modulation of the wave train in a manner which is determined by the nature of the source, its distance from the point of observation, and the depth of water. As the pattern expands, the amplitudes of all the individual waves are, on the average, diminished because the wave system contains a finite and constant amount of energy which is diffused with increasing time or distance. This effect can be resolved into two factors: dispersion, due to the increase in wave length and number of individual waves; and geometric expansion, caused by the increase of crest length necessary to circumscribe progressively larger radii.

Most of these features are well illustrated in Fig. I-1, which shows three successive stages in the development of an explosion-generated wave train. The vertical and horizontal axes in this figure are dimensionless distance $R = r/h$ and dimensionless time $T = t\sqrt{g/h}$, respectively. This diagram is therefore appropriately called an R-T diagram. The three computer-generated oscillatory curves show the amplitude-time histories of a wave train generated at the origin as they would be recorded at the non-dimensional distances, R = 2, 4, and 6. The symmetrical dashed curves bounding the wave trains, comprise the wave envelope, and serve to define the distribution of energy within the train. The precise shape of the envelope depends upon the initial source conditions, whereas the space-time coordinates of the individual waves are independent of the source and depend only on the water depth. A characteristic of the wave envelope is that any identifiable portion of it - say, a node or antinode - propagates at uniform velocity, as shown by the straight lines o-a connecting the origin with the nodal points delimiting the beginning (wave front) and o-b ending points of the first envelope maximum in Fig. I-1. In contradistinction, the space-time trajectories of all waves of the system are curves, concave upwards, because the waves are continuously accelerating towards the limiting phase velocity $c_o = \sqrt{gh}$ of the wave front. Thus the waves travel faster and pass through the successive nodes of the wave envelopes, and therefore there are progressively more waves in each envelope segment with increasing time or distance. For large explosions in the deep ocean, by the time the wave system has traveled a distance equivalent to 300 water depths, there will be more than 100 waves between the front and the first nodal point.

A second important feature of the wave envelope is that its amplitude, as measured along any straight line through the origin of the R-T diagram, is inversely proportional to its distance from the origin. Thus the height of the highest wave in the upper wave train of Fig. I-1 is about 1/3 that of the corresponding wave in the lower train, the latter having traveled three times farther. The above features, together with the experimentally determined result that the linear dimensions of explosion cavities scale over large ranges as a power function of the yield, results in the often used and over-simplified expression:

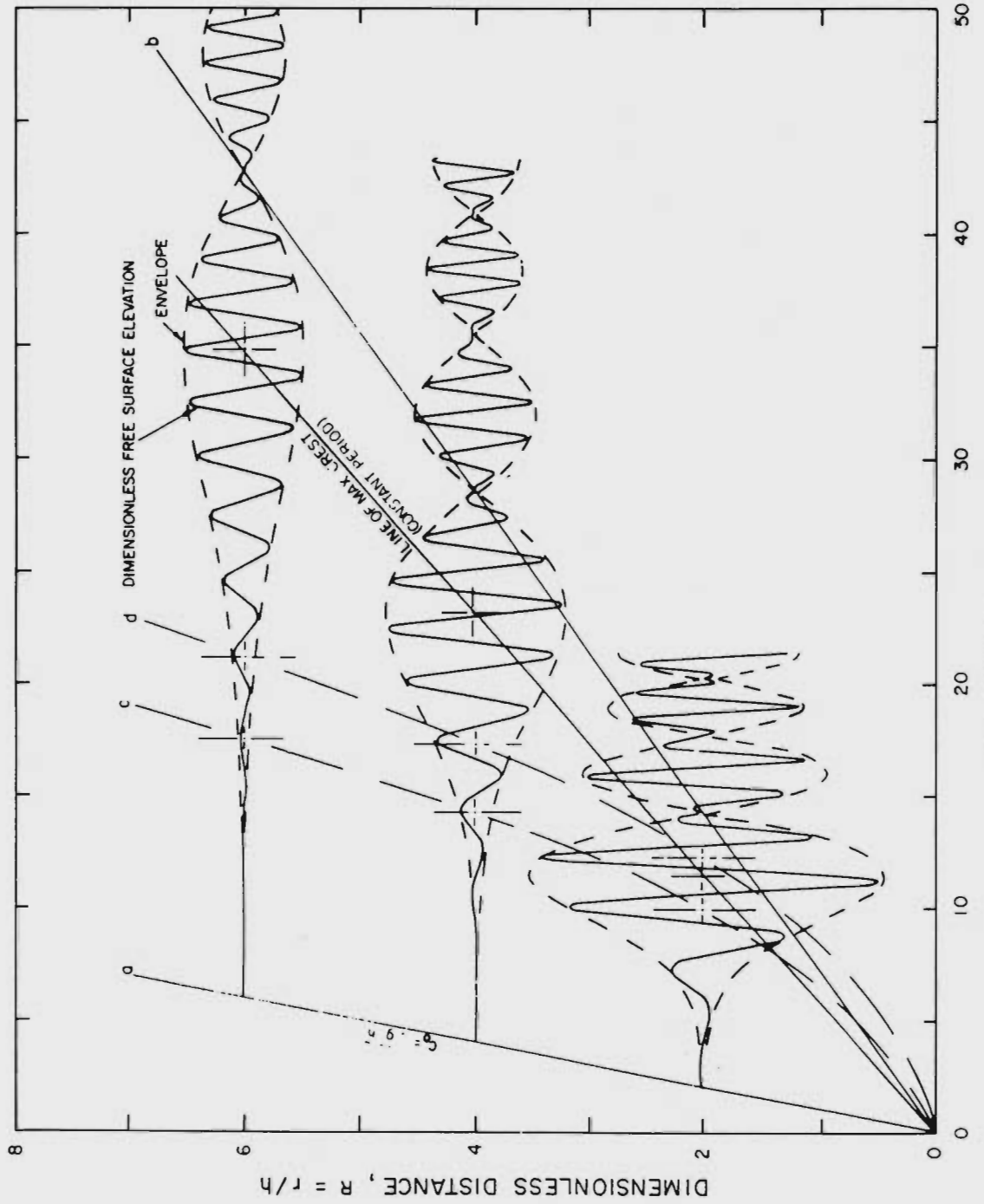

Figure I-1 Schematic Drawing of Wave Trains

$$Hr/Y^p = F$$

where H is the wave height, usually taken at the first envelope maximum (i.e., the highest wave in the train), r is distance from the explosion, Y is the charge weight (yield), F is an empirically determined function of charge depth and water depth (relative to the charge weight). According to scale law the exponent p is one-half for a small explosion in a deep, perfect fluid with no atmosphere. The most reliable experimental results give a somewhat higher value (p = 0.54), possibly owing to the prior-mentioned hydrostatic pressure difference across the explosion cavity, which increases with yield.

Now in nature the water depth is rarely uniform and since the propagation speed of individual waves depends in a rather complicated way upon the water depth and the local wave length (itself an implicit function of depth), the initial symmetry of the wave pattern soon becomes somewhat distorted, the shallower portions being slowed down. This effect, analogous to phase distortion in optics, is most marked at the outer margins of the pattern. Here, the longer wavelengths are more sensitive to depth variations than the shorter waves near the center. As in optics, the influence of any small topographic irregularity (compared with the local wavelength) is averaged out, and only larger features can appreciably alter the symmetry.

Under these circumstances the wave system development can no longer be simply presented on a dimensionless R - T diagram. Its behavior and characteristics at any time and place must be calculated step by step over the real topography. Since these calculations depend upon the local wavelength, the results are no longer scaleable in terms of yield unless the water depth is relatively deep in comparison to all wavelengths of interest.

These physical wave characteristics can be summarized as follows:

1. The waves travel radially from the location of the explosion.
2. At a given location they appear as a succession of waves of decreasing period.
3. Wave amplitudes vary with time so that they appear as a

succession of wave groups, the number of waves per successive group decreasing towards a constant limit.

4. The period of each wave increases with distance traveled.
5. The number of waves per group increases with distance.
6. The length of a group increases with distance.
7. The average wave height in a group decreases with distance traveled.
8. The period of the maximum wave in a group is constant.
9. The maximum wave height of successive groups at a given location decreases with time.

While the relative variation of wavelength with distance is a significant feature of dispersive waves in deep water, this variation becomes less pronounced in shallow water and with distance. Relative variation of wave period from one wave to another also decreases with decreasing depth or distance from the explosion. For these two reasons, the waves generated by a large deep water explosion far from the continental slope can be treated as a succession of quasi-periodic waves on the slope and shelf. If the explosion is near the slope, the dispersive effect is still significant so that the variation of wavelength across the slope must be considered.

I-3 WAVES ON THE CONTINENTAL SHELF AND COASTAL EFFECTS

When the waves approach the continental slope, a small part of the energy of the leading waves is reflected seaward. A fairly accurate estimate of the reflection coefficient can be made by assuming that each wave behaves as a periodic wave of the same period. From a hydrodynamic viewpoint, continental slopes are so gentle that, for most practical purposes, conservation of energy flux obtains, and reflections can be ignored.

As the waves from such a system approach the shoreline and pass into shallow water, the individual wave amplitudes tend to become larger and their length shorter as the energy increment within each wave is concentrated in an increasingly smaller volume of water. This effect opposes the tendency for waves to become smaller because of dispersion and geometric spreading, and there will therefore exist for each wave of the system a minimum amplitude at some point in its history. Eventually, as shoaling and wave growth continue, the local wave amplitude will amount to an appreciable fraction of the water depth. In this "shallow water" regime, additional modification of the wave system is brought about by amplitude distortion, which is nonlinear, has no precise parallel in optics, and is due to the fact that the phase speed of a free gravity wave in very shallow water is also a function of wave amplitude, a higher wave tending to travel faster than a smaller wave of the same length.

In shallow water, nonlinear effects become important, and some damping is produced by bottom friction. Due to convective inertia, the individual wave profile may become unstable, each wave subdividing into a succession of two or three undulations, which travel either as solitary waves or as undular packets separated by long flat troughs. Ultimately, as shoaling and wave growth continue, each wave becomes unstable and, depending on its steepness and the bottom slope, either breaks or surges up upon the shore.

Wave behavior in the immediate vicinity of the shore is very complex,

depending not only upon the slope and curvature of the shoreline, but also upon the history of each previous wave in the train, such that, in general, the point of breaking and the extent of local run-up are unique for every wave and for every point along the shore. Moreover, even more than with offshore propagation, these effects are not scaleable in terms of charge weight because the local effects depend upon the absolute wave height and length near shore. For this reason any prediction method must consider each critical area of the coastline independently, and calculate enough different situations so as to be sure to bracket all critical conditions, before general statements can be made about susceptibility to wave attack from large explosions.

Aside from the direct effects of run-up on the shore, large explosions can, under appropriate circumstances, produce very large waves in deep water, which may break upon the continental shelf many miles from shore. Since the wave spectrum for large explosions is peaked at wave periods substantially longer than the longest prevailing swell or surf, the net result is the creation of a breaker zone covering a very large area, and which can persist for several hours. Such waves could pose unusual and potentially severe problems to coastal navigation, not only through direct dynamic effects, but also because of cumulative effects such as inducement of resonant harbor oscillations and the scouring or deposition of sediment in regions ordinarily immune to normal storm conditions.

CHAPTER II

WAVE GENERATION MECHANISM

II-1 THE SOURCE MODEL

The theory for wave generation by explosions is not really a physical theory, but a mathematical model, based upon highly idealized source conditions that, having been once adjusted to describe the time variations of water surface elevations as observed at some point not too close to the source of an actual explosion, will thereafter reasonably predict them at any other distance or time. This mathematical model is scaleable in terms of explosion energy (yield). Since, however, it is manifest that the violent motions immediately following real explosions in water are not converted entirely into waves, no physical reality can be ascribed to the initial conditions assumed for the model, except to state that the same wave system would have resulted. Thus the choice of initial conditions is arbitrary to the extent that several model solutions can be forced to fit an observed wave train, and the particular solution presented here is only one of several proposed in the literature, although it appeals because of its mathematical simplicity.

The most general treatment is that of Kajiura (1963) although Kranzer and Keller (1959) have given a class of axi-symmetric solutions. (See also Van Dorn (1964), Whalin (1965), Hwang and Divoky (1967), for applications.)

In all such solutions, the wave train is considered to have originated from within a bounded disturbed region where the distribution of some forcing function within the region is the known initial condition. The function can be an initial elevation or depression of the surface, an impulse on the free surface, a given velocity distribution, or any combination thereof. Solutions also exist for functions that are time-dependent, although these have not been studied so extensively. But regardless of the form assumed for the initiating disturbance, it is treated thereafter as a problem of inviscid, incompressible potential flow, in which the resulting wave system may be thought of as a spectral continuum that can be subdivided into component frequencies ω, each of which propagates radially at its characteristic group velocity v in water of depth $h(r, \theta)$ given by

$$v = d\omega/dk = \tfrac{1}{2}(gk^{-1} \tanh kh)^{\frac{1}{2}} (1 + 2kh/\sinh 2kh) \qquad \text{(II-1)}$$

which is obtained by direct differentiation of the equation

$$\omega^2 = gk \tanh kh, \qquad \text{(II-2)}$$

where k is the wave number, r and θ are polar coordinates. Consideration of Eqs. (II-1) and (II-2) reveals that, in general, low frequencies propagate faster than high frequencies, asymptotically approaching a limiting value $v \to \sqrt{gh}$ as $\omega \to 0$. Thus the individual frequency elements are separated as they travel away from the source, which process has been given the name dispersion.

The distribution of energy among frequencies is determined by the spatial dimensions of the source and/or its speed of occurrence (intensity), tending to be maximized at a frequency corresponding to a wavelength $L = 2\pi/k$ which is of the order of the spatial dimensions of the source in a given direction. Hence, a crude method of determining the source dimensions consists of observing which frequencies dominate the spectrum made from a recording of the wave train at a distance.

At any instant of time, a three-dimensional physical model of the energy distribution might consist of two identical, elastic spider webs placed one above the other and separated by a vertical distance corresponding - at every point - to the square root of the local energy density. The peripheral strands of the web can be likened to the instantaneous positions of discrete adjacent frequencies all propagating outward in the directions indicated by the radial arms of the web. The total energy in the system which can be thought of as subdivided by the web into discrete patches is (Van Dorn, 1965)

$$E_t = \rho g \int_0^{2\pi} \int_o^{\infty} H^2 \, d\theta \, d\omega = \text{constant} \qquad \text{(II-3)}$$

where H is the vertical web separation, or the height any wave would have if it occupied that region of space at the particular time in question, ρ is density and $d\theta \, d\omega$ is the patch area. At a later instant of time the webs have

been stretched to a greater radius in all directions, with a corresponding reduction in the spacing between them, since the total energy is constant. Such a "quantization" of the energy into patches (hydrons) has been proposed by analogy to the phonons of acoustic radiation (Synge, 1962).

The velocity of the leading disturbance ($\omega = 0$) is given by

$$v = \sqrt{g\,h} \tag{II-4}$$

The energy, of course, is manifested by an annular gravity wave system, interposed between the web meshes such that the crests and troughs just touch the webs. The individual waves of the system travel at a characteristic phase velocity given by

$$c = \omega/k = \frac{dr}{dt} = (g\,k^{-1}\tanh k\,h)^{\frac{1}{2}} \tag{II-5}$$

Comparing Eq. (II-1) with Eq. (II-5), it is apparent that, in general, $c > v$, but that $v \to c \to \sqrt{g\,h}$ as $\omega \to 0$, and therefore the waves travel faster than the energy patches given by the web elements. Equation (II-5) has solutions of the form

$$\cos 2\pi\,(\omega\,t - k\,r - \bar{\varphi}) = \text{constant} \tag{II-6}$$

where r is the space coordinate of a particular wave phase at time t, and $\bar{\varphi}$ is a phase parameter which, depending upon the initial source conditions, ranges from $0 < \bar{\varphi} < \pi/2$. If Eq. (II-5) is integrated with the aid of Eq. (II-6) to obtain the trajectory of a particular wave in a space-time coordinate system, it will be found that, as this wave accelerates past the slower-traveling patches, it will always possess, instantaneously, the frequency and wave number appropriate to the patch it is passing. All of the foregoing properties are very elegantly compressed into the two equations relating the pertinent variables (see Kinsman, 1965):

$$\frac{\partial k}{\partial t} + v\frac{\partial k}{\partial r} = 0; \qquad \frac{\partial \omega}{\partial t} + v\frac{\partial \omega}{\partial r} = 0 \tag{II-7}$$

which can be derived very generally from the linear theory of dispersive waves. These equations give the distribution of wave number and frequency in the R-T plane.

Consider now the particular example of an initial surface deformation of height $\bar{H}_o(R, \theta)$, where $\bar{H}_o$ is small compared with the uniform water depth h (Fig. II-1). Taking the origin of polar coordinates within the disturbed region, the resulting local anomaly of surface elevation $\eta(R, T)$ can be shown to be (Kajiura, 1963)

$$\eta(R, T) = \frac{1}{2\pi}\int_o^\infty \sigma \cos \Omega T \int_o^{2\pi}\int_o^\infty \bar{H}_o(R, \theta) J_o(\sigma R)\, R\, d\, R\, d\theta\, d\sigma \tag{II-8}$$

where the following quantities have been nondimensionalized in terms of h:

$R = r/h$ (distance) $\qquad \Omega = \omega\sqrt{h/g} = \sqrt{\sigma \tanh \sigma}$ (frequency)

$T = t\sqrt{g/h}$ (time) $\qquad V = v/\sqrt{gh}$ (group velocity)

$\sigma = k\,h$ (wave number)

Equation (II-18) requires the evaluation of three integrals. The second and third integrals represent the summation of contributions from an infinite number of point sources having polar dimensions dR and $d\theta$ and height $\bar{H}_o$, while the first integral is the Hankel transform of the initial deformation $\bar{H}_o$. If we now restrict our attention to cases where the disturbance has circular symmetry with respect to the origin of the explosion (a single explosion), Eq. (II-8) can be reduced to

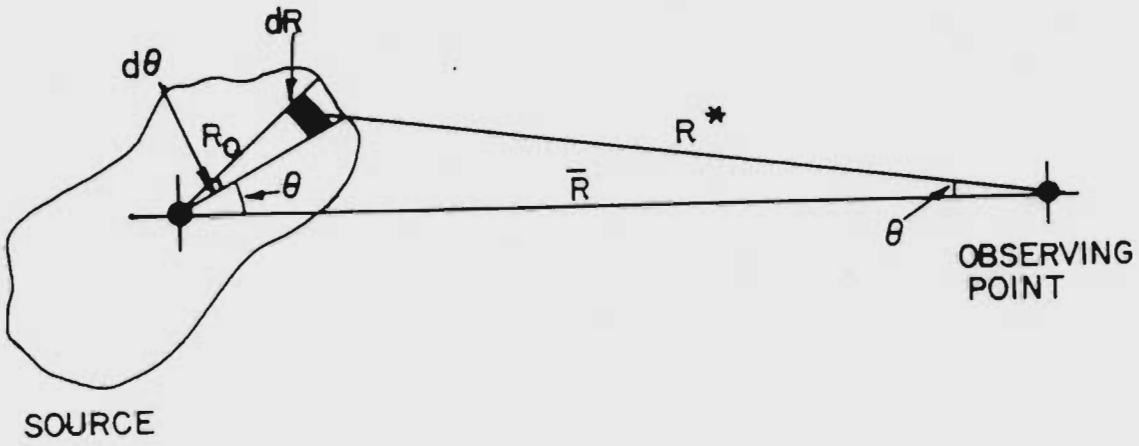

Figure II-1 Schematic Source Distribution

$$\eta(R, T) = \int_0^\infty \sigma \cos(\Omega T)\, I_o(\sigma)\, J_o(R\sigma)\, d\sigma \qquad \text{(II-9)}$$

where

$$I_o(\sigma) = \int_0^\infty \bar{H}_o(R)\, J_o(R\sigma)\, R\, dR \qquad \text{(II-10)}$$

is the zero-order Hankel transform of the initial elevation $\bar{H}_o(R)$. The integration of Eq. (II-9) in σ can now be performed by the approximate method of stationary phase, giving results that are valid everywhere except near the source.*

$$\eta(R, T) = \frac{1}{R} I_o(\sigma) \left(- \frac{\sigma V}{d V / d \sigma} \right)^{\frac{1}{2}} \cos(\sigma R - \Omega T) \qquad \text{(II-11)}$$

The evaluation of the remaining integral, $I_o(\sigma)$, in (II-11) can be performed algebraically if the function $\bar{H}_o(R)$ falls within a restricted list of those having known Hankel transforms, although it is possible on a computer to take the numerical transform of an arbitrary function. There are enough transformable functions, however, to construct approximate solutions for almost any form of $\bar{H}_o(R)$ from sums and differences of these functions, although the result may not satisfy the continuity requirement that no water is added or lost by the assumed disturbance, viz,

$$2\pi \int_0^\infty \bar{H}_o(R)\, dR = 0 \qquad \text{(II-12)}$$

While a number of source models (Whalin, 1965, and Van Dorn, 1964) have been studied, the procedure followed has been essentially the same.

---

* The accuracy of the asymptotic solution has been carefully examined and found to be much better than one would ordinarily suppose from the assumptions involved (Whalin, 1965).

One makes a guess as to the most appropriate transform from the shape of the observed wave spectrum, and computes a number of small variations until the best fit is obtained. This result is then compared to the results of other wave experiments and further modified, if desired. At the present writing, an initial function that satisfies the above requirements and which results in solutions that can be normalized to closely resemble the wave systems from actual explosions under widely varying geometries is given by

$$\begin{aligned} \overline{H}_o(R) &= b\left[2\,(R/R_o)^2 - 1\right] \qquad R \le R_o \\ &= 0 \qquad\qquad\qquad\qquad R > R_o \end{aligned} \tag{II-13}$$

where b is called the cavity height and R_o is the cavity radius. This function consists of a parabolic cavity superimposed upon a cylindrical elevation. Perhaps coincidentally, this shape physically resembles the free surface deformation observed at early times in small-scale model photographs of near-surface explosions (Fig. II-2). Its transform $I_o(\sigma)$, easily derived from known functions, is

$$I_o(\sigma) = \frac{bR_o}{\sigma} J_3(\sigma R_o) \tag{II-14}$$

and the final form of the solution becomes

$$\eta(R,T) = \frac{bR_o}{R}\left[-\frac{V/\sigma}{d\,V/d\sigma}\right]^{\frac{1}{2}} \cdot J_3(R_o\sigma)\ \cos(\sigma R - \Omega T) \tag{II-15}$$

This equation is most easily evaluated numerically by assigning successively equal increments to the wave number σ, and performing the indicated computations iteratively for each increment. The time of arrival of each wave number increment at a given radius, and the corresponding wave period at that time, are then explicitly determined by the definitions of group velocity and frequency.

The above form of the solution has interesting properties, in that wave

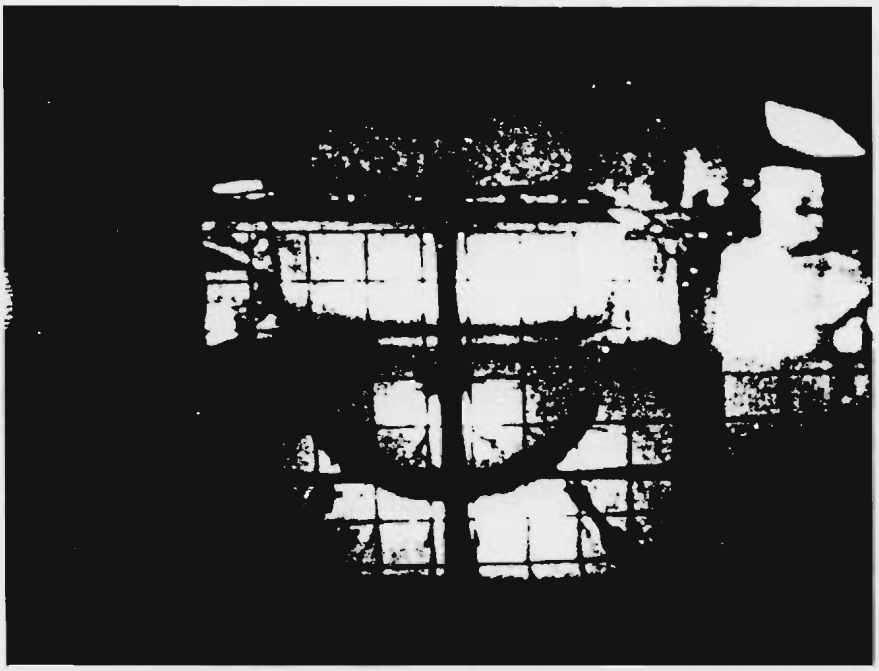

Figure II-2 A High Speed Photograph of Initial Cavity Shape
Taken Under the Following Conditions:

Charge Size	0.175 gram. TNT Equivalent
Ambient Pressure	0.003 Atmosphere
Charge Depth	2.0 inches
Bottom Depth	60.0 inches

(Photography by courtesy of URS)

amplitude (spectrum) and wave position (phase) at any time are given by separate factors, either of which can be computed independently. This fortuitous circumstance allows us to predict the local wave height at any time or place without having to worry about the waves at all, although the latter can be put in later, if desired. Since the phase function contains no information about the source disturbance, the wave system is immutable, depending only upon the (constant) water depth. That is, from a given point of observation, the same wave system will be produced by any (symmetrical) disturbance whatever, and only the height of the waves depends on the source conditions.

The general features of this solution were shown in the R - T diagram of Fig. I-1, where three consecutive time histories $\eta(t)$ of the same wave train were computed for the (fixed) distances R = 2, 4 and 6, respectively, as it has been discussed previously. The time scale of this figure has been compressed so as to better proportion the wave envelope dimensions. Wave amplitude, while plotted in the R-direction, should be recognized as normal to the plane. With reference to Eq. (II-15), at each stage of its development the wave system consists of an oscillatory wave train where both amplitude and frequency are varying with time. The frequency variations are governed by the phase factor, which has a maximum at the wave front, indicated by the straight line so labeled passing through the origin. However, the wave amplitude, governed by the amplitude spectrum, is zero at the front, increases smoothly to an initial - and highest - maximum, and oscillates thereafter in accordance with the Bessel Function $J_3(R_o\sigma)$, as indicated by the dashed lines bounding the wave patterns. Succeeding nodal points in the three envelopes correspond to the zeros of J_3, and can be connected by other straight lines, the slopes of which give the local values of group velocity. These lines can also be thought of as joining regions of constant frequency and wavelength, as well as boundaries delineating zones of constant total energy.

The local wave amplitude, governed by the magnitude of the amplitude

function along any such line, varies inversely with time or distance, owing to the factor R^{-1} in Eq. (II-15). This factor should more properly be written $R^{-\frac{1}{2}} \cdot R^{-\frac{1}{2}}$, the first factor being due to geometric spreading of the wave pattern, and the second due to dispersive separation of adjacent frequencies.

The trajectories of individual waves, two of which are shown in this figure (oc and od) by dashed lines connecting consecutive positions of corresponding wave crests, are parabolic curves in this representation, because the phase velocity of a wave of a given frequency or wavelength is greater than the group velocity everywhere except at the wave front. As a result, individual waves tend to propagate through the envelopes giving the energy distribution, as already described, thus crossing lines of constant group velocity (and frequency). They have the interesting property that, while the period and wavelength of the waves passing a fixed point of observation continuously decrease with increasing time, they both appear to increase with time to an observer traveling at wave speed. Since no wave can ever catch the one ahead, the net result of these differential motions is to accumulate more waves between any two group velocity lines with increasing time and distance; that is, within any proportional segment of the wave envelope.

If it seems surprising that we have not, until now, mentioned either the wave period or the wavelength, which, together with the wave amplitude, comprise the three most physically obvious features manifested by wave motion, the reason is that the ordinary definitions of these variables do not accurately apply to a system of dispersive waves. That is, the wavelength is only very approximately the distance between consecutive waves, and the period approximately equal to the coresponding time interval – and this approximation becomes increasingly poor nearer the wave front. This is because they are not properties of individual waves. Both wavelength and period should more properly be thought of as functions

of the dimensionless wave number; viz:

$$L = 2\pi h/\sigma \tag{II-16}$$

$$\tau = 2\pi (h/g\,\sigma \tanh \sigma)^{\frac{1}{2}} \tag{II-17}$$

Both period and wavelength are theoretically infinite at the wave front, descend hyperbolically, and diminish with increasing time like T^{-1} and T^{-2}, respectively.

II-2 THE SCALING LAWS

While the non-dimensional generation model (Eq. II-15) is useful in describing the general features of axisymmetric wave systems, the effects of varying the initial geometry (water depth and charge position) and the relative energy (yield) of an explosion can better be discussed by considering the same model in dimensional form:

$$\eta(k) = \frac{b\, r_o}{r} \left[- \frac{v/k}{d\, v/\, dk} \right]^{\frac{1}{2}} J_3 (r_o k) \qquad \text{(II-18)}$$

where the phase factor has been omitted as irrelevant to the discussion of wave amplitude. Equation (II-18) states that the amplitude spectrum $\eta(k)$ when viewed from a fixed observing distance r, depends only upon the initial source dimensions b and r_o, and the water depth h. The former can be supposed, in turn, to depend upon the charge yield, Y, and the charge depth, Z, relative to the free surface (Z = 0).

II-2.1 Effect of Water Depth

Consider, first, the effect of changing the depth only, all other input conditions remaining constant. Figure II-3 shows $\eta(\sigma)$ computed for five values of the ratio h/r and plotted as a function of $\sigma = kh$. For clarity, only the first maxima of the wave envelopes are shown. When the depth is large, the significant regions of the amplitude spectra become independent of depth. This is because, as in all water wave problems, the mechanism of surface motion becomes independent of water depth when the latter exceeds a substantial fraction of a wavelength ($h > L/2$). As the relative depth progressively decreases ($h/r < 1$), the spectrum undergoes distortion, and the maximum wave amplitudes (as shown by the solid line) first decrease to about half the deep-water value, and then increase inversely as the depth decreases without limit. But this latter increase is inconsistent with the very limited data available on explosions in shallow water (see Section II-3). Moreover, the theory becomes increasingly inaccurate for small values of kh. If, however, one accepts the

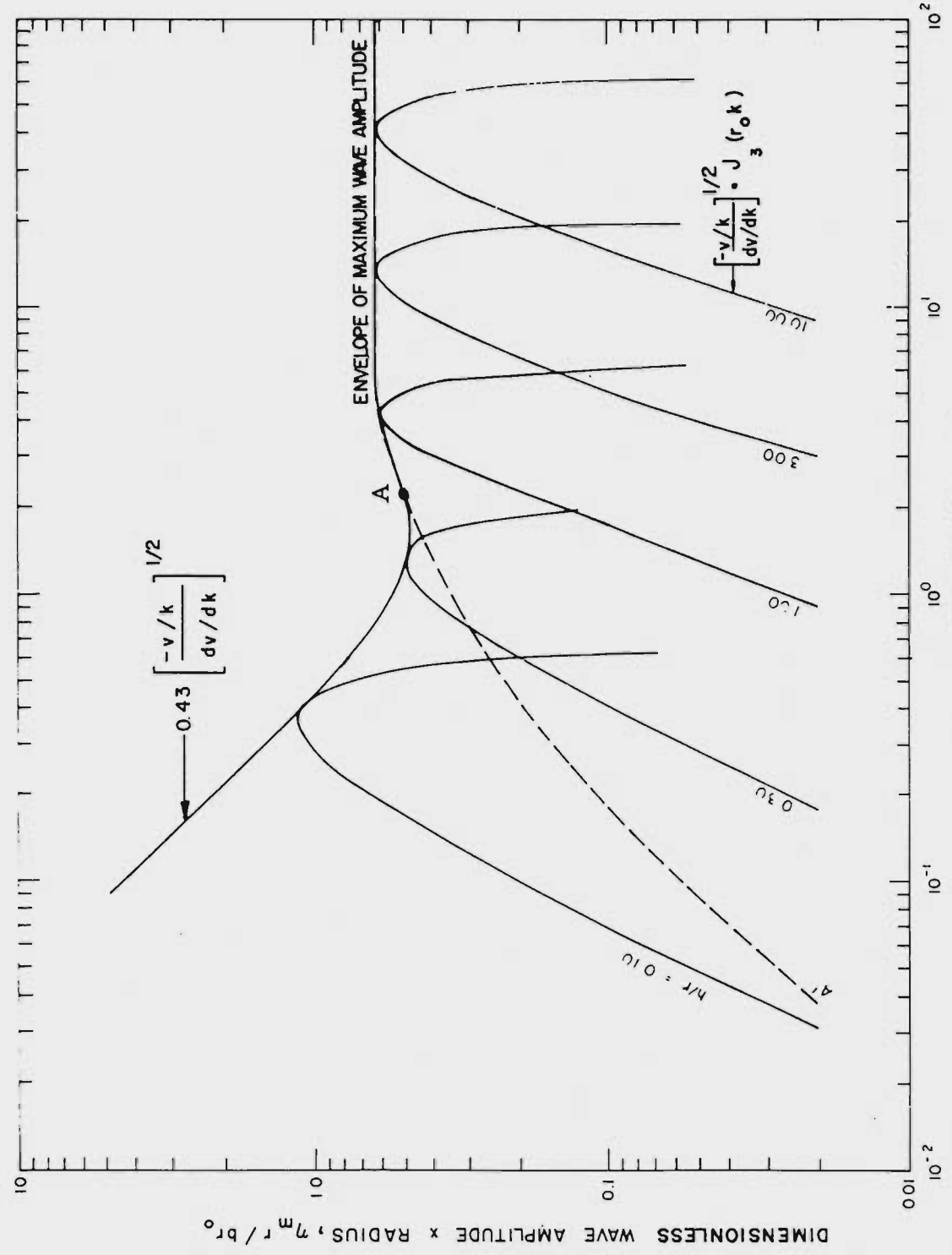

Figure II-3 Effect of Water Depth on Wave Height Generated by Explosion Obtained by Use of Kranzer and Keller's Solution

physically intuitive argument that the maximum wave height can never substantially exceed the water depth,

$$\eta_m \leq 0.39h, \qquad r = r_o \tag{II-19}$$

where η_m will diminish toward zero as the water depth diminishes, as suggested by the dotted branch A-A' in Fig. II-3.

II-2.2 Effect of Charge Depth

We consider now the effect of varying the charge depth Z, while holding the yield and water depth constant. Since our model is not based on the physics of wave generation, it says nothing about charge depth, and its generality as a prediction model depends upon the above-cited assumption that the experimentally-determined effects of charge depth variation can be incorporated in the parameters b and r_o (Eq. II-18), and in a manner (hopefully) scaleable with yield.

The influence of charge depth on wave production has probably been studied more intensively on an experimental basis than any other single factor. Yet today, there is no satisfactory explanation for all of the observed effects, typically illustrated in Fig. II-4, which is a plot of maximum observed wave amplitude time radius $\eta_m r$ vs. charge depth Z for a constant yield (Y = 385 lbs. TNT) and radius of observation. As the charge position is moved downwards from a relatively unexplored geometry just above the free surface (wherein wave effects are known to be small or unimportant), the curve exhibits a very high, narrow maximum for shots very slightly beneath the surface, followed by a minimum, and a second - but lower - maximum, after which the widely scattered results suggest that successively lower cycloidal maxima may occur. The first two maxima have been named the "upper and lower critical depths", respectively, because the largest waves occur at these charge depths. At least the second minimum can be linked to the emergence of the explosion

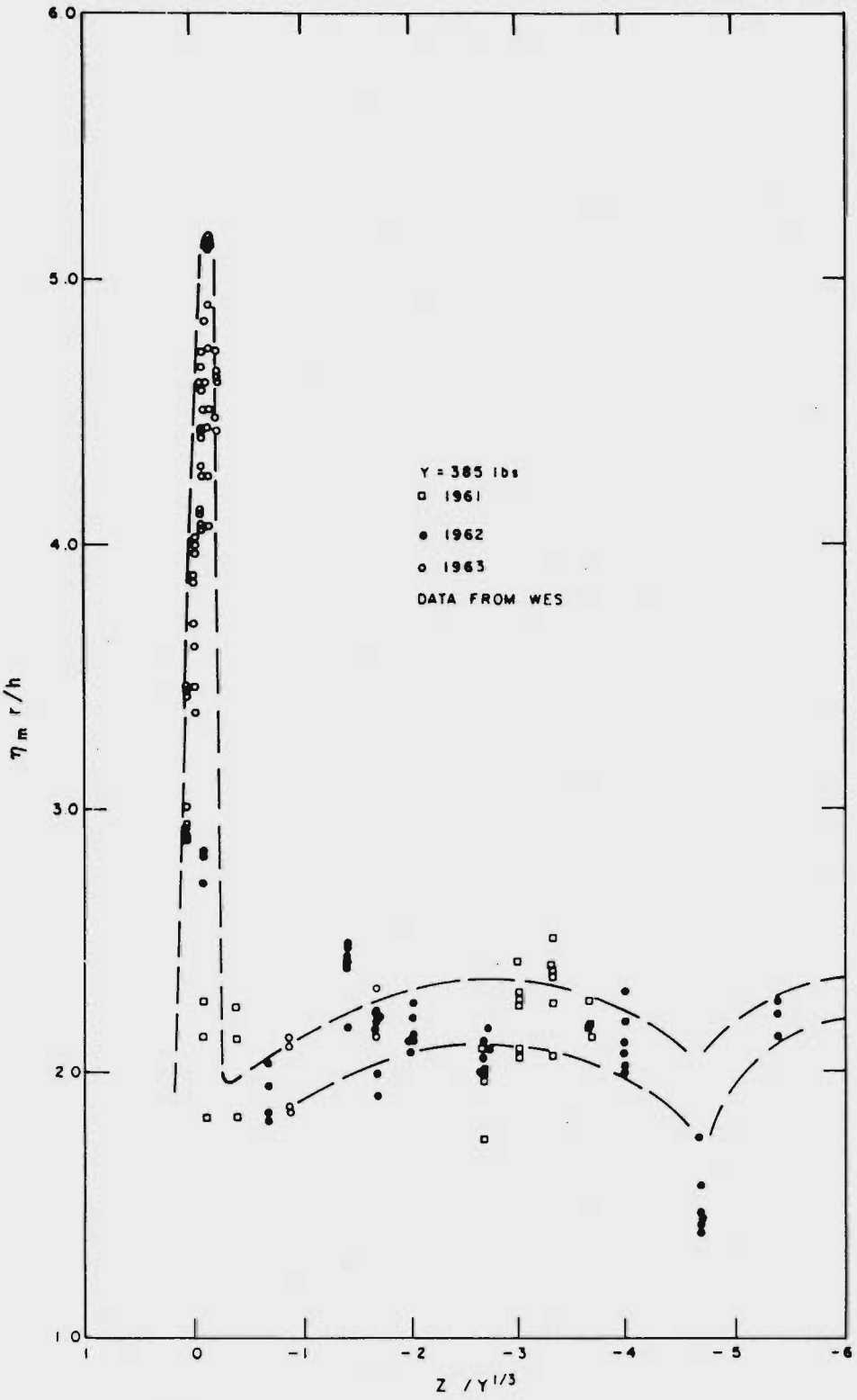

Figure II-4 Effect of Charge Depth, Z, on η_m r (for a given yield, Y = 385 lb)

bubble at the surface in a contracted phase following its first expansion.

While the lower critical depth is understandably analogous to the maximum observed in similar plots of radii and depths of explosion craters in solid materials, no sound physical explanation has yet been advanced for the upper critical maximum, although a recent theoretical model suggests that it may be due to restriction of surface venting because of surface shock reflection (Kriebel, 1968). This effect is so far unverified experimentally. However, since the entire region interior to this maximum is filled with data, it would appear to be a precarious stability condition that results in maximum effects, and one that is not readily reproducible. Nevertheless, the possibility that a near-surface explosion might produce waves of this magnitude cannot be ignored when making wave predictions.

An additional experimental observation (but one which may be of principally academic interest, since the precise arrival times of individual waves are not ordinarily of military significance) is a change of phase between the corresponding waves of trains generated by explosions above, or below the upper critical depth, respectively. Such a change, in fact, is predicted between theoretical models of wave trains generated by an initial impulse and an initial elevation, respectively. This fact, together with physical intuition, suggests that an impulse model may be more appropriate for above - or near-surface explosions. However, since neither model is based on physical reality, and since the deformation model can be suitably adjusted to give adequate predictions for surface explosions, the latter is employed exclusively hereinafter.

Turning now to the question of scaling, empirical curves, as shown in Fig. II-5, which is similar to Fig. II-4, have been obtained for a variety of chemical (HE) charge weights within the range $\frac{1}{2}$ lb < Y < 14,500 lbs (TNT equivalent), but with a steadily increasing scatter in wave amplitudes with increasing charge weight and charge depth. While some of this scatter can be attributed to differences in the experimental conditions, much of it appears to lie in an inherent

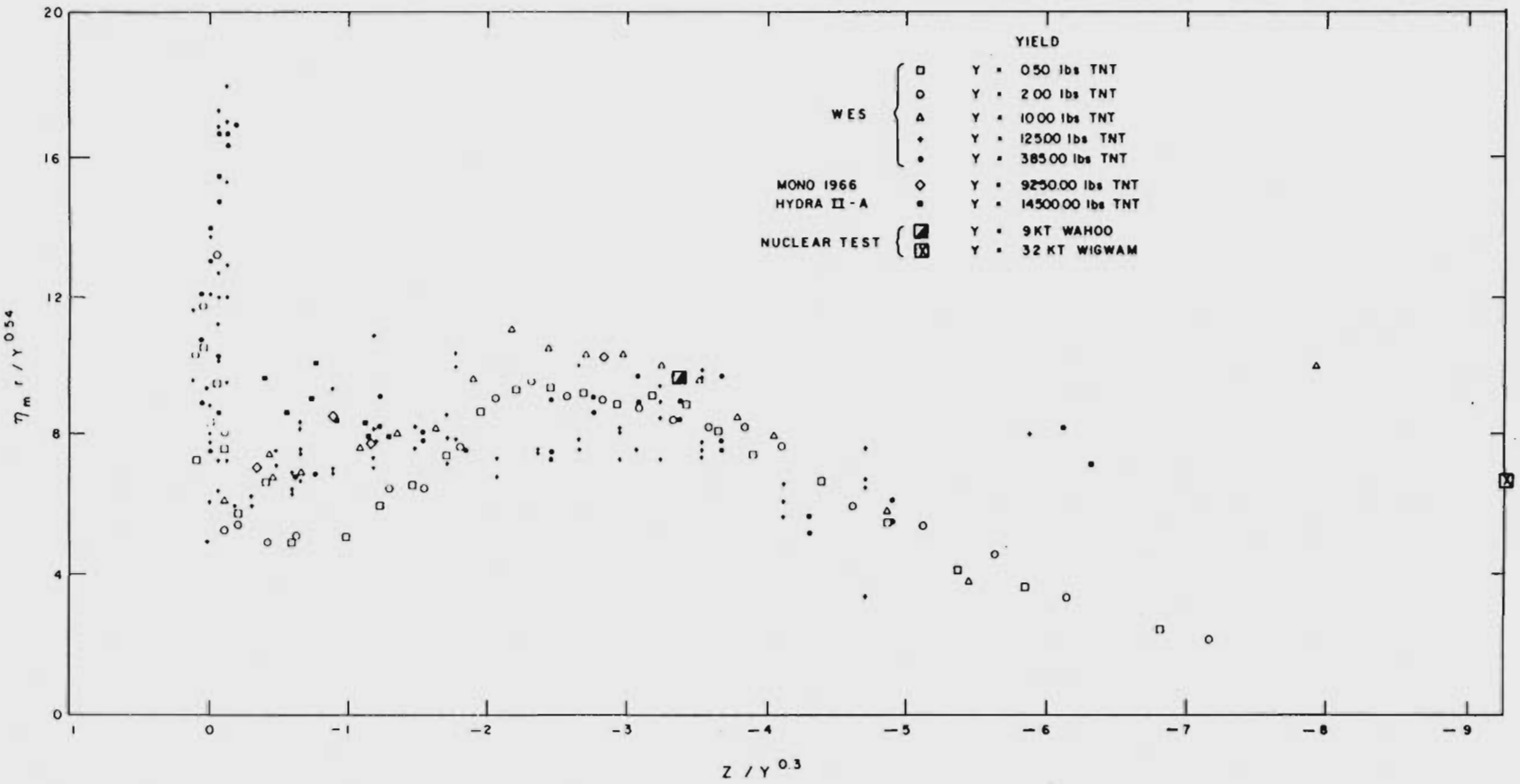

Figure II-5 An Empirical Curve for the Relationship Between Values of $\eta_m r$, Charge Depth and Explosion Yield

irreproducibility of wave effects from larger explosions, the latter exhibiting no well-defined amplitude maximum either at or below the surface. In fact, the maximum waves for large charges were produced by relatively deep explosions. However, the significant features of the depth-of-burst curves at smaller charge weights were only obtained by hundreds of repetitive tests, and an upper critical maximum is still clearly present with charges as large as 385 lbs.

Because most of the above testing was performed before the development of a suitable hydrodynamic model, earlier attempts to relate pertinent variables were restricted to dimensional analysis. Unfortunately, the water depth was not considered to be important, and most of the larger tests were carried out over uneven bottom, which has made the wave records difficult to interpret. Nevertheless, attempts have persisted to force rather widely scattered results into the framework of the mixed-dimensional relation

$$r\,\eta_m/Y^p = G(Z/Y^q) \qquad \text{(II-20)}$$

where η_m is the largest recorded wave amplitude at a distance r and G is an empirical function (hopefully) to be determined from the optimum composite curve of all test data obtained by trial adjustments of the exponents p and q. On a purely kinematic basis one expects that, if explosions of different sizes produce geometrically similar disturbances, then one should find that $p = 1/2$, $q = 1/3$. Unfortunately, nature is not quite so kind, and the most careful review of experimental data for HE in the light of hydrodynamic theory indicates that, while the general form of Eq. (II-20) is valid over an impressive range of Y, the best value of the exponents p and q seem to be slightly different from the above values, and that, because of atmospheric pressure, Z is not simply scaleable as a power of Y, as shown below.

First note that Eq. (II-18) shows that whenever $\sigma > 3$, $\eta_m r$ is a function of the explosion parameters only, in accordance with Eq. (II-20).

In addition to Eq. (II-20), we must establish the scaling law relating wave number to source radius for events where the charge depth Z is suitably scaled. Based on experimental results, it is suggested that

$$r_o k Y^c = F(Z) \qquad \text{(II-21)}$$

Charge depth scaling, particularly for surface-venting explosions, raises the problem of accounting for energy partition between atmosphere and water on the cavity history. These effects are manifestly different for chemical, relative to nuclear, explosions. Unfortunately, the bulk of empirical data fall within the former category where the physics of energy partition is least understood. It therefore is more appropriate to first consider scaling of subsurface explosions.

Using dimensional arguments, and assuming that a constant percentage of explosion energy goes into shock, for charge depths great enough so that the explosion cavity does not rupture the surface at first expansion, Penny (1945) suggests that the scaling law for Z should be

$$\left(\frac{Z_2}{Z_1}\right)^3 \left[\frac{Z_2 + P_a}{Z_1 + P_a}\right] = \frac{Y_2}{Y_1} \qquad \text{(II-22)}$$

where P_a is the atmosphere pressure head. This relation shows that Z scales like $Y^{1/3}$ for small charges ($P_a >> Z$) and like $Y^{1/4}$ for very large ones ($P_a << Z$).

Figure II-5 is a plot of $\eta_m r/Y^{0.54}$ versus $Z/Y^{0.3}$ for all available TNT explosions, where the water depth was large enough so that the wave number $\sigma_m \geq 3$. Data were excluded when the products $\eta_m r$ at different ranges from a given event failed to agree within 10%. The amplitude scale-factor $Y^{0.54}$ was determined by minimizing the vertical RMS data scatter about the arithmetic mean within integer zonal multiples of $Z/Y^{0.3}$. It is clear that practical limits for prediction purposes can be expressed as

$$\frac{\eta_m r}{Y^{0.54}} = 18, \quad 0.25 > Z/Y^{0.3} > -0.25 \qquad \text{(II-23)}$$

for surface explosions, and

$$\frac{\eta_m r}{Y^{0.54}} = 10, \quad Z/Y^{0.3} < -0.25 \qquad \text{(II-24)}$$

for subsurface explosions.

II-2.3 Scaled Source Coefficients

Returning, now, to Eq. (II-21), if we let $k = k_m$ at $\eta = \eta_m$ signify the wave number of the maximum wave in the time-record of a wave train observed at a distance r, then k_m can be evaluated from experimental data knowing the (uniform) water depth and arrival time of η_m. Figure II-6 shows the variation of k_m with yield Y for the data of Figure II-5 which, again, are practicably divisible into two groups, given by the power laws

$$\text{surface} \qquad k_m = 0.44\, Y^{-0.3}, \quad 0.25 > Z/Y^{0.3} > -0.25 \qquad \text{(II-25)}$$

$$\text{subsurface} \qquad k_m = 0.39\, Y^{-0.3}, \quad Z/Y^{0.3} < -0.25 \qquad \text{(II-26)}$$

The scatter of data for wave number is very much smaller than that for wave amplitude, since the dispersion is a function only of the water depth and source radius. Equation (II-21) is thus verified for explosions deep enough so that $k_m h > 3$, because the largest waves η_m will occur when $r_o k_m = 4.2$; giving the scaled source radii

$$\text{surface} \qquad r_o = 4.2/k_m \doteqdot 9.6Y^{0.3}, \quad 0.25 > Z/Y^{0.3} > -0.25 \qquad \text{(II-27)}$$

$$\text{subsurface} \qquad r_o = 4.2/k_m \doteqdot 10.8Y^{0.3}, \quad Z/Y^{0.3} < -0.25 \qquad \text{(II-28)}$$

It is significant that $Y^{0.3}$ is also found to be the optimum scaling exponent for crater radii in solid materials (Nordyke, 1962).

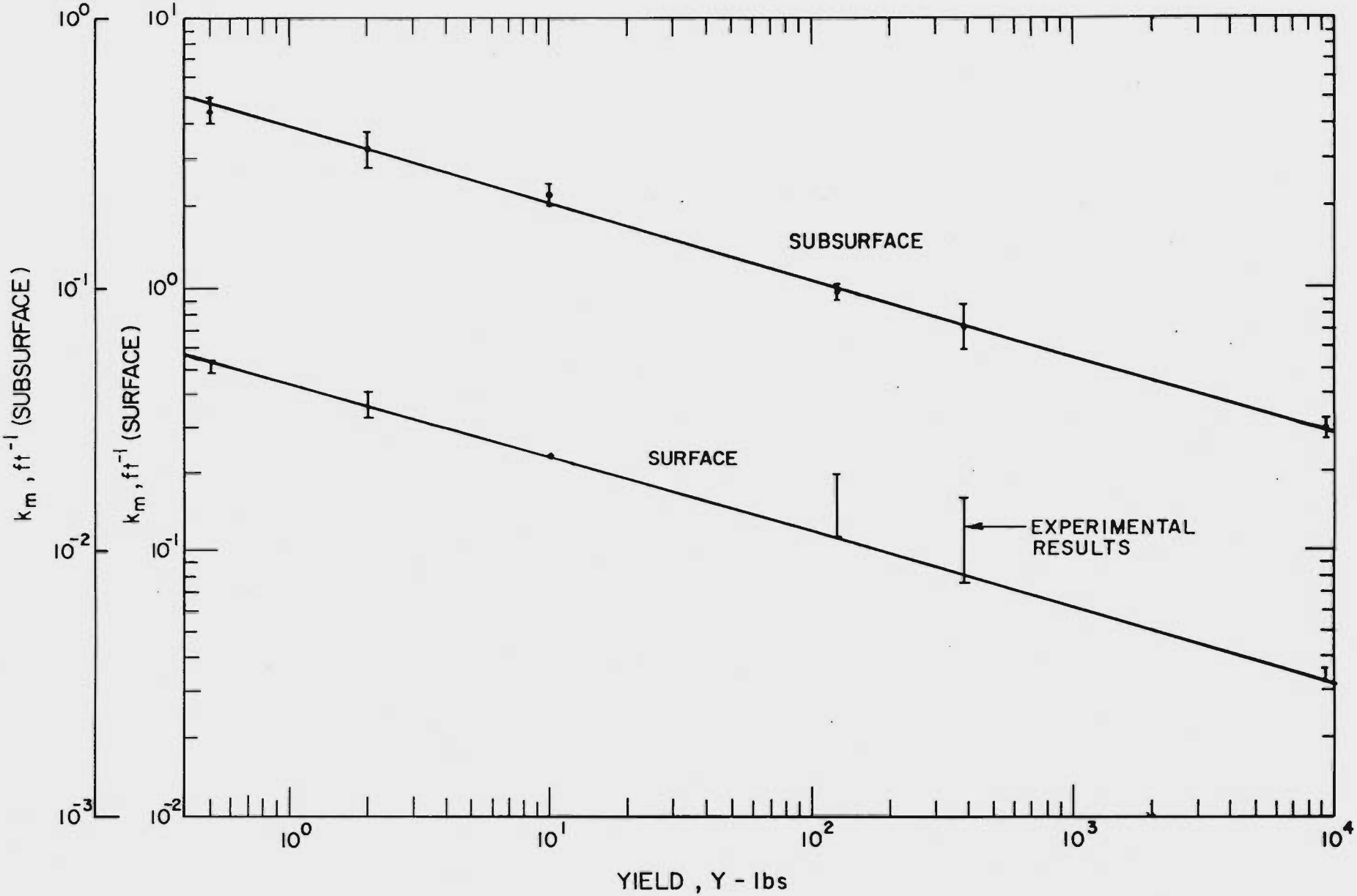

Figure II-6 The Relationship Between Wave Number and Yield for Subsurface and Surface Explosions

Now, combining Eqs. (II-23), (II-24) and (II-27), (II-28), and noting that for $k_m h > 3$, $\eta_m r = 0.63\, b r_o$, we obtain the source amplitudes,

$$\text{surface} \qquad b = 2.8\, Y^{0.24}, \quad 0.25 > Z/Y^{0.3} > -0.25 \qquad \text{(II-29)}$$

$$\text{subsurface} \qquad b = 1.6\, Y^{0.24}, \quad Z/Y^{0.33} < -0.25 \qquad \text{(II-30)}$$

Again, $Y^{0.24}$ scaling has also been found to be most appropriate for crater depths in solid materials, although there is no corresponding upper-control maximum in the latter media.

Since not only crater radii but also crater depths in solid materials diminish as the charge depth is decreased towards zero, the anomalous increase in maximum water wave amplitude at the upper critical depth can only be the result of the kinetics of water motion following initial expansion, probably abetted by the better impedance match between water and air than that for most solids.

As evidence of the general applicability of the model, Fig. II-7 shows wave envelopes computed from Eq. (II-18) (phase factor omitted) normalized to the stated maximum amplitudes η_m for three wave trains recorded during the 1966 Mono Lake test series (Pollard and Wallace, 1967). (The standard subsurface prediction [$b = 1.6\, Y^{0.24}$, $r_o = 10\, Y^{0.3}$] would have given uniform maximum envelope amplitudes $\eta_m = 0.38$ ft. at $r = 3600$ ft, thus over-predicting for the shallower shots by about 22% and 35%, respectively. This is necessarily the case with scattered data; the prediction must cover the possible maximum case.)

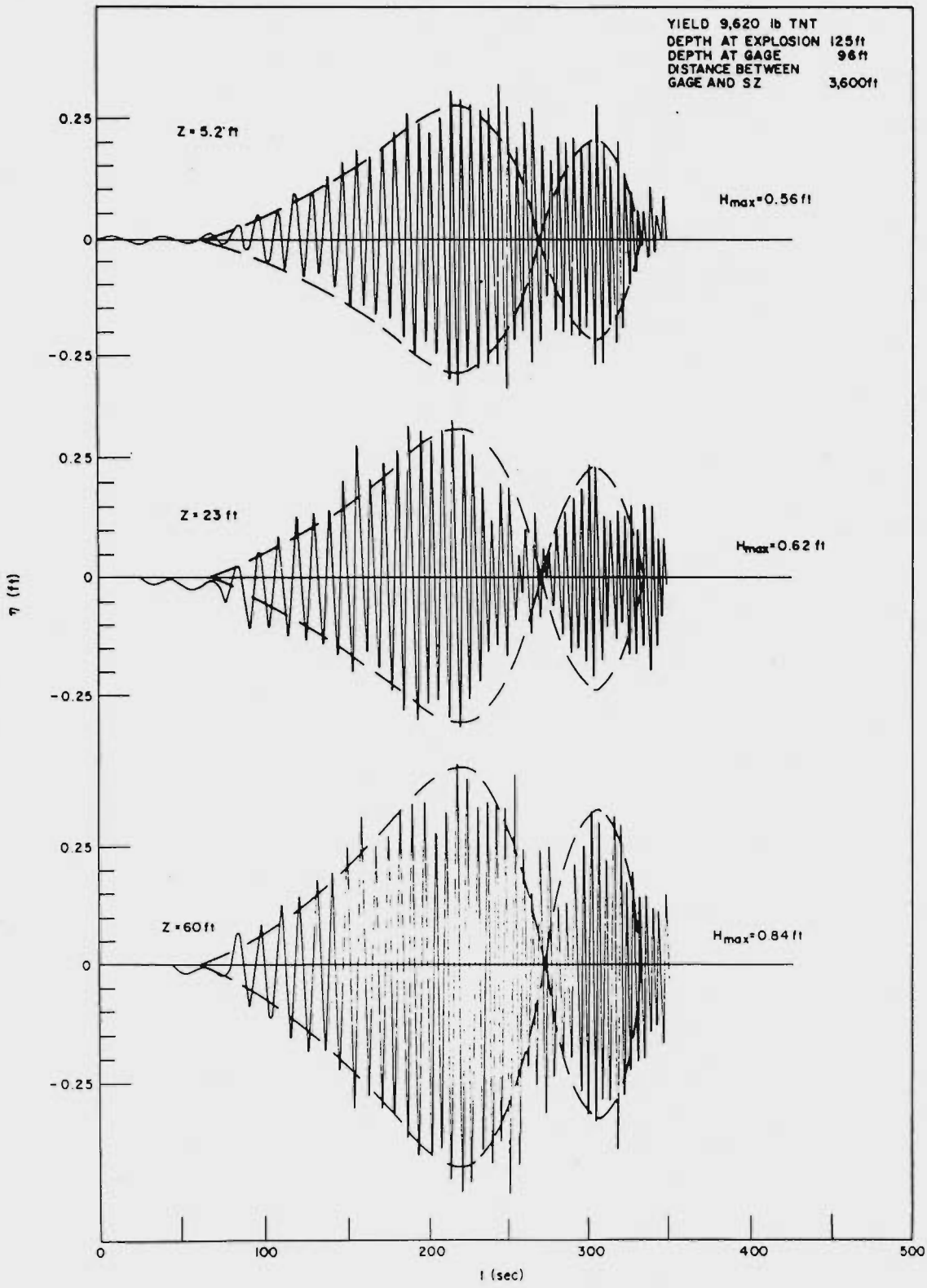

Figure II-7 Comparison of OSI 1966 Mono Lake Experiments with Theory

II-3 SHALLOW WATER WAVE GENERATION

Interest in shallow water generation stems from the fact that, although the wave-making efficiency is smaller than that for an equivalent explosion in deep water, a greater fraction of the resulting wave energy goes into the leading waves of the train. This is because the cavity radius, which controls the wavelength of the principal waves (Eq. II-27), is substantially independent of the water depth. Moreover, because of their low steepness ($\eta_m k_m < h k_m < 1$), such waves are less apt to break on gentle slopes, and hence are potentially capable of a higher absolute shoreline run-up than steeper waves of the same height. Thus, the tendency for greater run-up is opposed by decreasing available wave energy as the generation depth decreases, and it is desirable to inquire whether the absolute run-up will increase or decrease in such circumstances.

While the deep water prediction model becomes invalid for $h < 6Y^{0.3}$ a general theory exists for shallow water generation (Kajiura, 1963). As with deep water generation, however, an acceptable prediction model must be normalized to an extensive set of experimental data. Unfortunately, present data are limited to a single small test series with 4-lb TNT charges (WES, unpublished) and two 9,250 lb. shallow water shots during the 1966 Mono Lake tests (Wallace, 1967). Figure II-8 shows the available data compared with that for deep water. The former have roughly the same charge depth dependence, but the $\eta_m r/Y^{0.54}$ values are only about half as great as the median (heavy) line for deep water tests. Although the WES original records are not yet available for analysis, Fig. II-9 shows the published wave records for shot 2 of the 1966 Mono Lake shallow water series (Wallace, 1967). As distinct from deep water records at similar distances, the wave trains are characterized by a large, long leading wave, followed by a series of shorter waves, whose amplitudes increase and then decrease with time. Such wave trains can be shown to be predictable by shallow water generation theory of Kajiura (1963).

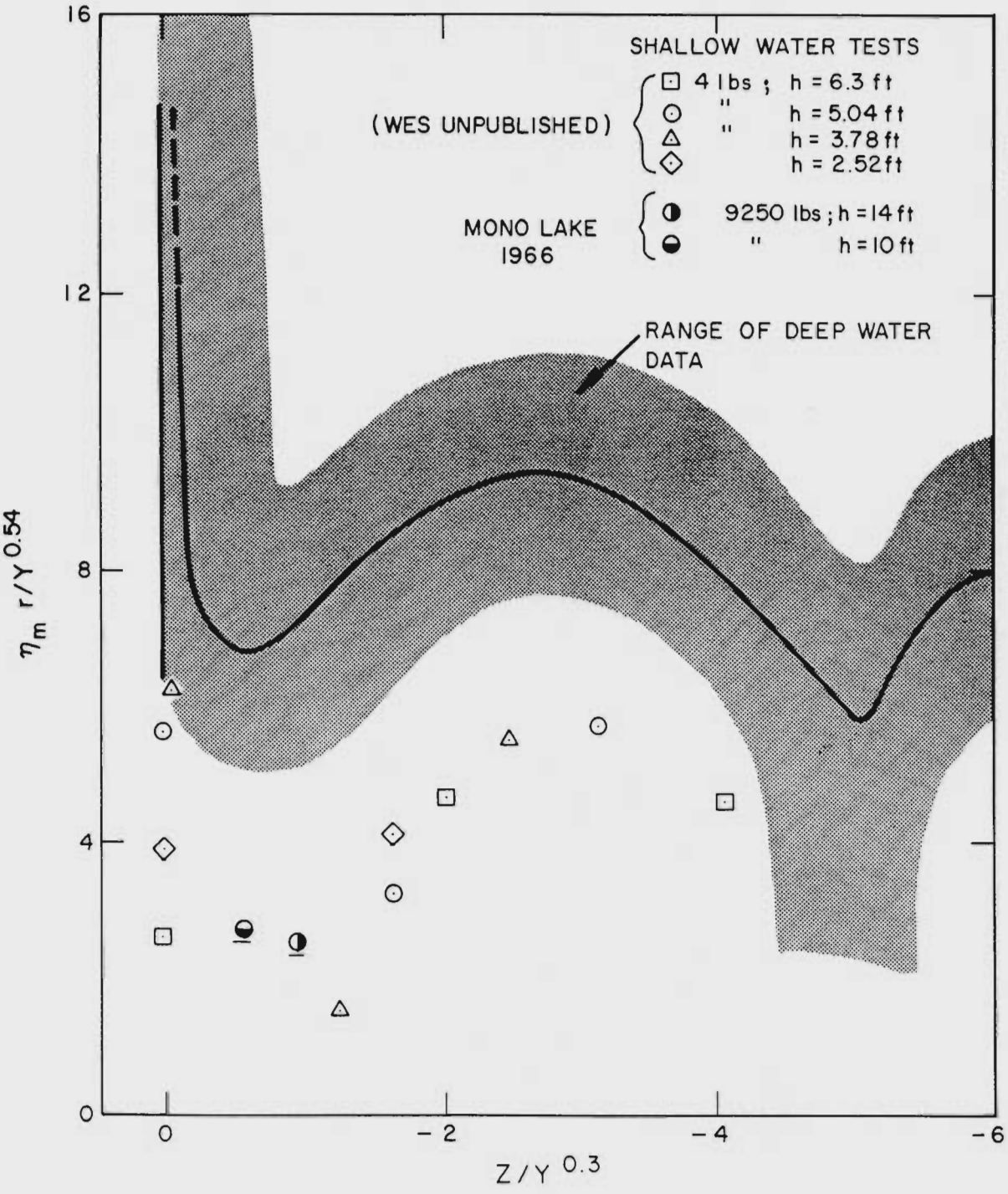

Figure II-8 Summary of Explosion Wave Data for explosions in shallow water underlined points are for bottom-denotated charges (Z = -h)

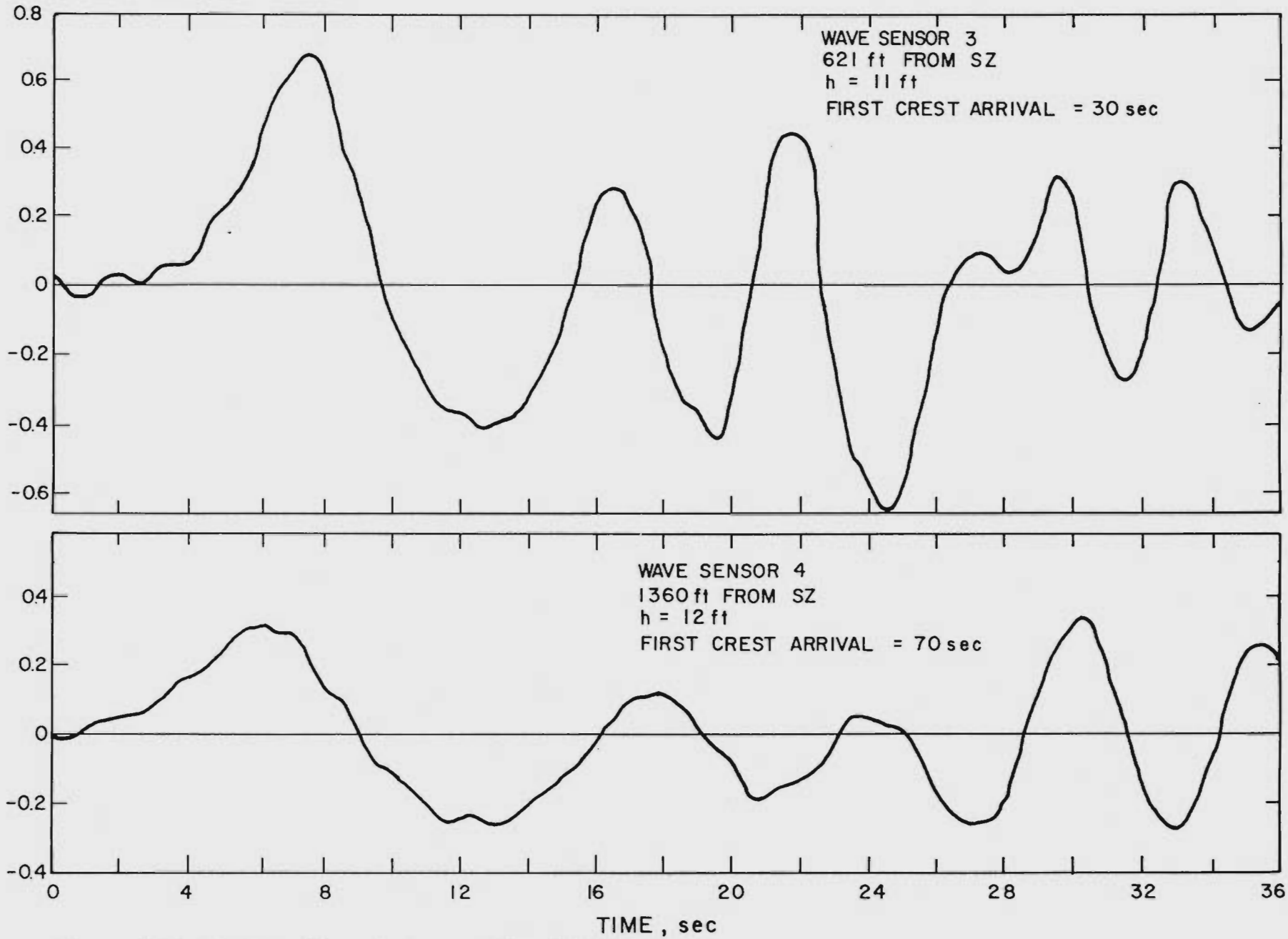

Figure II-9 Shot 2 - Wave Systems, Mono Lake Shallow-water tests. Charge weight W = 9,250 lbs. Burst depth 10 ft (on bottom) Data from Wallace (1967).

CHAPTER III

WAVE PROPAGATION

III-1 UNIFORM WATER DEPTH

When the water depth is uniform, or deep enough, relative to the explosion yield ($h > 6Y^{0.3}$) so that the principal waves are unaffected by the depth the wave system will have circular symmetry. The general characteristics of such an expanding wave system will resemble those of Fig. I-1.

As in the theory for wave generation discussed in Chapter II, the local wave amplitude at any place and time is calculated by summing the Fourier components which arrive simultaneously from all of the elemental regions comprising the source disturbance. The wave amplitude is a function of the local energy density, considered to be the property of an energy packet bounded by adjacent rays radiating outward at group velocity in the direction of the rays. The procedure is appropriately called the conservation of energy flux. Thus, the amplitude, of any individual wave is not a property of that wave, but will vary according to the wave amplitude envelope as each wave passes through. In order to determine the amplitude of any particular wave at a given point or time, one must first determine when the wave will arrive at that point, determine its local frequency from the dispersion relation (Eq. II-2), and then compute its amplitude from the general formula (Eq. II-18).

The local wave position is determined from the phase function (Eq. II-6). While it is known that the wave phase at a given point shifts by as much as 180° as the charge depth is varied, this shift is ordinarily of no importance to wave effects, and is ignored in the following discussion. Thus the calculated instantaneous position of any particular wave in the ensemble passing a given point will be uncertain with a half-wavelength or so, or its arrival time uncertain by half its period. This uncertainty will not ordinarily affect the local amplitude.

At any point in a space-time coordinate plot of an expanding wave train, any wave can be identified by the position of some point of constant phase (say, the wave crest), usually by assigning it an order number n, reckoned

inwards toward the source from that crest nearest the wave front. The locus of such points is called a phase trajectory, two of which are shown in Fig. I-1. Since a point of constant phase (point phase) is defined by $\cos(\omega t - kr) = m = \text{constant}$, wave crests will occur when $m = 1$, and the crest order numbers will be given by

$$\omega t - k r = \pi (2n - 1) \qquad n = 1, 2, \ldots, p \tag{III-1}$$

In view of the auxiliary equations for group velocity and frequency for a point of stationary phase,

$$v = r/t = (\omega/2k)(1 + 2kh/\sinh 2kh) = \frac{d\omega}{dk} \tag{III-2}$$

$$\omega^2 = g k \tanh kh$$

Equation (III-1) can be revised to a pair of equations relating n and r or t to the wave number k and the (constant) water depth h.

$$\frac{\pi (2n - 1)}{r} = k\left[\frac{1 - 2kh/\sinh 2kh}{1 + 2kh/\sinh 2kh}\right] \tag{III-3a}$$

$$\frac{\pi (2n - 1)}{t} = \frac{1}{2}(g k \tanh kh)^{\frac{1}{2}}(1 - 2kh/\sinh 2kh) \tag{III-3b}$$

Equations (III-3) might be called the field equations for wave number in the r-t plane (similar to R-T plane). Knowing either r or t, h and n, k can be found from a curve or table, and the unknown variable determined by substitution. More commonly, h, r, and t are known and n is desired. In such cases, no exact solution is possible, but the closest integer value $p(n)$ can be found by determining k from Eq. (III-2) and substituting in either of Eqs. III-2.

Simplifications of the above procedure can be made when the water depth h is substantially greater than the wavelength L at the frequency considered, as defined by

$$kh = 2\pi h/L > 3 \quad \text{(deep water)} \tag{III-4}$$

In this case, Eq. (III-3) becomes

$$\pi (2n - 1) = k r = \frac{t}{2} (g k)^{\frac{1}{2}} \qquad \text{(III-5)}$$

from which, by eliminating k,

$$\pi (2n - 1) = \frac{g t^2}{4 r} \qquad \text{(III-6)}$$

Thus the trajectories of individual waves in the r-t plane are first order parabolae, whose consecutive arrival times at any point, R will be in the ratios

$$T : \frac{T}{\sqrt{3}} : \frac{T}{\sqrt{5}} \quad \ldots \text{ etc.}$$

Similarly, at any instant of time, T , the consecutive crest radii will have the ratios

$$R : R/3 : R/5 \quad \ldots \text{ etc.}$$

III-2 NON-UNIFORM DEPTH

III-2.1 Method of Approach

There is no uniformly valid theory for predicting the evolution of an explosively-generated wave system in water of non-uniform depth. This is because depth variations act to disturb the uniform radial flux of energy and speed of wave propagation by processes of refraction and/or reflection in a manner too complicated to permit simple generalization. Moreover, these perturbations depend upon the local wave frequency, which, itself, is varying with time. Lastly, such nonlinear processes as finite wave height and frictional dissipation, that can be ignored in deep water, must be considered in shallow-water propagation.

As a result, in order to make meaningful predictions, a piece-wise continuous computation scheme is used, (see Section III-3.2), by which energy and waves can be propagated over a greatly simplified step-like topography, suitably selected to approximate the actual sea floor over a limited region. The validity of such a model depends upon a number of simplifying assumptions or approximations, each of which have been separately investigated. The most important of these factors are reviewed in the following sections. Because of the greater simplifications afforded, in most previous theoretical and experimental work, it has been assumed that the waves are periodic. While ultimately, one has to rely upon a theory valid for dispersive waves, the importance of wave reflection, nonlinearity, and bottom dissipation can more easily be assessed by assuming that the waves are quasi-periodic.

III-2.2 Wave Reflection

The many theoretical attempts to derive a suitable formulation for the reflection coefficient for periodic progressive waves in water of non-uniform depth have been reviewed by LeMéhauté (1966). Of these, the work of Miche (1944) and Roseau (1952) have the most general application to the problem of explosion waves advancing shoreward from deep water. The Roseau theory applies to a particular family of bottom profiles, some

of which quite closely resemble the continental shelves and their terminal escarpments. Application of this theory to the explosion wave problem (LeMéhauté, et al, 1965) indicates that the correction for wave reflection by the continental slope is insignificant for all frequencies of practical interest, even for the long leading wave. In the limiting case of small reflection, the Roseau theory tends to the linear conservation of energy flux (in one dimension). This conclusion is further supported by wave tank experiments (LeMéhauté, Snow, and Webb, 1966).

Since the reflection coefficient for waves advancing at oblique incidence will always be less than that for normal incidence, the effect of reflection is ignored in the present prediction model.

III-2.3 Wave Shoaling and Peak-Up Phenomena

The method of conservation of energy flux is one of several approximate methods available for calculating the transformation of a wave propagating from deep water to the shore. It has the advantage that it is easily applied to practical predictions. This method assumes a priori that there is no friction either internally in the fluid or at the boundaries. Moreover, it is assumed that there is no reflection of the wave energy due to the sloping bottom, and that the wave motion may be described locally by the solution to the corresponding problem for a horizontal bottom. Caldwell (1949) showed experimentally that reflection is negligible for slopes less than 4.5 degrees. Roseau (1952) substantiated this finding theoretically.

This method has been used by numerous investigators to obtain the transformation of waves. Some differences between these various investigations are attributable to different mathematical approximations for the waves. The simplest case is when the wave is taken to be a linear progressive wave. In this case the shoaling coefficient H/H_o is a function only of the group velocities v_o and v in deep and shallow water, respectively.

$$\frac{H}{H_o} = \left[\frac{v}{v_o}\right]^{-\frac{1}{2}} = \left[\tanh \sigma \left(1 + \frac{2\sigma}{\sinh 2\sigma}\right)\right]^{-\frac{1}{2}} \qquad \text{(III-7)}$$

For waves of finite height, more precise methods are required. By taking the third order gravity wave theory, LeMéhauté and Webb (1964) computed the transformation of waves, assuming conservation of energy flux. Their results indicate a larger shoaling coefficient than predicted by the linear theory (see Fig. III-1 and III-2), and the deviation increases with increasing deep water wave height, H_o. The same trend (i.e., larger shoaling coefficient for larger initial wave height) was obtained from a similar analysis, using the fifth order theory (Koh and LeMéhauté, 1966) as shown in Fig. III-3, but the fifth order wave theory is not applicable when the water is too shallow. This is because at shallow depth, we have exceeded the limit of applicability of the Stokes wave theory since the series is non-uniformly convergent. (Actually, the fifth order theory ceases to be valid for $\sigma > 0.6$.)

Basically, the problem of wave propagation, as investigated herein, possesses three geometric characteristic lengths: namely, the depth h, the wavelength L, and the wave height H. From these it is possible to form two dimensionless quantities H/L and H/h. The fifth order theory expands the solution, using essentially H/L as the parameter of expansion, without paying much attention to the other parameter, H/h. It was implicitly assumed, therefore, that in the theory the quantity H/h is unimportant. In the present investigation of wave shoaling, this quantity is certainly not uniformly small in the physical region of interest. In particular, for small depth (and hence larger H/h) the fifth order theory appears to be a poorer approximation to experimental results than the corresponding third order theory. In the limit as $h \to 0$, the third order theory is poorer than the linear theory. It is concluded that the third order results should be used for calculations of wave shoaling, where extreme accuracy is desired, but that the first order theory is adequate for most cases where the topography is imperfectly known.

When waves arrive at a depth smaller than approximately 1.4 times the breaking depth, a sudden increase in wave height is observed experimentally (LeMéhauté, Snow and Webb, 1966). Figure III-4 illustrates this phenomenon. Even though the general results given by previously mentioned nonlinear wave theory indicate this trend, there is presently no satisfactory theory

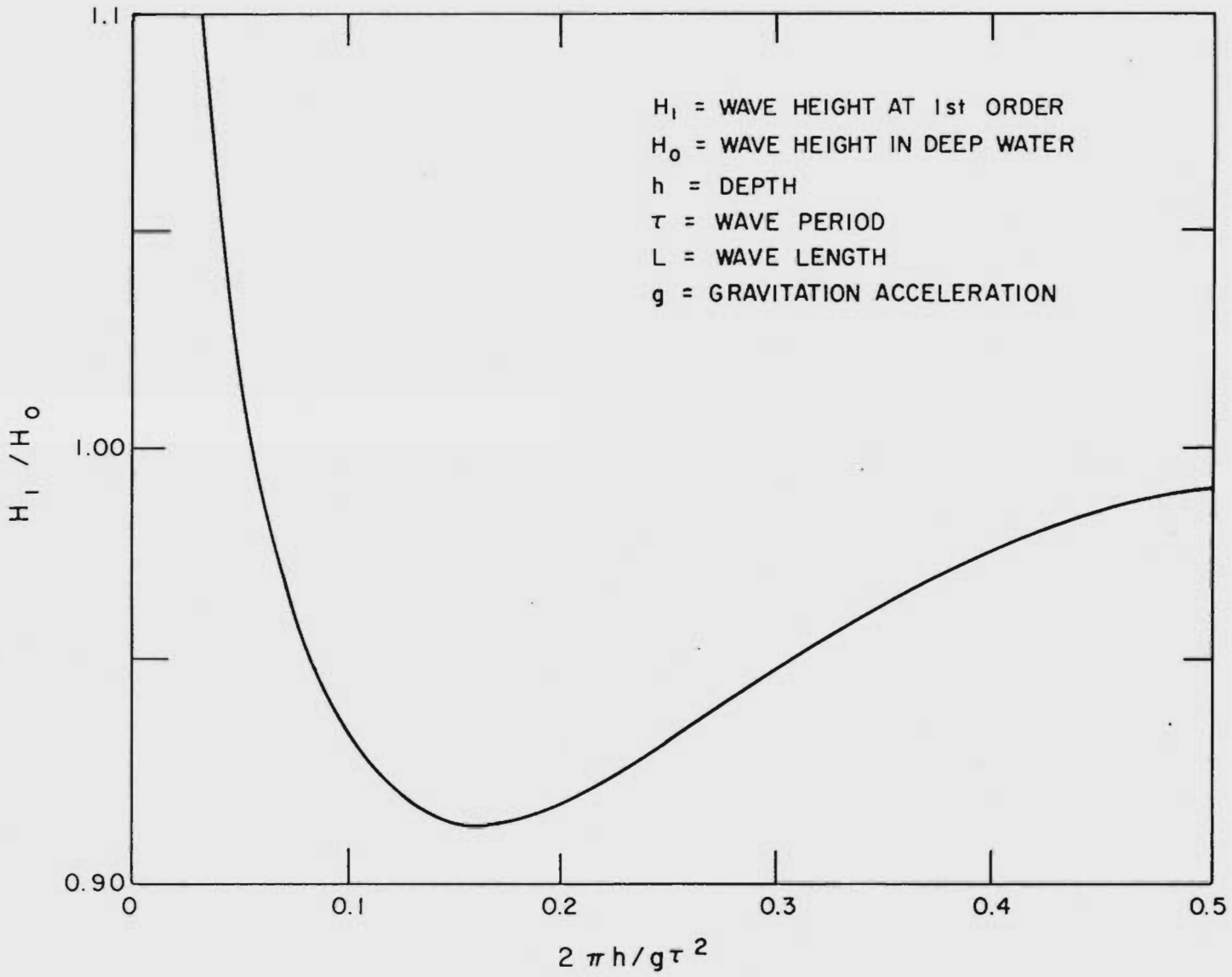

Figure III-1 The Shoaling Coefficient at the First Order of Approximation

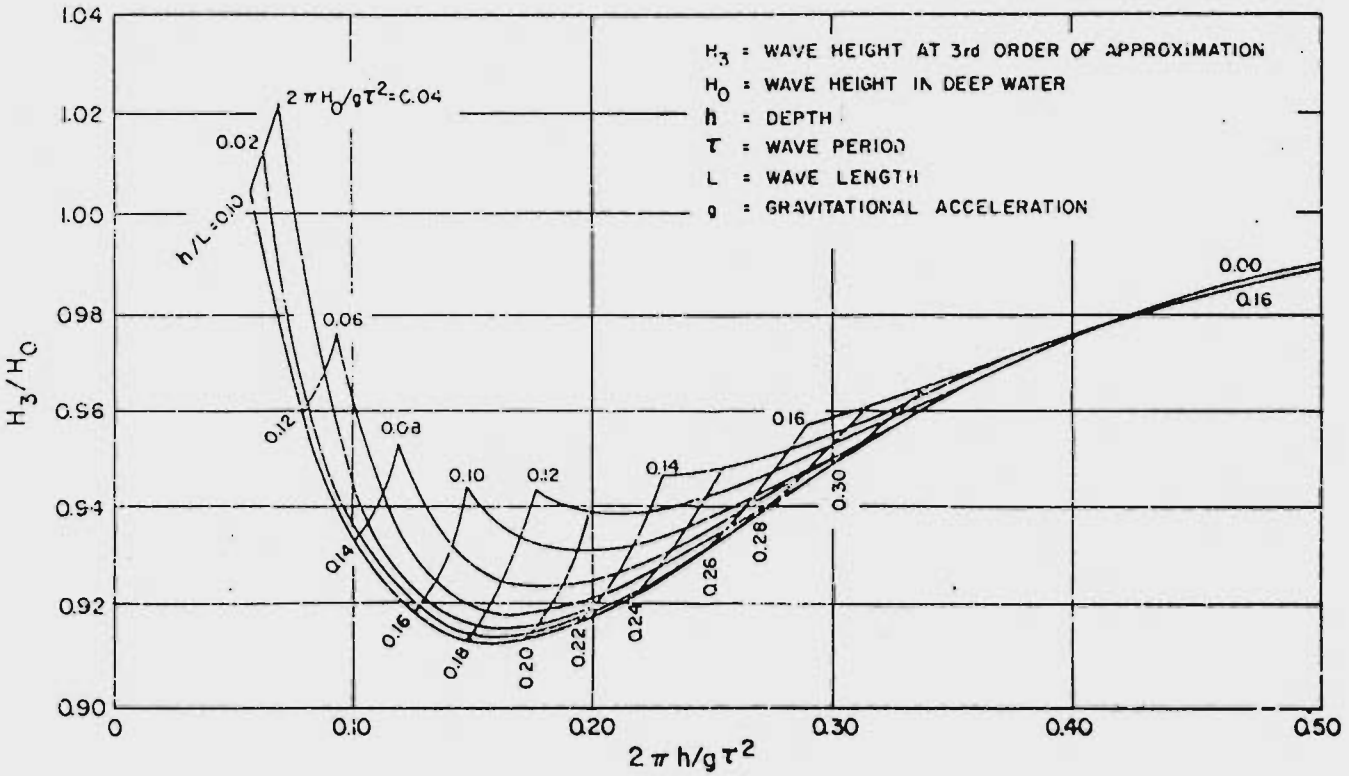

Figure III-2

The Shoaling Coefficient at the Third Order of Approximation (Non-dimensional Variables)

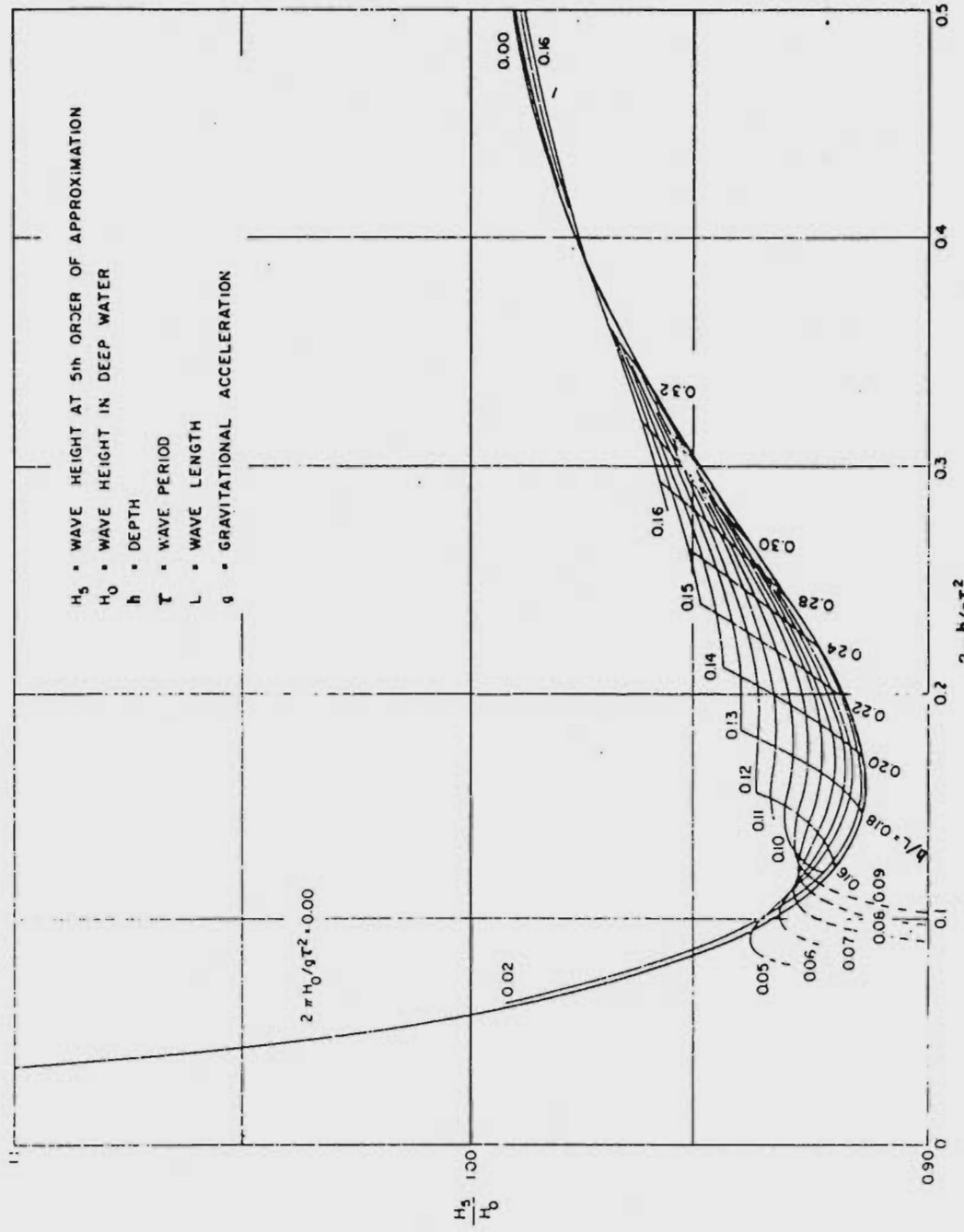

Figure III-3 The Shoaling Coefficient at the Fifth Order of Approximation

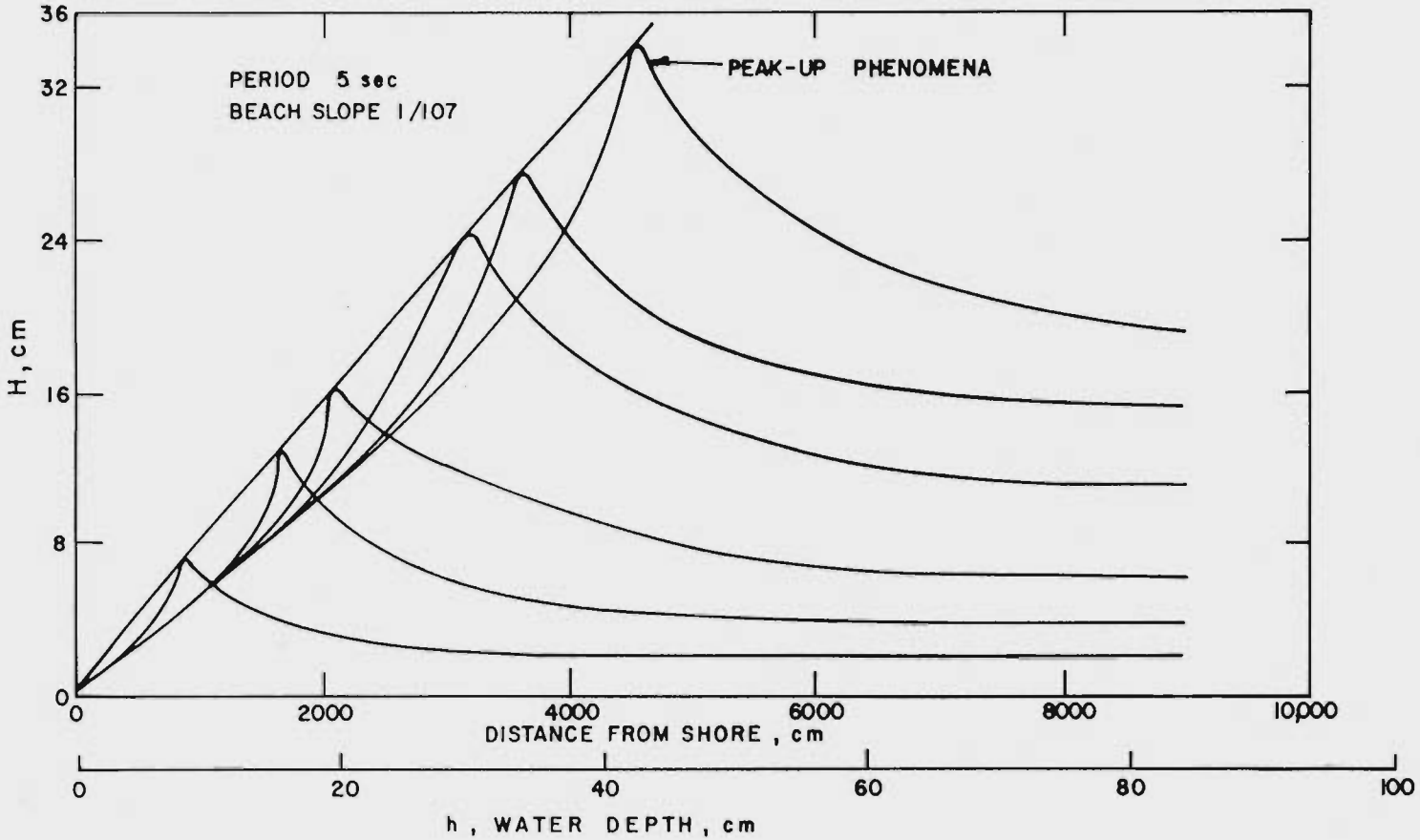

Figure III-4 Experimental Peak-Up Loci of Periodic Waves Near the Point of Breaking Inception

which can match the experimental facts, although Van Dorn (1966) suggests that such a peaking up is to be expected for waves on a slope when the local Ursell parameter $\frac{H}{h}\left(\frac{L}{h}\right)^2 > 100$. As a practical ground rule, we can consider that the wave height suddenly increases prior to breaking by a factor of 1.4 above the value given by conservation of energy flux.

III-2.4 Beating Phenomena Due to Reflection

While reflections can generally be neglected in waves advancing from deep to shallow water over the continental slope, upon reaching the shoreline, a dispersive wave train is, to some extent, reflected seaward; the leading portions arriving back at any intermediate relevant point before later portions have yet passed that point on the way to the beach. That is, the observed offshore surface motion consists of a quasi-standing wave system, composed partly of incident waves and partly of reflected waves, the exact motion depending on their relative heights and phases. Hence, we see a beating effect at various offshore points. It is to be noted that the envelope of the run-up history does not evidence such beating, since there is always an antinode at the shore.

The beating phenomena associated with reflection of dispersive wave trains has been theoretically investigated (Le Méhauté, Hwang et al, 1967) for the case of total reflection, corresponding to non-breaking waves. The wave pattern was calculated at various distances from the shore, and it was found that the irregularities due to superposition of the reflected wave increases as the distance from the shore increases. Figure III-5 is an example of a computed time history for an offshore point, and shows a beat superimposed on the normally smooth modulation envelope.

This result is confirmed by the experimental observations of Van Dorn (1966). Figure III-6 shows dispersive waves (records made at four positions)

in a tank with a sloping beach. Results are shown for several water depths along the slope, and it can be seen that the beats are most prominent at some distance from shore, tending to lessen in very small (near-shore) depths. The asymmetry of the shallowest record is due to wave breaking.

If the waves are breaking, this beating phenomenon will be attenuated, but there will still remain some residual discrepancy between the unreflected theoretical model for the incoming wave and the measured one, since beaches never totally absorb wave energy.

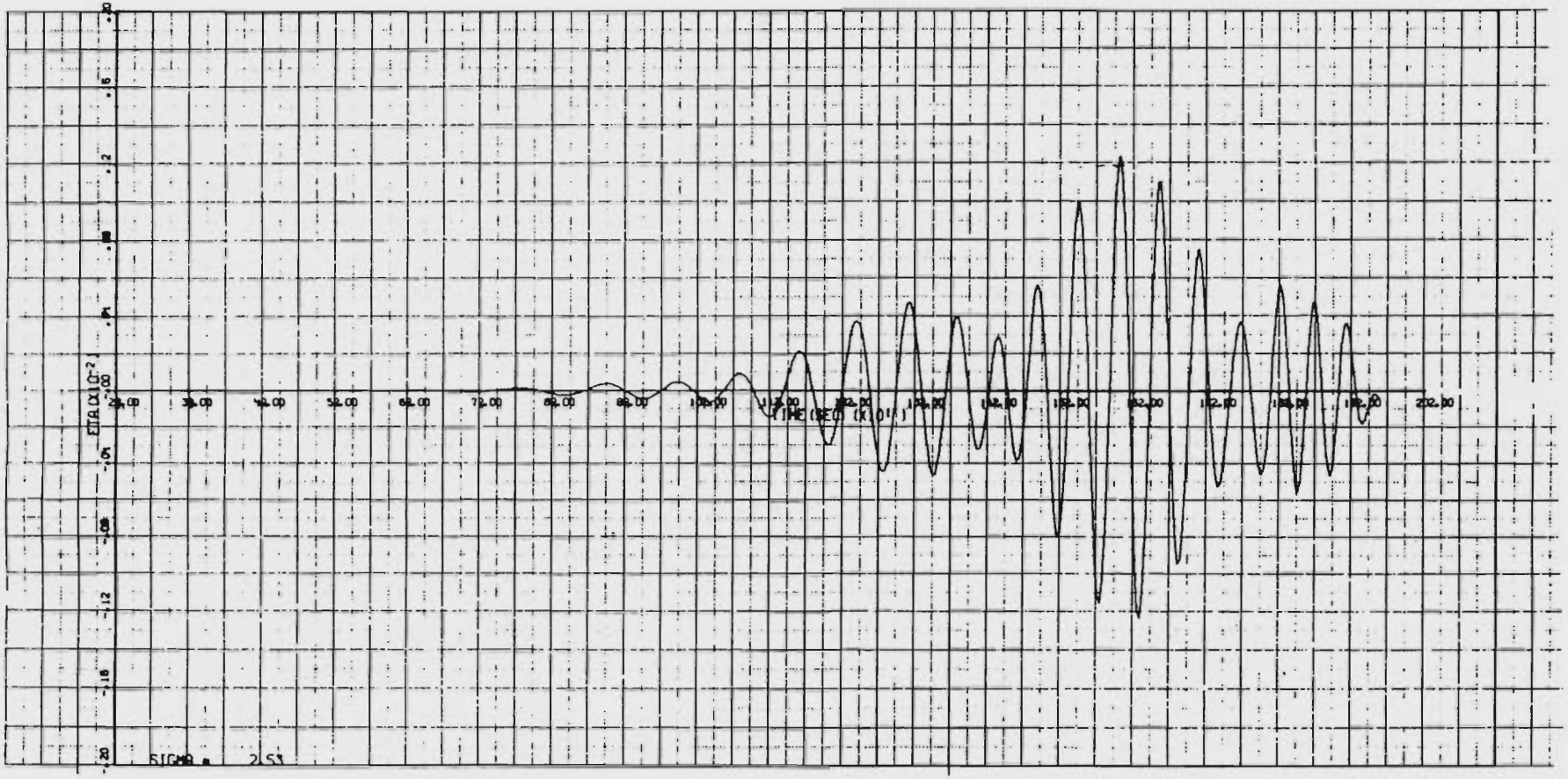

Figure III-5 Computed Example of Beating Phenomena Associated with Total Reflection of a Dispersive Wave Train from a Uniform Slope (from Le Méhauté and Hwang, 1967)

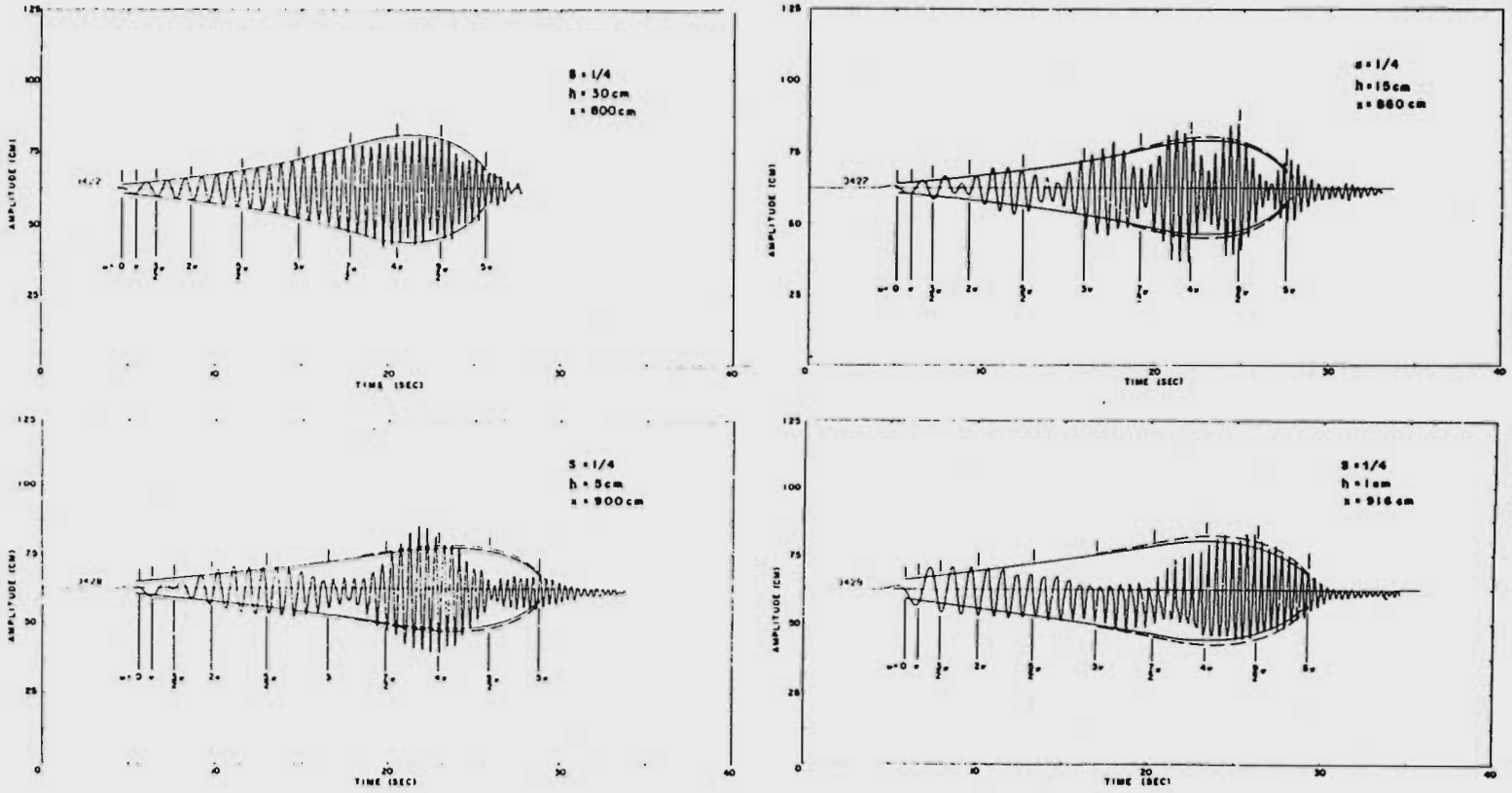

Figure III-6 Experimentally Observed Dispersive Wave Envelopes Measured over a Uniform Slope at Four Different Locations on a Slope S = 1/4 (Van Dorn, 1966)

III-3 PRACTICAL METHOD OF CALCULATION OF DISPERSIVE WAVES WITH NON-UNIFORM DEPTH

III-3.1 Wave Transformation - Basic Principles

With non-uniform depth, wave generation can still be computed by the methods of Chapter II, and the local wave amplitude determined by the conservation of energy flux, but the procedure is more complex. Whereas in uniform depth both frequencies and phase points propagate in coincident straight lines, when the depth is variable not only do frequencies and (constant) phase points propagate at different - and varying - speeds, but, in general, by different paths; moreover, these paths are no longer straight lines, but are curves that must be separately determined prior to the amplitude computation. These curves have, somewhat loosely, been given the name rays, and no confusion results from this terminology in the case of monochromatic wave systems, wherein a moving phase point (say, a wavecrest) is always associated with a constant frequency. In a dispersive system, however, the distinction must be made between the propagation paths for frequency elements and phase points. The word ray will be defined here as the curve generated in a space-time coordinate system by an energy packet propagating at group velocity, while orthogonal refers to the analogous path for a phase point moving at phase velocity. Both the rays and orthogonals have in common that the travel time for frequencies and phase points, respectively, is a minimum between any two points on these curves; this statement is, in fact, a definition of a ray in geometric optics. .

In order to determine the spectral energy at a remote point in water of variable depth, then, one must first determine the rays connecting the source and the point of observation for a given frequency, and then integrate the equation (Eq. II-1) for this frequency along the ray to find its arrival time. Since, in a continuum, energy is considered to be conserved within a wavepatch bounded by adjacent rays and adjacent frequencies, the above process is then repeated with small changes in the ray direction and frequency in order to determine the energy intensity at

the observation point. This procedure must be repeated for enough frequencies to define the energy spectrum of the disturbance as a function of frequency and time.

In an entirely similar fashion the phase of the disturbance can also be determined as a function of time by computing the required orthogonals, and then integrating (Eq. II - 5) along them to determine the arrival times of the consecutive phase points. Although, in principle, the computations must again be repeated for each of the elements comprising the source, for remote observation points the travel paths will be sufficiently similar that this latter complication can usually be avoided.

It is apparent from the foregoing that the task of computing the wave history at even a single observation point is apt to be very complicated and laborious. Although the differential equations for the rays (II-7) can be written down in the most general form, they cannot be solved explicitly for arbitrary topography. No similar equations exist for finding the orthogonals. In general, the rays and orthogonals must be found by graphical constructions on a trial-and-error basis or computed by iterative numerical techniques for each frequency concerned.

Fortunately, however, as in the theory of generation, simplifying assumptions make possible quantitatively satisfactory calculations of wave characteristics in regions where they can be justified. These assumptions, in order of consideration, are:

1) That within an angular zone of interest with its apex at the explosion point all depth contours can be approximated by straight lines.
2) That the laws of geometric optics apply to the construction of wave rays and the computation of wave amplitudes. These laws essentially require that the wave amplitude be small enough so as not to affect the wave speed; that the water depth does not change by a significant fraction in a wavelength at any frequency considered; and that the local wave speed be equal to that if the local depth were uniform everywhere.

3) That the distance along a ray connecting any two points does not differ significantly from that along an orthogonal connecting the same two points; that is, that phase travel times may be computed by integrating along a ray in lieu of constructing separate orthogonals.

III-3.2 Practical Method of Calculation

III-3.2.1 Outline of Procedure

The following simplified procedure (Van Dorn, unpublished, LeMéhauté, Hwang, et al 1967) can be used to compute the wave characteristics at any place or time following an explosion, subject to the above assumptions.

1) The wave envelope spectrum obtained from Eq. (II-18) is first subdivided into a number of component frequencies ω_i, each identified by an initial amplitude $\eta_1(\omega_i)$ in water depth h_1 at the explosion site, which is taken as the origin of cartesian coordinates for further calculations with the x-direction shoreward.
2) The region shoreward of the explosion point, 0', assumed to be the area of interest, is subdivided into zones radiating from 0', and a suitable number of depth contours are approximated by drawing straight lines C_i across each zone (Fig. III-7).
3) A family of wave rays for each above frequency is then computed to further subdivide each zone. Such subsets of contours intersected by refracted rays comprise elemental regions within which energy is to be conserved for each frequency.
4) The wave amplitude at every contour is then computed from the conservations of energy flux, as well as its arrival time, wavelength, period, and other number by which the local wave phase can be identified. Test criteria are also applied to determine whether the local wave phase is stable and satisfies the assumed linearity conditions (IV-2), or whether it breaks and must therefore be treated differently.
5) Step 4 is then repeated contour by contour until some reference contour near shore is reached, after which the run-up can be computed by the methods of Chapter V.

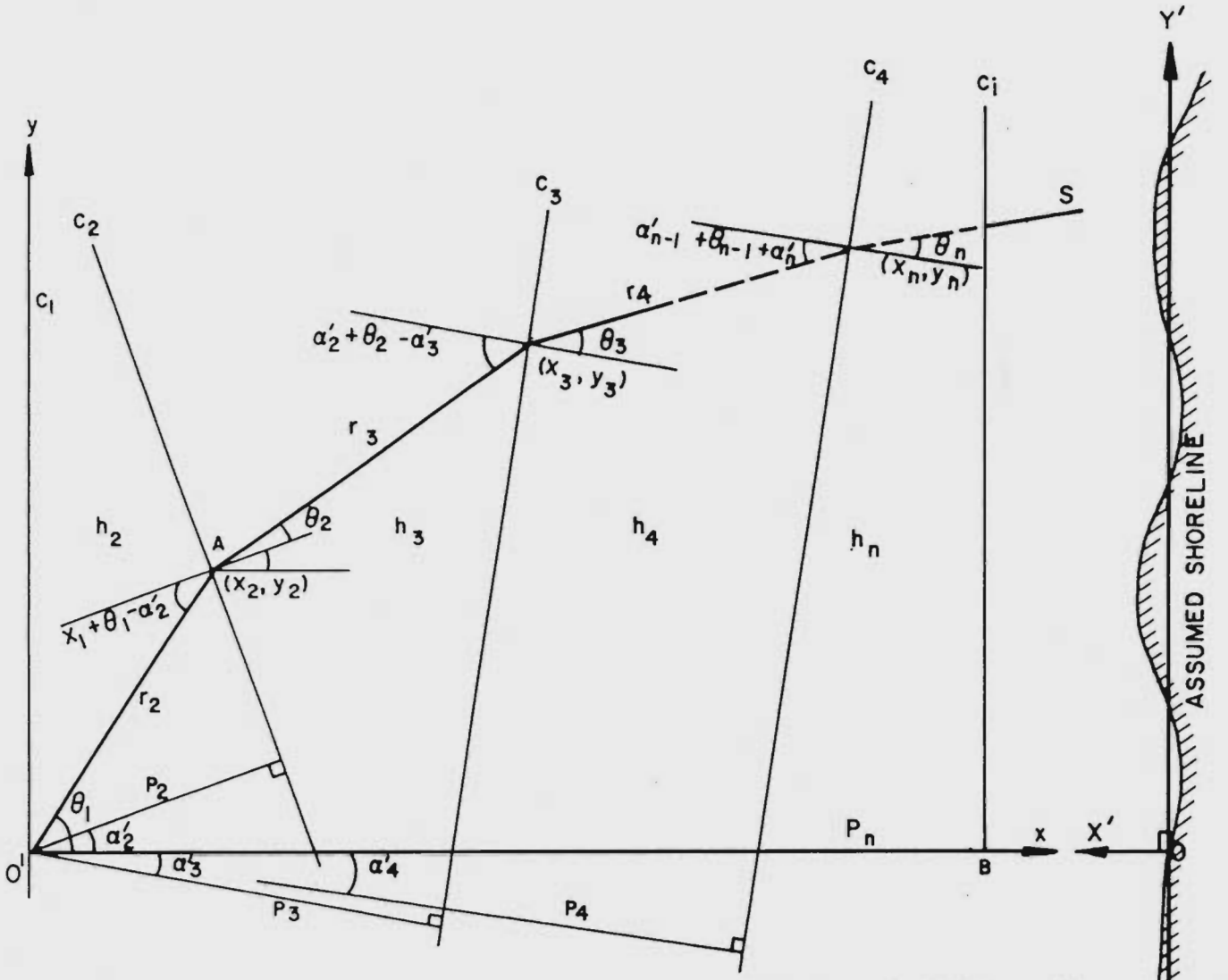

Note: Two different coordinate systems are used in the calculation with the first origin O' at the location of the explosion (x O' y) and the second, O, at the assumed shoreline (X' O Y')

Figure III-7 Notation Used for Calculation of Wave Rays

6) Steps 5 and 6 are then repeated for each ray and each frequency to determine the time history of the wave field as a function of distance along shore within each zone.

In general, each such calculation differs from every other, which explains why the prediction of wave characteristics over complex topography cannot be generalized in any convenient fashion, although the gross results can be presented ultimately in relatively simple form.

III-3.2.2 Computation of the Ray System Within a Zone

As a frequency element propagates at group velocity towards shore it will be refracted according to Snell's law for geometric optics. Figure III-7 illustrates the segmental refraction of a ray originating at 0' at an angle θ_1 to the shoreline normal 0'-x. The ray is approximated by straight line segments r_i in crossing the intervals between discrete contours C_i, each of which intervals is assumed to have a uniform depth h_i, until it eventually reaches a limit contour C_s beyond which the two-dimensional theory of run-up takes over.

Adopting the nomenclature of Fig. III-7, one can calculate a ray path as follows. Let $Q(x_n, y_n)$ denote the point of intersection between the ray and the n^{th} contour. Then the nth coordinate of the point can be related to the previous coordinate by

$$x_n = \frac{p_n - \left[Y_{n-1} - x_{n-1} \tan (\alpha'_{n-1} + \theta_{n-1}) \right] \sin \alpha'_n}{\cos \alpha'_n + \sin \alpha'_n \tan (\alpha'_{n-1} + \theta_{n-1})} \qquad \text{(III-9)}$$

$$y_n = y_{n-1} + (x_n - x_{n-1}) \tan (\alpha'_{n-1} + \theta_{n-1}) \qquad \text{(III-10)}$$

and the distance between points $Q(x_{n-1}, y_{n-1})$ and $Q(x_n, y_n)$ is

$$\Delta r_n = \left[(x_n - x_{n-1})^2 + (y_n - y_{n-1})^2 \right]^{\frac{1}{2}} \qquad \text{(III-11)}$$

The relationship between θ_{n-1} and θ_n is given by

$$\theta_n = \sin^{-1} \left[\frac{v_{n+1}}{v_n} \sin (\alpha'_{n-1} + \theta_{n-1} - \alpha'_n) \right] \qquad \text{(III-12)}$$

where

$$v_{n+1}/v_n = \frac{dk_n}{dk_{n+1}} = \left[\frac{h_n - h_{n+1}}{h_{n-1} - h_n}\right]\left[\frac{\sigma_{n-1} - \sigma_n}{\sigma_n - \sigma_{n+1}}\right] \qquad \text{(III-13)}$$

is the group velocity ratio across the corresponding contour.* The time required for propagation across Δr_n is

$$\Delta t_n = \frac{\Delta r_n}{v_n} = \frac{2\Delta r_n}{\left(\frac{gh_n \tanh \sigma_n}{\sigma_n}\right)^{\frac{1}{2}}\left(\frac{1 + 2\sigma_n}{\sinh 2\sigma_n}\right)} \qquad \text{(III-14)}$$

and the total propagation time from surface zero to point (x_n, y_n) is equal to the sum of the propagation times across Δr_n; that is

$$t = \sum_{j=1}^{n} \Delta t_j \qquad \text{(III-15)}$$

III-3.2.3 Wave Amplitude Change Along a Ray

The changes in wave (spectral) amplitude associated with propagation of a wave packet of constant frequency in water of variable depth has been given for the special case where the direction of propagation is normal to the bottom contours (Van Dorn, and Montgomery, 1963). In such cases the conservation of energy flux is given by:

$$\frac{E(\omega)}{\pi \rho g} = \eta_1^2 \left[k_o \int_{r_o}^{r_1} \frac{dr}{k}\right] \cdot \left[v_1 \int_{r_o}^{r_1} \frac{\partial}{\partial k}\left(\frac{-1}{2v^2}\right) dr\right] = \text{constant} \qquad \text{(III-16)}$$

Where $E(\omega)$ is energy per unit frequency, and r is distance measured from the origin along a ray. The first factor in brackets gives the effect of ray separation (geometric spreading) and the second factor the effect of dispersion (frequency separation).

---

* The group velocity is used here instead of phase velocity because an energy packet of constant frequency is being refracted instead of a point of constant phase.

In the coordinate system of Fig, III-7, the amplitude change in going from the origin r to the point $r = r_i$ can be written as

$$\eta = \eta_1 \frac{r_i}{\Delta r} \left[\frac{v_1 \beta_1}{v_i k \sum_1^n (1/k_i) \cdot \sum_1^n \beta_i} \right]^{\frac{1}{2}} \tag{III-17}$$

where Δr is the interval between two contours, $\beta_i [k(h)] = \partial (1/2\, v_i^2)/\partial k_i$

$$= [8/(g \tanh k_i h_i)] \left[\frac{1/4 - k_i h_i / \sinh 2k_i h_i - k_i^2 h_i^2 (1 - 2 \cosh 2k_i h_i)/\sinh^2 2k_i h_i}{(1 + 2k_i h_i / \sinh 2k_i h_i)^3} \right] \tag{III-18}$$

and, again, $k_i(h_i)$ is obtained from

$$\omega^2 = g\, k_i \tanh k_i h_i$$

When the rays are not normal to the contours, the effect of refraction can be included by multiplying (III-17) by the ray-spacing factor

$$\left[\frac{\cos \theta_1}{\cos \theta_i} \right]^{\frac{1}{2}} \tag{III-19}$$

appropriate to each successive contour.

Recalling, now, Eq. (II-18) for the wave amplitude $\eta(\omega)$ in water of uniform depth h, the corrected spectral amplitude η after crossing the i^{th} contour and traveling a total distance $r_i = \sum_1^i \Delta r$ along the j^{th} ray will be, upon substitution for ω and t their equivalent stationary phase formulae

$$\eta_i(\omega_i) = \frac{b\, r_o}{\Delta r} \left[\frac{-v_1/k_1}{dv_1/dk_1} \right]^{\frac{1}{2}} J_3 (r_o k_1) \cdot \left[\frac{\cos \theta_i}{\cos \theta_1} \cdot \frac{\beta_1 (v_1/v_i)^{\frac{1}{2}}}{k_1 \sum_1^i (1/k_m) \cdot \sum_1^i \beta_m} \right]^{\frac{1}{2}} \tag{III-20}$$

and its time of arrival $t_i = \sum_1^i \Delta_i / v_i$. The wave order number corresponding to the frequency ω_j will be the integer nearest to

$$N_i(\omega_j) \equiv \Sigma \Delta r_i k_i \cdot \left[\frac{1+2k_i h_i}{1-2k_i h_i} \right]^{\frac{1}{2}} \qquad \text{(III-21)}$$

A schematic drawing used for such a calculation is shown in Fig. III-8, where 7 frequencies are shown initially propagating at an angle θ with shoreline normal 0'-0. Each frequency follows an independent path. Since each has its own initial amplitude, it will have a unique amplitude-distance history (shown above schematically for the highest waves) and break at a different point. In this example, the contours are assumed to be parallel to shore. A more realistic case would show more irregular rays and more variation between them.

The actual breaking point and subsequent history of each wave in very shallow water can then be treated by methods discussed in the following chapters.

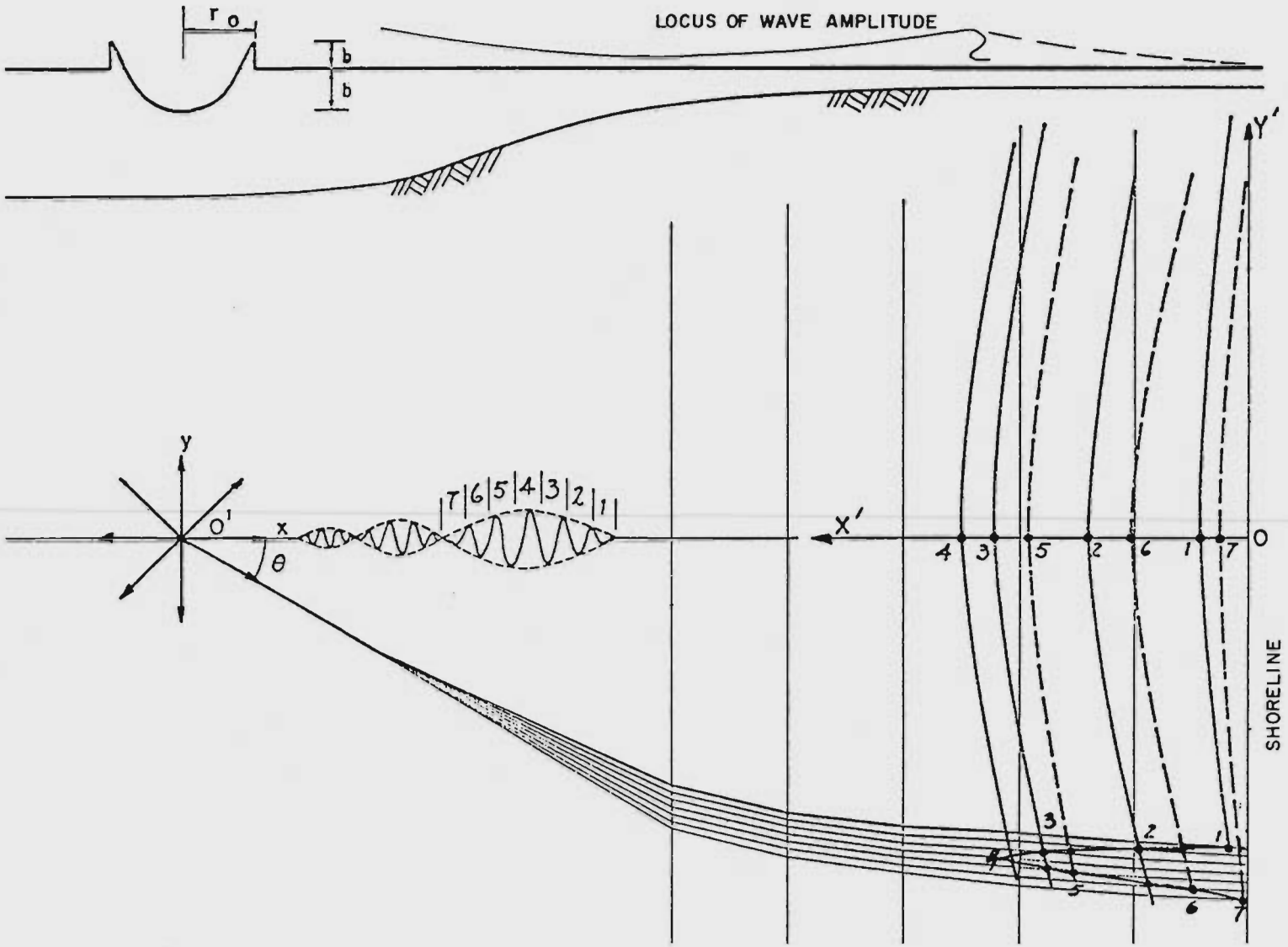

Figure III-8

Schematic Illustration of Procedures

CHAPTER IV

SHALLOW WATER WAVES

IV-1 INTRODUCTION

Waves in shallow water are important to the purposes of this handbook for several reasons. Firstly, the wave height generated in deep water usually amplifies as the wave propagates toward shallow water. It has been shown (Le Méhauté, et al., 1967) that the wave-making potential of very large explosions is sufficient to produce abnormal breaking in relatively deep water on the continental shelves, thus posing operational problems for ships and submarines. Secondly, the abnormal waves are potentially capable of producing semi-permanent local changes in undersea sedimentary deposits through the processes of erosion and wave-induced littoral transport. Any such changes are undesirable from the standpoint of navigation and possible damage to cables or other undersea installations. Lastly, the understanding of wave propagation in shallow water and its breaking is of primary importance in the prediction of wave run-up on the shore. Thus an understanding of the wave behavior in shallow water, such as velocity field, breaking, breaking wave propagation and its effects, is of great importance.

IV-2 THE ESSENTIAL CHARACTERISTICS OF WAVE THEORIES

Ship and submarine motions are dependent upon the velocity and acceleration fields of the wave environment. If one wants to investigate the motion of a ship, it is, therefore, important to find out which theory can best represent the wave motion. Before an appraisal of the validity of different wave theories, let us give a brief discussion of the essential characteristics of wave theories which are commonly used in practice.

1. The linear theory of Airy in Eulerian coordinates gives the essential characteristics of the wave pattern in a simple formulation: the free surface is sinusoidal, particle paths are elliptic and follow a closed orbit (zero mass transport); lines of equipressure are also sinusoidal. The terms in $\left(\frac{H}{L}\right)^2$ are neglected. (See Stoker, 1965.)

2. The linear theory of Airy in Lagrangian coordinates gives also elliptic particle paths, but the free surface and lines of equipressure are now trochoidal, as in the wave theory of Gertsner (Biesel, 1952).

3. The linear long wave theory is the same as the theory of Airy where it is assumed that $\frac{h}{L}$ is small; as a consequence, the formulae are simplified considerably. The pressure is hydrostatic and the horizontal velocity distribution is uniform. The wave velocity is simply $\sqrt{g\,h}$ (Wiegel, 1964).

4. The theory of Stokes at a second order of approximation is characterized by the sum of two sinusoidal components of period τ and $\frac{1}{2}\tau$ respectively. As a result, the wave crests become peaked and the troughs become flatter. The wave profile can even be characterized by the apparition of a hump in the middle of the wave trough. Similarly, the elliptical particle path is deformed and tends to hump under the crest and flatten under the trough. In this theory as in all the following wave theories, there is mass transport as a result of irrotationality and nonlinearity. However, phase velocity, wave length

and group velocity are the same as in the linear theories. The terms in $\left(\frac{H}{L}\right)^3$ are neglected. (See Wiegel, 1964.)

5. The theory of Stokes at a third order of approximation is characterized by the sum of three sinusoidal terms of period τ, $\frac{1}{2}\tau$, and $\frac{1}{3}\tau$ respectively. The same logical results are found. Phase and group velocity exhibit nonlinear corrections. The coefficients of $\left(\frac{H}{L}\right)$ which are functions of $\frac{h}{L}$ tend to infinity when $\frac{h}{L}$ tends to zero so that the theory cannot be used in very shallow water. The series is non-uniformly convergent. The terms in $\left(\frac{H}{L}\right)^4$ are neglected. (See Skjelbreia, 1959.)

6. The theory of Stokes at a fifth order of approximation is the sum of five sinusoidal terms. The coefficients of $\left(\frac{H}{L}\right)^n$ are functions of $\frac{h}{L}$ and tend to large values for $n > 3$ even sooner than in the case of the third order theory ($n \leq 3$), i.e., for larger values of $\frac{h}{L}$. Consequently, the fifth order wave theory is less valid than the third order wave theory for small values of $\frac{h}{L}$ and cannot be used when $\frac{h}{L} < 0.1$. The terms in $\left(\frac{H}{L}\right)^6$ are neglected. (See Skjelbreia and Hendrickson, 1962.)

7. The theory of Keulegan and Patterson belongs to the cnoidal family of water wave theories. It follows the same physical approach as the theory of Korteweg and de Vries (1895). From a purely mathematical viewpoint, there are some inconsistencies as some third order terms are included while some other second order terms are neglected; however, it gives apparently good results. The horizontal velocity component varies with depth. (See Keulegan and Patterson, 1940.)

8. The cnoidal wave theory of Laitone obeys a rigorous mathematical treatment: at a first order of approximation, the vertical distribution of horizontal velocity is uniform. There is no mass transport. The terms in $\left(\frac{H}{h}\right)^2$ are neglected. (See Laitone, 1961.)

9. The theory of Laitone at a second order of approximation gives a non-uniform velocity distribution. There is mass transport. The

vertical distribution of mass transport velocity is uniform. The second order term becomes larger than the first order term as $\frac{H}{h}$ increases. ($\frac{H}{h}$ is not necessarily a small parameter as $\frac{H}{L}$ always is.) The series is non-uniformly convergent. The terms in $\left(\frac{H}{h}\right)^3$ are neglected. (see Laitone, 1961.)

10. The solitary wave theory of Boussinesq is the result of a purely empirical approach. The vertical component of velocity is initially assumed to be linearly distributed from the bottom (equal to zero) to the free surface (equal to the linearized free surface velocity $\partial\eta/\partial t$). The vertical distribution of horizontal velocity is assumed to be uniform. As a result a correction due to path curvature (vertical acceleration) is added to the hydrostatic pressure.

The equations of motion are linearized vertically but remain nonlinear horizontally, i.e., convective inertia terms where the vertical component of velocity appears are neglected, but the product $u u_x$ remains. The solution is then exact.

As in any solitary wave theory, η has always a positive value and there is mass transport equal to the volume of the wave above the S. W. L. The terms in $\left(\frac{H}{h}\right)^2$ are neglected. (See Munk, 1949.)

11. The solitary wave theory of McCowan obeys a more rigorous treatment and satisfies the kinematic free surface boundary condition exactly. It corresponds to a higher order solution of the theory of Boussinesq. The vertical distribution of horizontal velocity is non-uniform. The terms in $\left(\frac{H}{h}\right)^3$ are neglected. (See Munk, 1949.)

12. The theory of Goda is actually an empirical modification of Airy theory and considers only the horizontal particle velocity. (See Goda, 1964.)

IV-3 THEORETICAL DETERMINATION OF VALIDITY OF WAVE THEORIES

While a universal theory which will be valid for all values of h/L, H/L and H/h does not exist, it is to be expected that some may present a better fit than others within certain ranges of these parameters.

The limit of validity of the linear wave theory depends, of course, on the relative importance of the nonlinear terms. Since the second order term of the theory of Stokes is a nonlinear correction to the first order term obtained by linear approximation, one can have a realistic appraisal of its importance by assessing the value of the ratio of these terms quantitatively.

The potential function for a Stokes wave or irrotational periodic gravity wave traveling over a constant finite depth at a second order of approximation is found to be (Wiegel, 1964):

$$\Phi = -\frac{H}{2}\frac{\omega}{k}\frac{\cosh k(z+h)}{\sinh kh}\cos(kx - \omega t)$$

$$+\frac{3}{8}\left(\frac{H}{2}\right)^2 \omega \frac{\cosh 2k(z+h)}{\sinh^4 kh}\cos 2(kz - \omega t)$$

The series being convergent, and since the term in H is the solution obtained by taking into account the local inertia only, while the term in H^2 is the first correction due to convective inertia, i.e., the most significant one, the relative importance of the convective inertia term can be described by the ratio of the amplitude of these two terms. In particular, in very shallow water, since $\cosh kh \to 1$ and $\sinh kh \to kh$, it is seen after some simple calculations that the ratio of the amplitude of the second order term to the amplitude of the first order term is

$$\frac{3}{16}\frac{1}{(2\pi)^2} \cdot \frac{H}{L}\left(\frac{L}{h}\right)^3$$

When $U_R = \frac{H}{L}\left(\frac{L}{h}\right)^3$ is very small, the small amplitude wave theory is

valid. The group denoted by U_R is known as the Ursell parameter.

If, instead of H, one uses the maximum elevation η_o above the still water level (η_o is equal to H/2 in the linear theory), the so-called Ursell parameter initially introduced by Korteweg and de Vries is obtained (Korteweg and de Vries, 1895). When $\frac{H}{L}\left(\frac{L}{h}\right)^3 \ll 1$, the linear small amplitude wave theory applies. In principle more and more terms of the power series would be required in order to keep the same relative accuracy as the Ursell parameter increases.

Also, in the case of very long waves in shallow water such as flood waves, bore, nearshore tsunami waves, and, in the present case, explosion waves, the value of the Ursell parameter which is supposed to be $\gg 1$ depends upon the interpretation given to L. The relative amplitude $\frac{H}{h}$ is then a more significant parameter for interpreting the importance of the nonlinear terms. In this case the vertical component of inertia force is negligible and the only term for convective inertia is $\rho u \frac{\partial u}{\partial x}$. Then it is possible to calculate the ratio of amplitude of convective inertia to the amplitude of local inertia $\left(\rho u \frac{\partial u}{\partial x} / \rho \frac{\partial u}{\partial t}\right)$ directly. Since in very shallow water $\frac{h}{L}$ is very small and $\cosh kh \to 1$ and $\sinh kh \to kh$, one has simply (here u is the horizontal velocity):

$$u = \frac{\partial \Phi}{\partial x} = \frac{H}{2} \frac{\omega}{kh} \sinh (kx - \omega t)$$

and it is found that

$$\frac{\rho u \frac{\partial u}{\partial x}\Big|_{max}}{\rho \frac{\partial u}{\partial t}\Big|_{max}} = \frac{H}{2h}$$

which demonstrates the relative importance of the ratio $\frac{H}{h}$. Despite these difficulties of interpretation, the Ursell parameter is a useful simple guide, but is not necessarily sufficient for judging the relative importance of the nonlinear effects.

Dean (1965) has attempted to determine the limit of validity of wave theories on the basis of the best fit with exact boundary conditions. According to Dean, this method has been successful for deep water wave conditions. However, for shallower water conditions, it appears that the error must be extremely small to be a reliable indicator of wave theory validity. In a word, the experimental results presented in a later section are the best methods for determining the validity of shallow water wave theories.

The above discussion summarizes the wave theories developed for non-breaking waves. The condition that the wave breaks and its breaking location have been investigated extensively for many years. A brief discussion of this topic is given in the next section.

IV-4 BREAKING CRITERIA

As waves propagate into shallow water, depending upon the bottom profile and their previous history, they will either break or surge up the beach. Occasionally, as was observed during the 1966 Mono Lake tests, an intermediate situation will arise wherein a wave will become unstable without breaking, but instead split into a succession of smaller undulations which travel together towards shore. Wave splitting has also been observed experimentally, but is so far unexplained. Since it will always act to lessen run-up, further consideration here is unwarranted.

Despite extensive efforts, and probably because of the large range of variables and its inherently nonlinear character, no uniformly satisfactory criterion for wave breaking has evolved.

For a variable offshore slope α, Keller (1961) has shown that both the linear and nonlinear small amplitude wave theory predict breaking when

$$\frac{H}{L} \geq \sqrt{\frac{2\alpha}{\pi}}\ \frac{\alpha^2}{2\pi}\left[\frac{v_o}{v}\right]^{\frac{1}{2}} \qquad \text{(IV-1)}$$

As the depth becomes large, $H \to H_o$, $L \to L_o$, $(v_o/v) \to 1$, formula (IV-1) differs only by the factor, $\frac{1}{2}$, from the stability limit proposed by Miche (1951) for relatively steep slopes

$$\left.\frac{H_o}{L_o}\right|_{max} = \sqrt{\frac{2\alpha}{\pi}}\ \frac{\sin^2\alpha}{\pi} \qquad \text{(IV-2)}$$

Figure IV-1 compares these results with experimental data and it can be seen that the theory generally allows steeper waves than are observed experimentally for moderate slopes, but that Eq. (IV-1) gives good results for relatively small slopes.

Figure IV-2 compares the above two criteria with a time history of the (one-dimensional) shoreline oscillations from an impulsive disturbance,

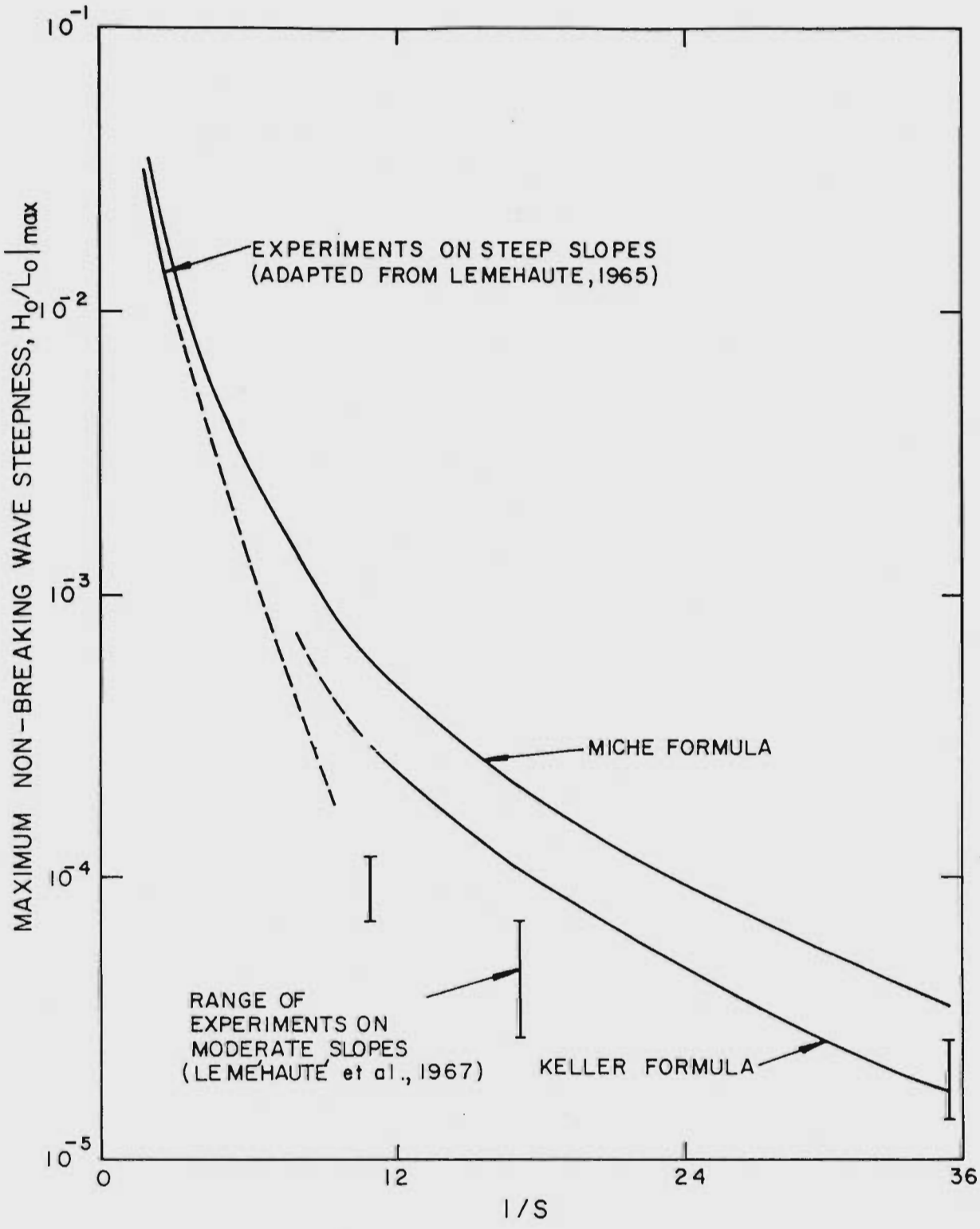

Figure IV-1 Summary of Breaking Criteria

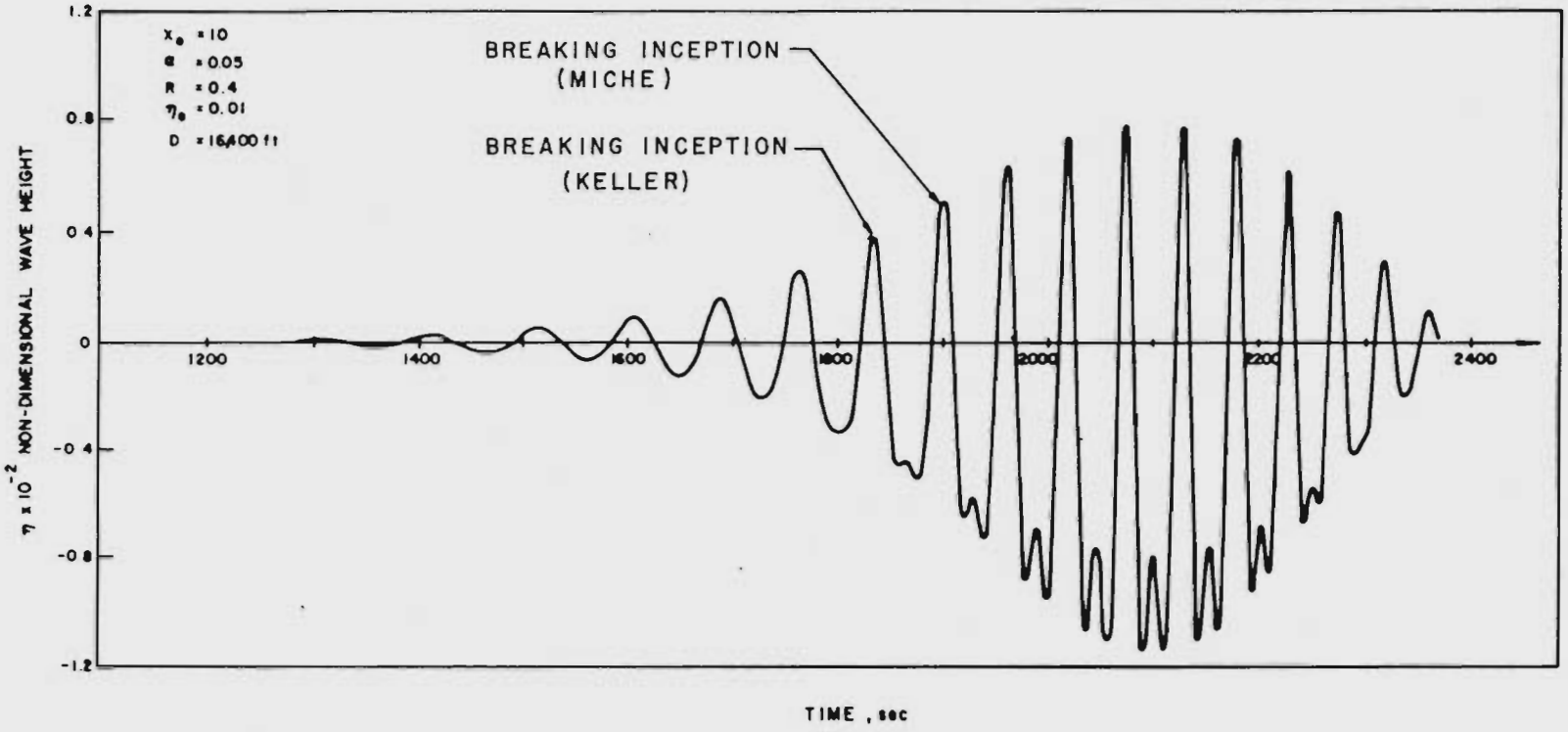

Figure IV-2 Comparison of the Breaking Criteria of Miche (1952) and Keller (1961) with LeMéhauté and Hwang's results (1967)

as computed from the theory of Carrier and Greenspan (Le Méhauté and Hwang, 1967). Perhaps significantly, instability develops in the computer solution midway between the Keller and Miche breaking criteria. This result shows the consistency of quite different theoretical models, and supports the previous assumption that theories developed for periodic waves are still valid for dispersive waves.

For a uniform bottom of depth h terminating in a uniform slope α, Keller and Keller (1964) give the stability limit

$$\frac{H}{h} \leq 2(\alpha/\Omega)^2 \left[J_o^2(2\Omega/\alpha) + J_1^2(2\Omega/\alpha) \right]^{-\frac{1}{2}} \qquad \text{(IV-3)}$$

where Ω is the dimensionless wave frequency, as defined in Chapter II.

In the same notation, Eq. (IV-3) can be compared with the empirical formula of Hunt (1959)

$$\frac{H}{h} \geq \frac{4\pi^2}{g} (\tan \alpha/\Omega)^2 \qquad \text{(IV-4)}$$

which is numerically very similar over a wide range of slopes and periods. Van Dorn (1966) has shown that Eqs. (IV-3) and (IV-4) acceptably divide breaking from non-breaking waves for a very large class of laboratory experiments with $\pi/2 > \alpha > \pi/100$.

While the above formulations provide a means of predicting, under rather special circumstances, whether or not a given periodic wave will break, they say nothing about the location of a wave at the instant of breaking. For lack of a valid breaking theory, and good experimental results, the breaking location for periodic waves is not well defined. However, numerious experimental data for solitary waves suggests that breaking occurs at $\frac{H_b}{h_b} = 0.75 + 25\,S$ for $S < 0.1$ (Street and Camfield 1966). Since the continental slopes, S, are of the order of 10^{-3}, the approximation

$\frac{H_b}{h_b} = 0.78$ is probably adequate for the calculation of the extent of the breaking region.

After breaking inception, the subsequent wave history will vary with local conditions. That is, should breaking inception occur on the continental slope or at some other location where the bottom slope is steep, one might see the so-called "plunging" breaker. In this case, vessels near the breaking inception point would experience the most violent environment. On the other hand, perhaps more likely, development may occur as a "spilling" breaker on a very gentle slope. In this case conditions would be relatively uniform within the entire breaking region. Whether violent "plunging" or more gentle "spilling" development will occur at a particular location can be determined through consideration of the local bottom slope and the deep water wave steepness. Figure IV-3 (Wiegel, 1964) illustrates three breaking classifications and indicates their dependence on slope; application requires wave-by-wave consideration at each breaking point. It appears that, in general, spilling breakers would occur in most cases, although this matter should be investigated further. Surging breakers are not to be expected in most coastal environments.

Once breakers are developed, they then enter a second phase of long duration characterized by an essentially stable pattern of propagation. That is, they progress as peaks of water separated by long flat troughs, sometimes followed by secondary undulations, dissipating their energy through breaking to maintain an essentially constant height to depth ratio. As they break, they leave behind a fraction of their momentum and volume; in this way, they are responsible for the phenomenon of wave set-up, a slight rise in the mean water level near the shore; this phenomenon will be discussed later.

In this latter regime, the processes of shoaling, energy dissipation through breaking, and bottom friction dissipation are in balance to maintain the breaker's form. It may happen that these effects and also

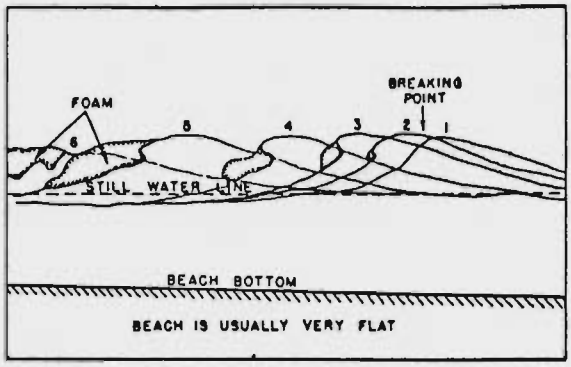

Spilling Breakers

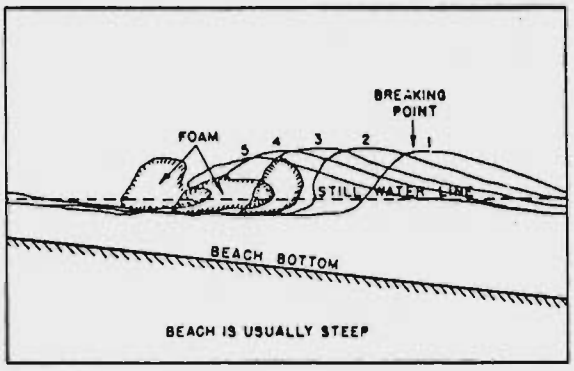

Plunging Breakers

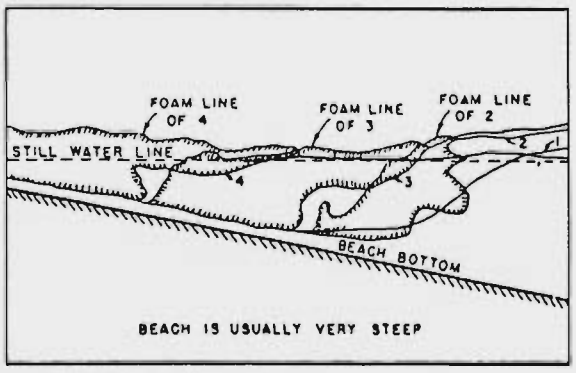

Surging Breakers

Figure IV-3
Three Types of Breakers

divergence of wave orthogonals through refraction, will cause a breaker to stop breaking, perhaps even separate into new waves, then reform and continue breaking toward the shore. Due to its relative importance, a detailed analysis of the change in breaking wave height H as the breaker proceeds toward shore is presented in the following section. It can be seen that, after a fast initial decrease in height near the breaking depth, h_b, the assumption that H/h is constant is sufficient for providing a first order of approximation of the breaker height. A more detailed investigation, where both the degree of breaking and bottom friction are incorporated into a theoretical model of the hydrodynamics of the breaker, gives a more complex variation of the breaker height.

IV-5 VELOCITY FIELD

During the phase of breaker propagation, the velocity and acceleration fields are of interest in order to establish resulting ship motions. Miller and Zeigler (1964) have performed a field experiment on measurement of the velocity field. An example of the results is shown in Fig. IV-4, illustrating the "very asymmetric" breaker, one of three classes found by Miller and Zeigler and said to correspond to a spilling breaker. It should be noted that in this study, backwash from the beach is of great importance, distorting the observed velocity field and wave profile, whereas, in the case of explosion waves on the continental shelf, backwash will not exist during most of the breaker propagation. Furthermore, the experiments have been performed on relatively steep slopes encountered on beaches in contrast to slopes of continental shelves. For these reasons, it is thought that these experimental results are not applicable to the determination of velocity field on the continental shelf.

An experimental program for measuring velocity profiles has just been completed at Tetra Tech (Le Méhauté, Divoky and Lin, 1968). Figures IV-5 through IV-8 represent a sample of this study. Figures IV-5 and IV-6 indicate a comparison of horizontal particle velocity with existing theories for non-breaking and near-breaking waves. Figure IV-6 shows the horizontal velocity under the crest for a breaking wave, while Fig. IV-7 shows a comparison of experimental results with different theories for the vertical particle velocity. The results of this study can be summarized as follows.

For non-breaking waves of the shortest period (length), Airy theory best agrees with the data. However, as the wave becomes longer, the data moves away from Airy theory which is superseded by Keulegan and Patterson (K&P) cnoidal theory, McCowan solitary theory, and the empirical form due to Goda. The Stokes waves, the first and second order cnoidal waves of Laitone (1st and 2nd cnoidal, for short), and the Boussinesq solitary wave are all less satisfactory.

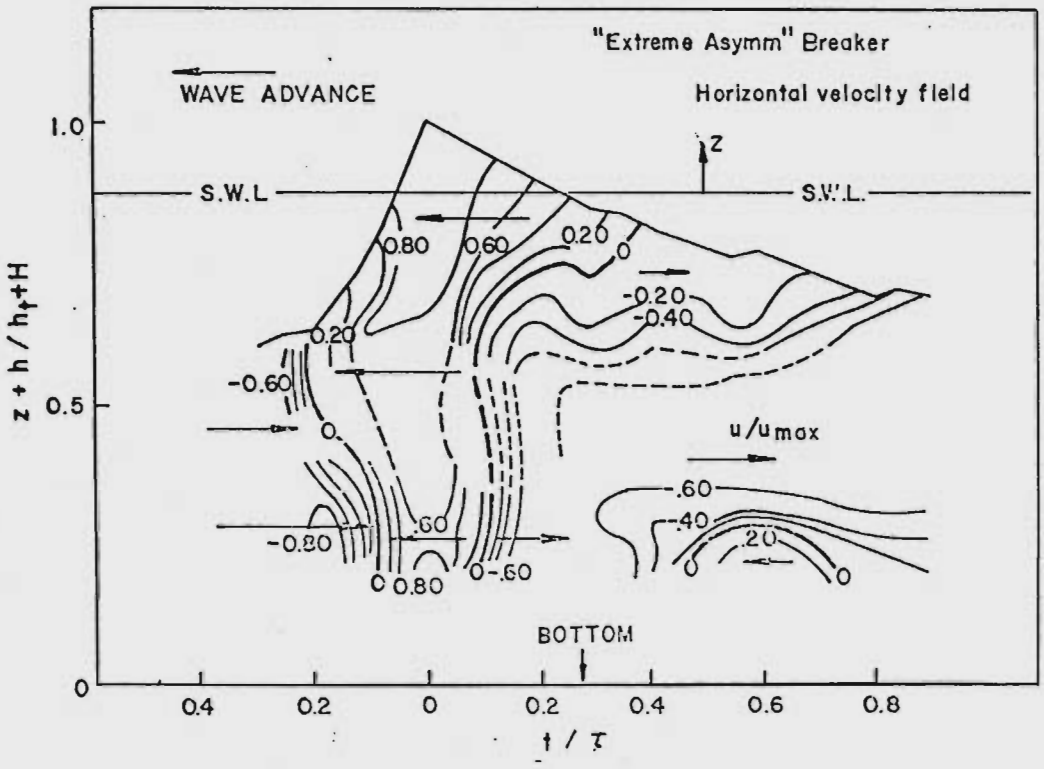

Figure IV-4 Velocity Field in a Breaker According to Observations of Miller and Zeigler (1964)

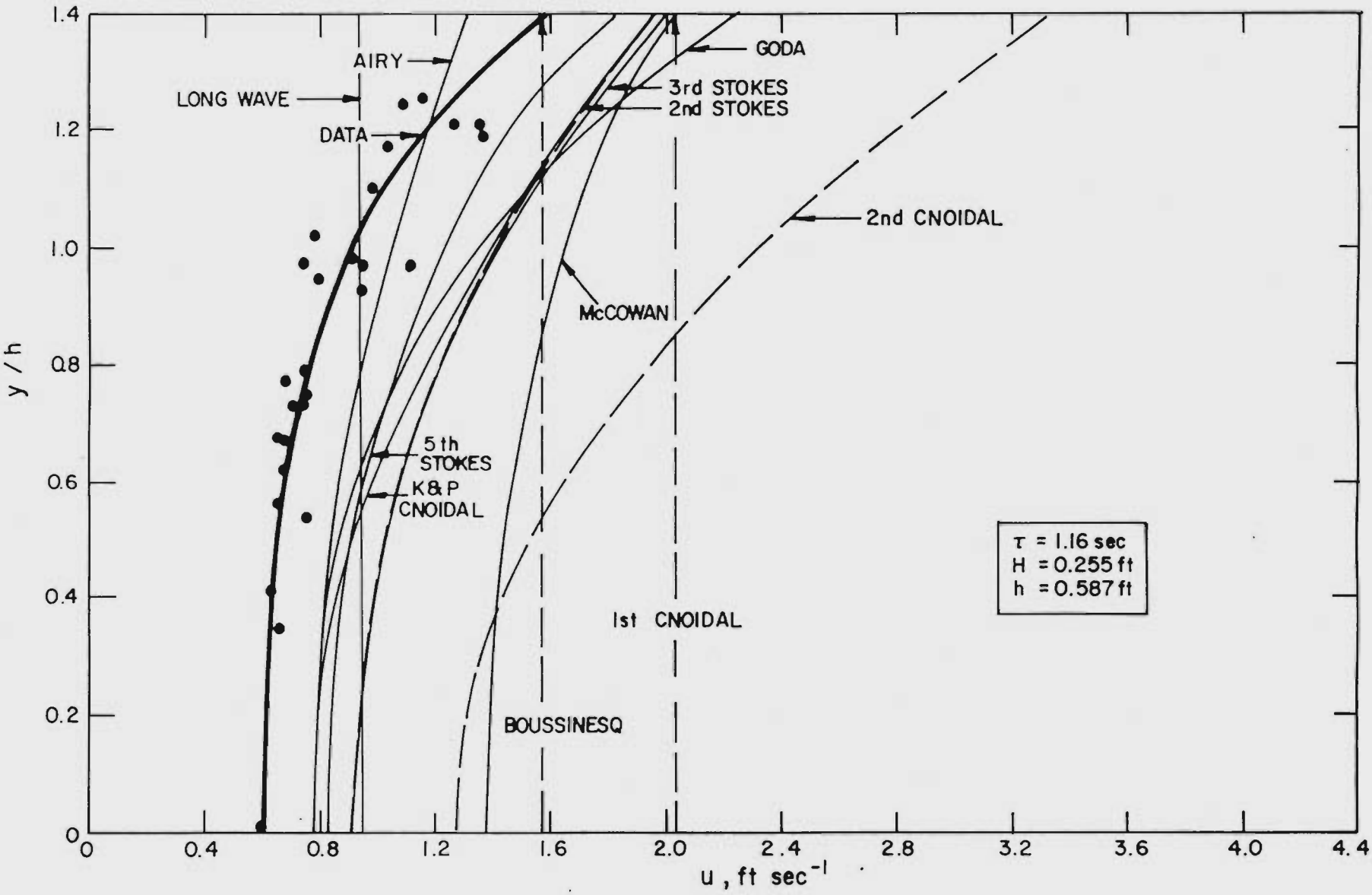

Figure IV-5 Horizontal Particle Velocity under the Crest - NON-BREAKING WAVES

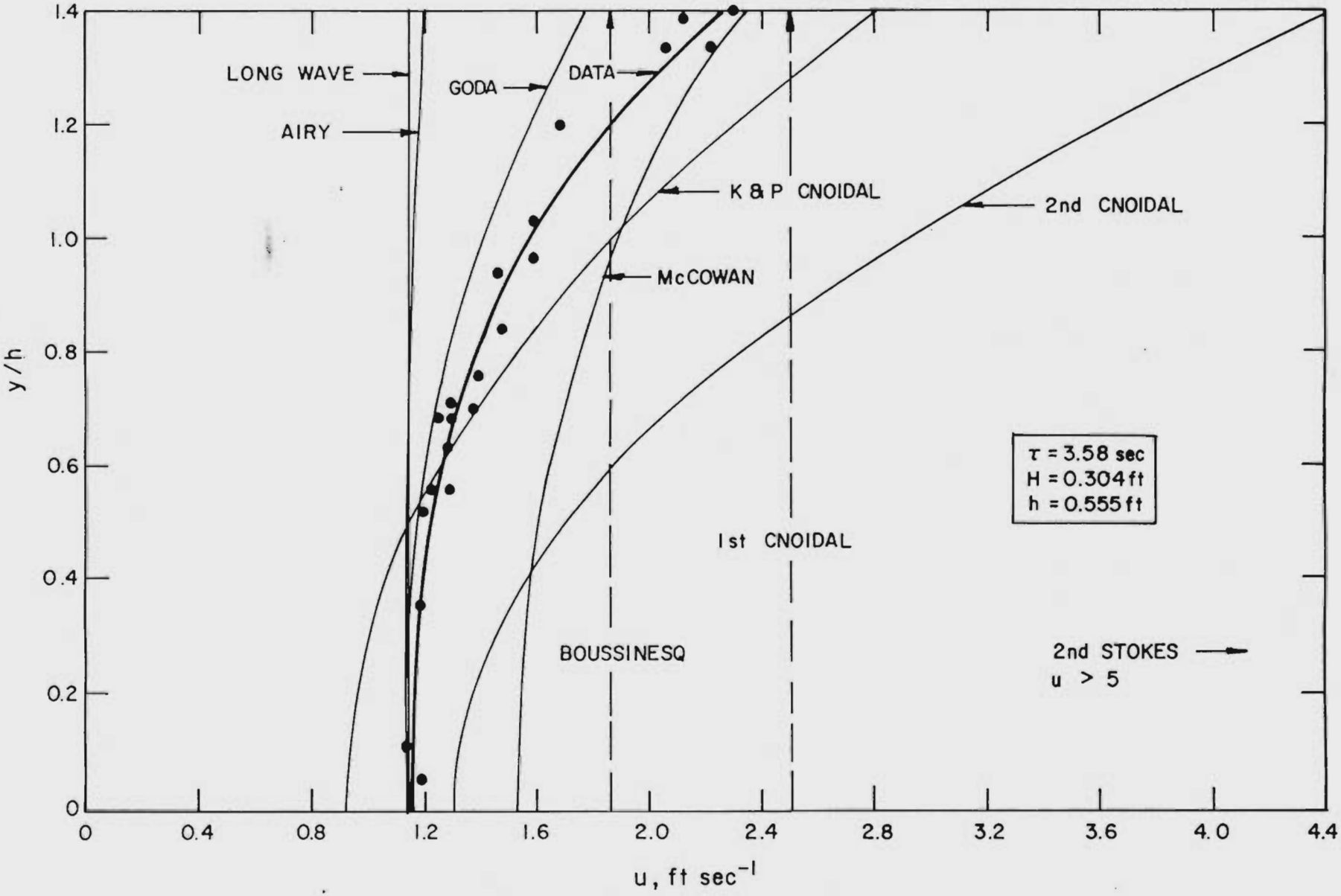

Figure IV-6 Horizontal Particle Velocity under the Crest - NEAR-BREAKING WAVES

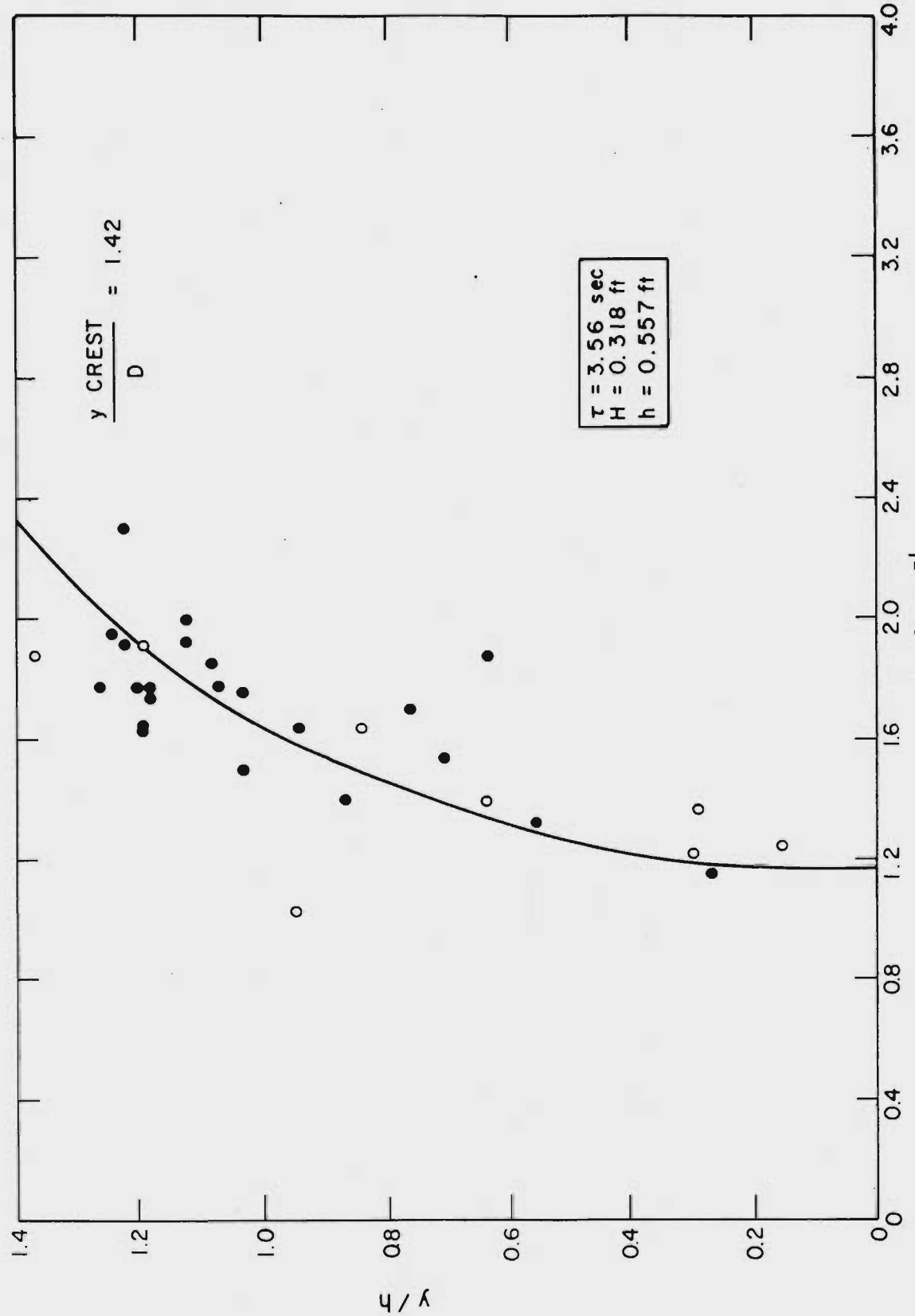

Figure IV-7 Horizontal Particle Velocity under the Crest - BREAKING WAVES

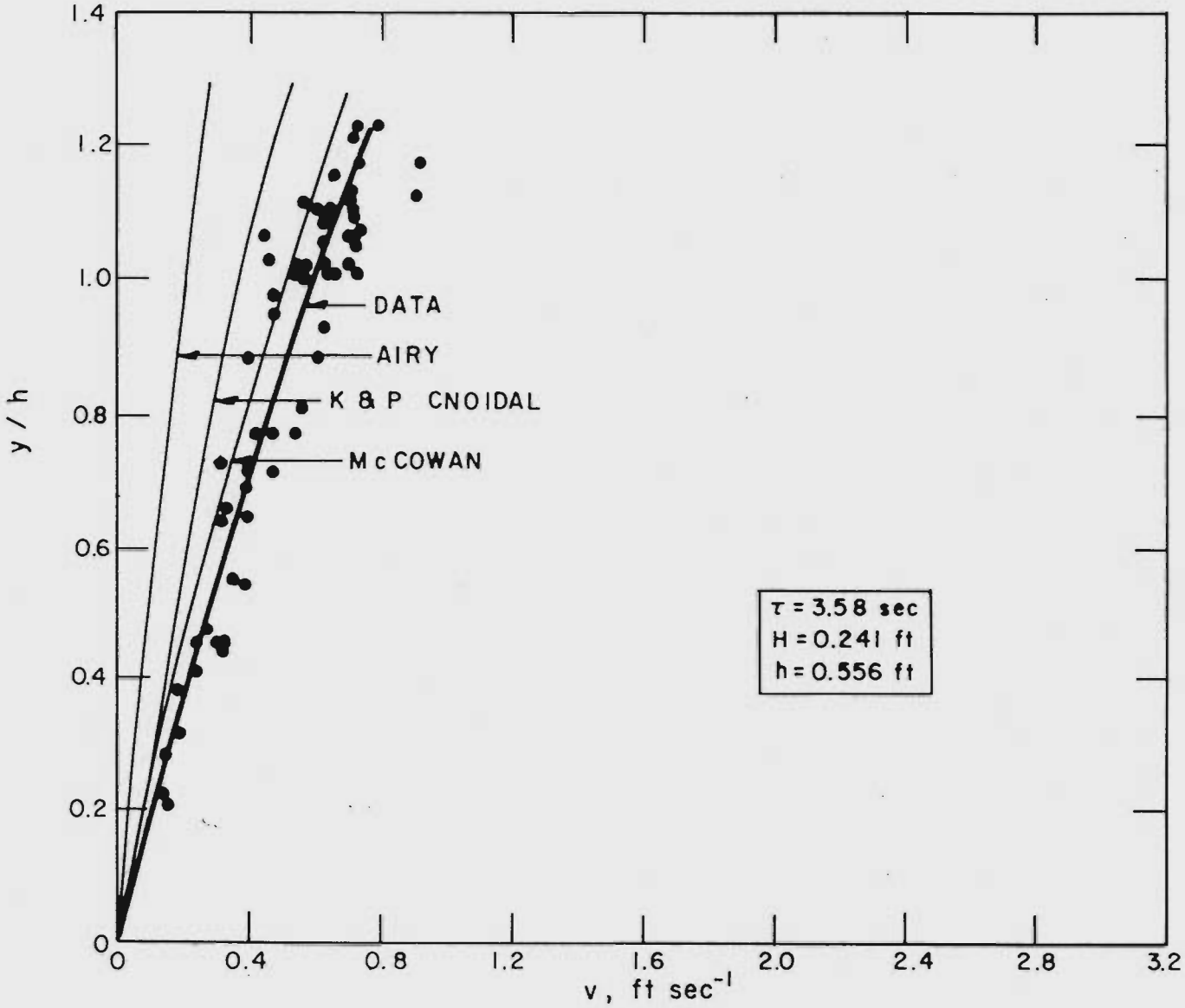

Figure IV-8 Vertical Particle Velocity where the Horizontal Velocity is Zero

For the near limit waves the situation is entirely similar, K&P cnoidal, McCowan, and Goda being best for the longer waves, while surprisingly perhaps, Airy theory is reasonably good for the shorter periods.

In specifying a theory adequate for long waves, however, the choice is immediately narrowed to three: Keulegan and Patterson cnoidal theory, McCowan solitary wave theory, and the empirical modification of Airy theory by Goda. Of these, one is inclined toward the analytical theories in the interests of generality and since Goda's results were developed for horizontal velocity component only.

As for the horizontal velocity profiles for breaking waves, it is interesting to point out that in passing from a limit non-breaking wave to the breaking wave of corresponding period and water depth, the velocity profile is sensibly unchanged. This may be seen, for example, by close comparison of Figs. IV-6 and IV-7. It can be seen that the two sets of data points overlap completely except, perhaps, in the near region of the crest where violent turbulent fluctuations occur in the breaking case.

This immediately suggests that, except in the foam region, one may apply non-breaking theories to the breaker with good results. Hence, the choice of the Keulegan and Patterson cnoidal theory is extended to gently spilling breakers. Again, the McCowan solitary wave theory may prove practical in some calculations due to its greater simplicity, and Airy theory may be adopted for pressure fluctuations. Within the foam region no theory will apply except that the mean motion may be expected to be given roughly. Of course, the turbulent fluctuations dominate so that this fact is not of great interest.

As the breakers propagate toward the shoreline, they are transformed into bores and run up the beach. In this phase, it is possible to treat them with the long wave equations by the method of characteristics (Freeman and Le Méhauté, 1964).

A detailed approach to the quasi-steady second region of breaking is

discussed in the following section where the theory of non-saturated breakers is developed, incorporating the most recent experimental results.

IV-6 BREAKERS ON CONTINENTAL SHELVES

IV-6.1 General Discussion

Considerable attention has been given to the hydrodynamics of breaking waves. The theoretical approaches which have been used fall roughly into two classes. The first is based essentially on the long wave theory, the horizontal velocity being assumed uniform along a vertical while the vertical velocity and acceleration are neglected; thus, the breaker obeys the equations of a fully developed bore. Representative papers are Ho, Meyer and Shen (1963) and Freeman and Le Méhauté (1964). Keller, Levine and Whitham (1960) present a method of calculation of the bore height as it travels toward shore based on these assumptions and the results of Whitham (1958). Such approaches from long wave theory require numerical procedures, such as the method of characteristics, which become unreliable as the involved distances (i.e., the number of computations) become large. Hence, they are more suitable for steep bottom slopes than for gentle slopes.

The second approach (presented below) is directed toward gentle slopes, and was proposed by Le Méhauté (1962) and later revised (Le Méhauté, Divoky and Lin, 1968). It is based on the principle of conservation of energy, and is called the Non-Saturated Breaker Theory.

IV-6.2 The Non-Saturated Breaker Theory

Consider a succession of waves traveling in a shallow channel of depth h, which may be constant or slope uniformly. Furthermore, the channel width δ may be constant or variable, allowing lateral concentration of wave energy, corresponding to waves propagating on the continental shelf, although particle motions are restricted essentially to the shoreward direction. It is also assumed that a theory that adequately describes a wave just before breaking will continue to describe the gross features of the wave after breaking provided that the bottom slope or side-convergence is sufficiently gentle. It is well known that, as waves arrive

in shallow water, their crests narrow and the troughs widen, with the result that successive waves can be treated as largely independent of one another. Hence, one is inclined to adopt cnoidal or solitary wave theory, especially in light of the experiments described earlier. For simplicity we choose the Boussinesq solitary wave theory although it is to be expected that a similar development in terms of cnoidal theory might better approximate actual conditions.

Assuming, after Boussinesq, the wave properties (Fig. IV-9)

$$\text{profile} \qquad \eta = H \operatorname{sech}^2 \left[\frac{\sqrt{3}}{2} \left(\frac{H}{h} \right)^{\frac{1}{2}} \frac{X}{h} \right] \tag{IV-5}$$

$$\text{phase speed} \qquad c = \left[g h \left(1 + H/h \right) \right]^{\frac{1}{2}} \tag{IV-6}$$

$$\text{energy} \qquad E = \frac{8}{3\sqrt{3}} \rho g \delta h^3 (H/h)^{3/2} \tag{IV-7}$$

where δ is the width of the wave orthogonals. The conservation of energy may be expressed as

$$\frac{dE}{dt} = c \frac{dE}{dx} = \left. \frac{dE}{dt} \right|_f + \left. \frac{dE}{dt} \right|_\nu + \left. \frac{dE}{dt} \right|_b \tag{IV-8}$$

where (see Le Méhauté, Divoky and Lin, 1968, for detailed discussion)

$$\left. \frac{dE}{dt} \right|_f = - \frac{4}{5} \frac{f c^3 H}{g h^3} E = \text{turbulent dissipation} \tag{IV-9}$$

$$\left. \frac{dE}{dt} \right|_\nu = - \frac{3}{2} \Delta c E = \text{viscous bottom dissipation} \tag{IV-10}$$

$$\left. \frac{dE}{dt} \right|_b = - \frac{3\sqrt{3}}{32} \frac{cE}{H+h} \left(\frac{H}{h} \right)^{3/2} \left[\frac{(1 - \beta')^3}{(1 + \beta' H/h)} \right] = \begin{cases} \text{breaking} \\ \text{dissipation} \end{cases} \tag{IV-11}$$

where f is a friction coefficient, $\Delta(\nu, \omega)$ is an exponential coefficient for viscous damping, and β' is "saturation" coefficient that is chosen to define the extent of the breaking region. Now, differentiating the left side of Eq. (IV-8), and combining it with Eq. (IV-9) and (IV-11) to eliminate the common factor cE, one obtains

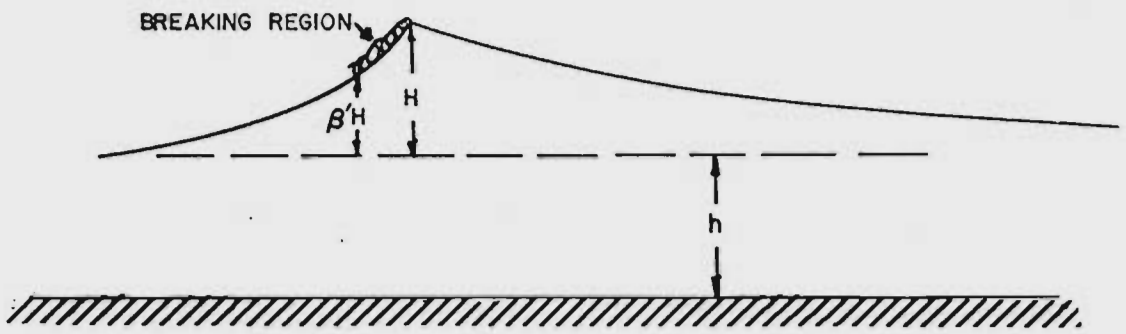

Figure IV-9 Extent of the Breaking Region

$$\frac{1}{\delta}\frac{d\delta}{dx} + \frac{3}{2}\frac{1}{h}\frac{dh}{dx} + \frac{3}{2}\frac{1}{H}\frac{dH}{dx} = -\frac{4}{5}\frac{f}{h}\frac{H}{h}\left(1+\frac{H}{h}\right) - \frac{3}{2}\Delta - \frac{3\sqrt{3}}{32}\frac{B}{(h+H)}\left(\frac{H}{h}\right)^{3/2} \qquad \text{(IV-12)}$$

where $B \equiv (1 - \beta')^3/(1 + \beta' H/h)$ (IV-13)

Clearly, when

$\beta' = 1$, $B = 0$: the wave is not breaking

$\beta' = 0$, $B = 1$: the breaker is fully developed

β' is small, $B \approx 1 - \beta'\left(3 + \frac{H}{h}\right)$

B can thus be considered as the ratio of the energy dissipated by the breaker to the maximum energy which could be dissipated by a bore of the same height. Note that a small variation in β' near zero corresponds to a larger variation in B; hence, a breaker may appear to be fully developed, or saturated, when it is not.

The problem, now, is that we have one equation, Eq. IV-12, containing two unknowns, H (or H/h), and B. It is to be expected that further study will enable us to write a second expression giving β' independently. For the present, however, we examine Eq. IV-12 in two idealized cases. Firstly, consider a very gentle bottom slope or channel convergence. In that case, H should follow the usual breaking criterion $H/h \approx 0.78$. Then, if

$$\frac{dh}{dx} = -S \quad \text{and} \quad \frac{1}{\delta}\frac{d\delta}{dx} = -P \qquad \text{(IV-14)}$$

we find

$$B \approx 48S - 18f + 16h\left(P - \frac{3}{2}\Delta\right) \qquad \text{(IV-15)}$$

For two-dimensional waves on the continental shelf ($P = 0$, $\Delta = 0$), B is zero if the slope is smaller than about $\frac{18}{48}f$, frictional dissipation being sufficient to damp the wave without breaking. On the other hand, if S is greater than $\frac{1 + 18f}{48} \approx \frac{1}{48}$ then $B \approx 1$ and the breaker is fully developed or saturated. In that case, however, the assumption that H/h is constant is not valid so that another approach is necessary.

Similarly, for waves in a converging channel of constant depth and such that $f \approx 0$, one has $B = 0$ for $P = \frac{3}{2}\Delta$. That is, the rate of convergence is too small to overcome viscous damping. When $P = \frac{1}{16h} + \frac{3}{2}\Delta \approx \frac{1}{16h}$, $B \approx 1$ so that the breaker is fully developed. Again, however, the assumption of small P and constant H/h is violated.

In the case of large slope or convergence, assume instead that B is constant while H/h is variable. Then again letting $\frac{dh}{dx} = -S$ and $\frac{1}{\delta}\frac{d\delta}{dx} = -P$ and linearizing Eq. IV-12, we get

$$\frac{dH}{dh} = H\left(\frac{\Delta}{S} - \frac{2}{3}\frac{P}{S}\right) + \frac{H}{h}\left(\frac{8f}{3S} + \frac{\sqrt{3}\,B}{16\,S} - 1\right) - \frac{\sqrt{3}\,B}{32\,S} - \frac{8f}{5S} \qquad \text{(IV-16)}$$

In case the orthogonals are parallel, P = 0, and viscous friction is neglected, the above equation can be solved to yield

$$\frac{H}{H_b} = \frac{h}{h_b}\left\{\left(\frac{h}{h_b}\right)^{-M} - \left(\frac{\sqrt{3}\,B}{16SM} - \frac{8f}{5SM}\right)\left(\frac{H_b}{h_b}\right)^{-1}\left[-1\left(\frac{h}{h_b}\right)^{-M}\right]\right\} \qquad \text{(IV-17)}$$

where $M = 2 - \frac{\sqrt{3}\,B}{16S} - \frac{8f}{3S}$.

This corresponds to a two-dimensional wave on the continental shelf. The result of this equation, for different values of slope S, is calculated and is shown in Fig. IV-10. On the other hand, one may evaluate β' by choosing a converging channel of constant depth with negligible friction (f=0) and constant wave height H. The result is

$$B = \frac{32}{\sqrt{3}}\,h\left(\frac{H}{h}\right)^{-3/2}\left(1 + \frac{H}{h}\right)\left(P - \frac{3}{2}\Delta\right) \qquad \text{(IV-18)}$$

where $B = \frac{(1-\beta')^3}{1+\beta'\frac{H}{h}}$ as has been specified in Eq. IV-13.

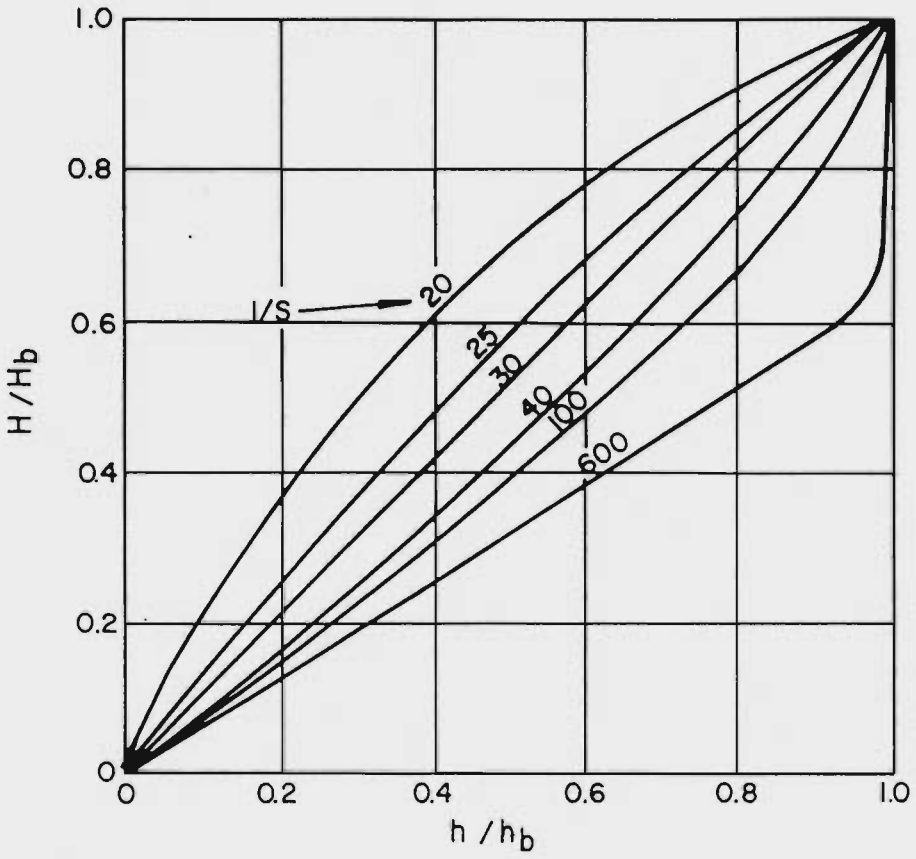

Figure IV-10 Height Variation after Breaking

IV-7 WAVE SET-UP

IV-7.1 Experimental Observations

During several of the ten 9,250 lb HE (High Explosive) run-up tests at Mono Lake in 1965, several of the shallow water records obtained within the breaker zone exhibited a remarkable, low frequency oscillation of mean water level of amplitude approaching that of the superimposed breaking waves from the explosion, an example of which is shown in Fig. IV-11. Figure IV-12 shows the set-up and the wave envelope which was superposed on the wave set-up. Since such oscillations were not apparent in wave records made outside the breaker zone, they were supposed to have originated as a result of wave breaking, and the interaction with the sloping beach (LeMéhauté, et al, 1966).

A similar effect was demonstrated in a series of wave tank experiments by Hwang et al. (1967), who found that the maximum wave set-up on the continental shelf can be as large as 0.2 times the height of the maximum wave of the train prior to breaking (Fig. IV-13). Because of its potential aggravation of run-up heights, some theoretical attempts to explain this phenomenon are given below.

IV-7.2 Wave Set-Up Due to Periodic Waves

Set-up of periodic non-breaking waves on a uniformly sloping beach has been investigated theoretically by Longuet-Higgins and Stewart (1960, 62, 63, 64), and Whitham (1962) by using a linear solution for periodic waves, and by Hwang, et al. (1967) by considering the waves as a quasi-periodic succession of solitary waves.

Experimental investigations by Londgren (1963), Bowen, Inman and Simmons (1968) and Saville (1961) generally confirm the validity of these theories: prior to breaking there is a set-down due to "radiation stress" (the tendency to expel water from regions of high waves) followed, after

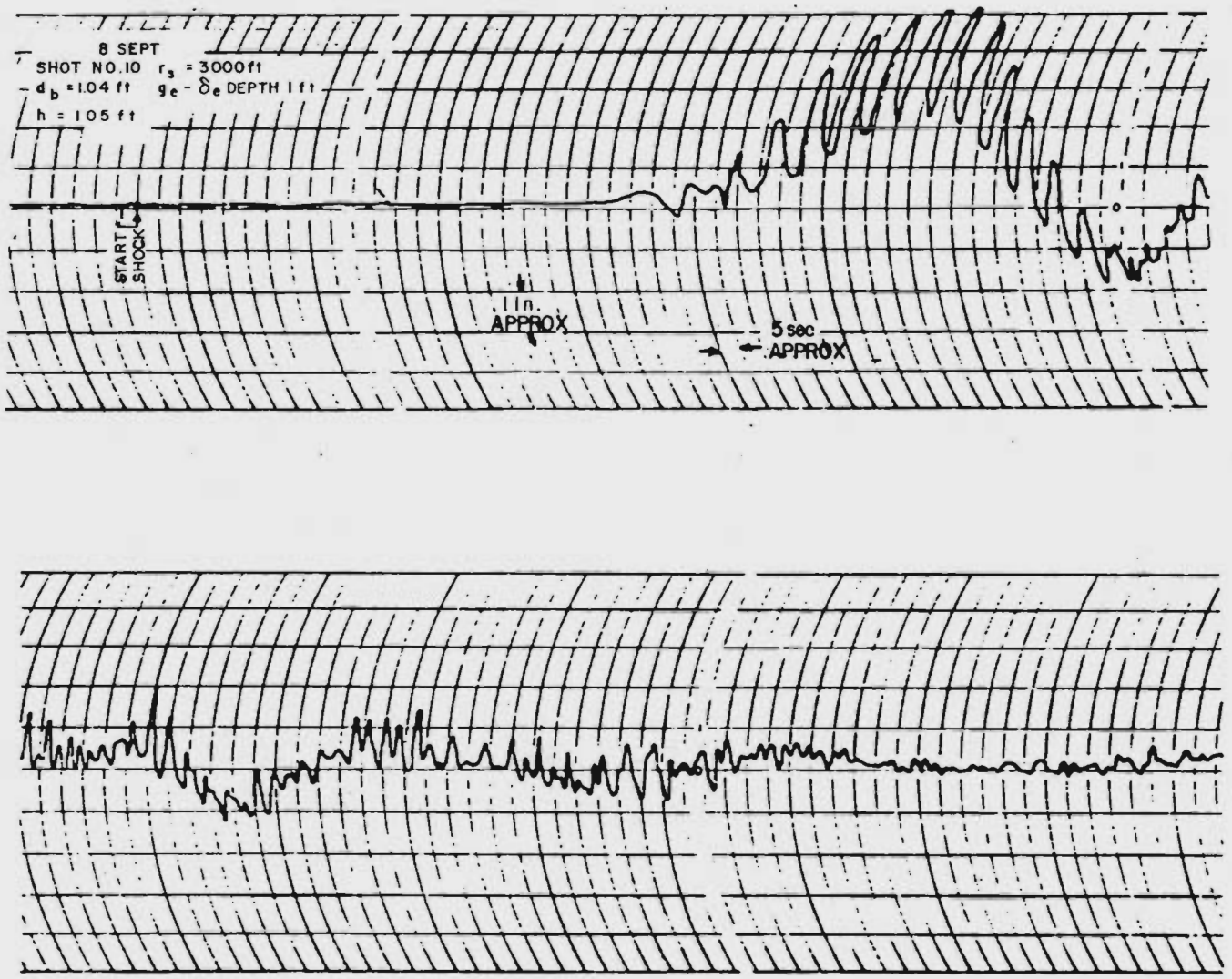

Figure IV-11 Sample record obtained by Dr. Van Dorn at Mono Lake in 1966

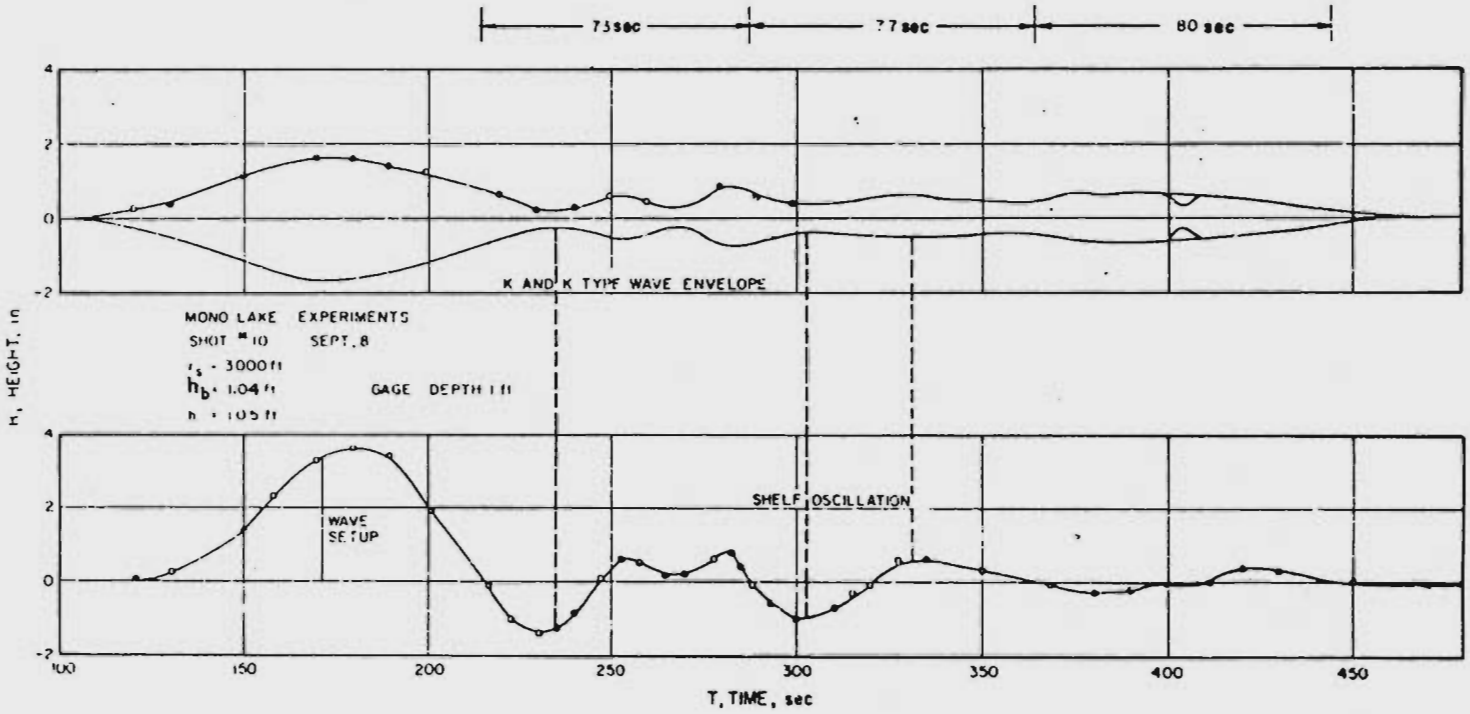

Figure IV-12 Wave set-up versus time

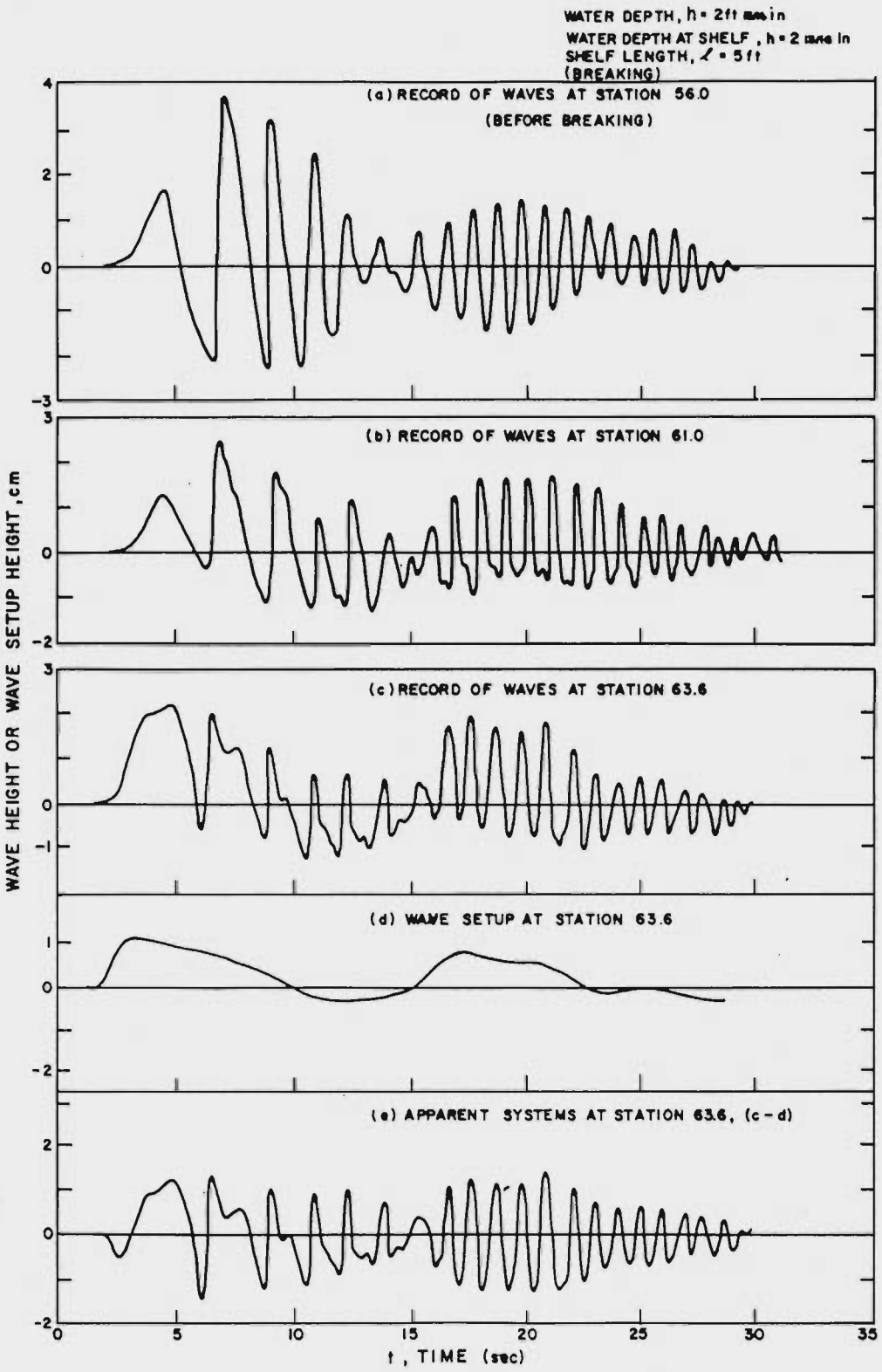

Figure IV-13 A sample of wave profiles and wave set-up. (The station number refers to the distance in feet from the wave generator; Hwang et al 1967)

breaking, by a nearly linearly increasing set-up shoreward as a result of mass transport due to breaking (see Fig. IV-14).

According to Hwang, the maximum wave set-up which can be observed on a shoreline as a result of long periodic waves is:

$$\zeta = -0.38\, h_b + 4.5\, \tau^{-1} g^{-\frac{1}{2}} h_b^{3/2} \qquad \text{(IV-16)}$$

which was approximately verified by his experiments.

IV-7.3 Wave Set-Up Due to Explosion-Generated Waves

The phenomenon of dispersive wave set-up is more complicated as a result of the unsteadiness of the momentum flux associated with individual waves in the wave train. It is a transient phenomenon which is difficult to evaluate. A numerical method of prediction has been proposed by Hwang, et al. (1967), but it is too complex to generalize here, despite a number of simplifying assumptions. Qualitatively, the mechanism can be explained as follows.

The wave set-up induced by the first wave envelope maximum induces shelf oscillation, which theoretically may be amplified or diminshed by the following maxima, depending upon their relative periods.

The shelf oscillation accompanying the first wave maximum can clearly be observed in the previous figures. It has been verified theoretically that these oscillations have periods which closely approach those of the fundamental oscillation of the shelf or its first harmonic. While resonant conditions can theoretically obtain if the wave envelope period (time interval between consecutive envelope nodal points) coincides with a low shelf harmonic, resonance was not observed in these experiments.

With respect to application to explosion waves on the continental shelf, where many low frequency modes of oscillation normally are detectable

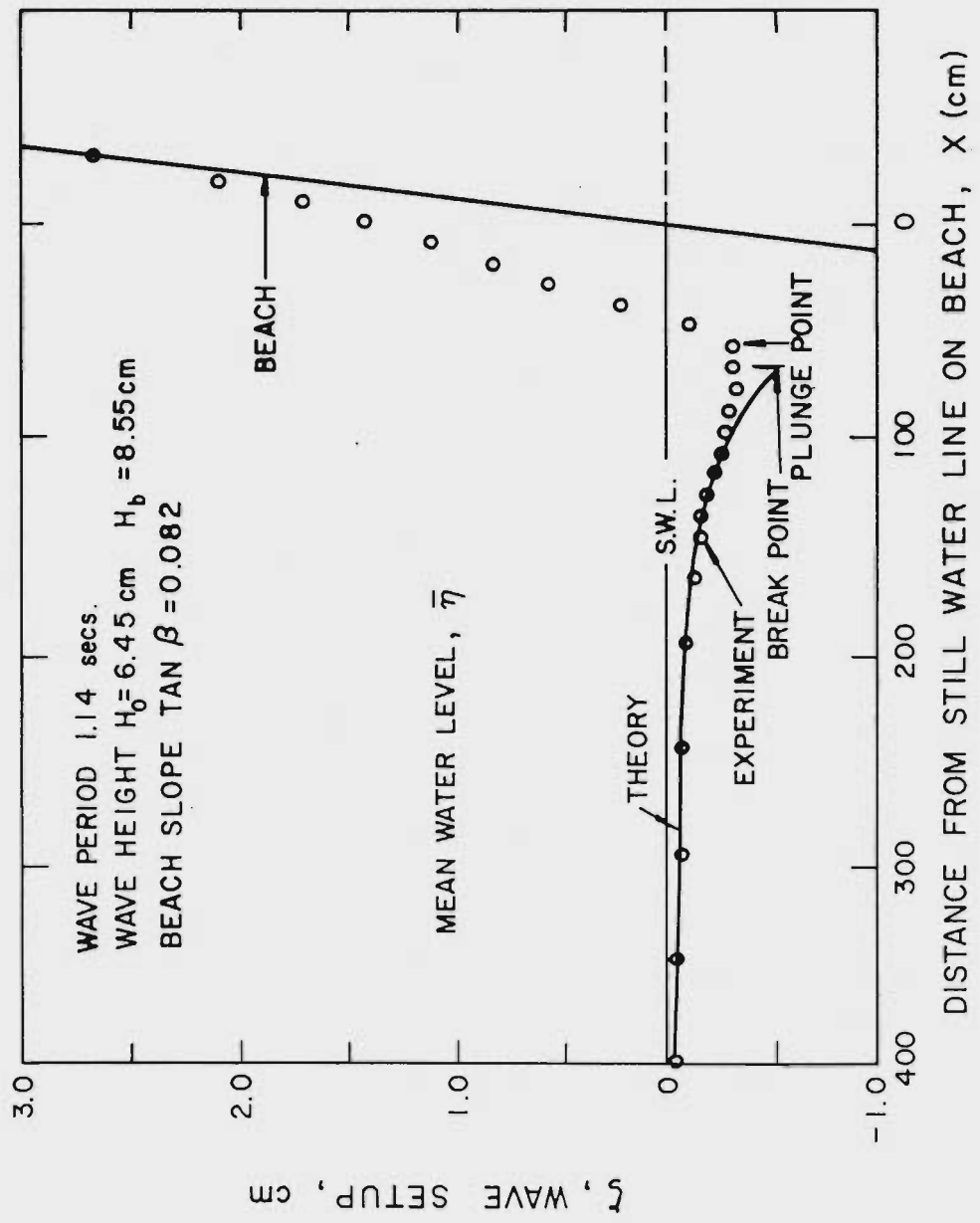

Figure IV-14 Profile of the wave set-up (The results obtained by Bowen, Inman and Simmons)

from wave spectra (Miller, etc. 1962), it is possible that such modes might be excited in a manner similar to that observed during naturally-occurring tsunamis (Van Dorn, 1965).

CHAPTER V

WAVE RUN-UP

V-1 INTRODUCTION

As the explosion-generated wave train propagates towards the shore, each wave ultimately terminates by running up the beach, possibly locally augmented or dimished by lower-frequency oscillations of the type discussed previously. The wave systems produced by large explosions in relatively deep water, aside from their potentially large amplitudes, represent a unique type of motion that does not occur in nature, and hence is outside the range of observational experience. The principal distinction here is one of frequency, the spectral maximum τ_m for significant events falling with the range 20 sec $< \tau_m <$ 100 sec, as compared with that for ordinary storm waves (5 sec $< \tau_m <$ 20 sec) and for tsunamis (100 sec $< \tau_m <$ 1 hour). For swell, the direct run-up dominates over local shelf oscillation (surf beat), while for tsunamis the reverse is true. Limited field observations during nuclear and high-explosive tests suggest that for explosion waves both factors are of importance.

Because of present uncertainties regarding the best interpretation of the run-up results from the recent Mono Lake tests (Rooke, et al., 1967 and Wallace and Baird, 1968), the following discussion of run-up is restricted to theory and experiments involving propagation in one-dimension.

There is no mathematical method available for predicting wave run-up which will be valid for all possible conditions. Many approximate theories are available, each with its own range of applicability. Theoretically, even in the case of regular waves, it is difficult to predict the run-up from the deep water wave characteristics. The theory must be equally valid in deep water and in shallow water near the shore where nonlinear effects must be taken into account. Furthermore, in most cases, the waves break before they reach the shoreline. The only well-known theory which includes breaking is the nonlinear long wave theory, where bores may be included in the computations. (However, this theory is known to predict the formation of a bore sooner than is observed experimentally.)

Finally, it must be emphasized that explosion waves are not regular but consist of dispersive waves with different periods, wave lengths, and amplitudes. However, it is felt that without a good basic physical understanding of periodic wave behavior, it is not possible to formulate a realistic approach to the problem of dispersive explosion-generated waves.

In the next section a brief discussion of run-up of periodic waves is given.

A more detailed discussion of some of the phenomena treated herein may be found in Van Dorn (1966) and Le Méhauté, et al. (1968).

V-2 A CLASSIFICATION OF PHENOMENA AND SIGNIFICANT PARAMETERS

Since a general approach for complex bottom profiles cannot be made, phenomena occurring on a simpler bottom geometry are studied and are interpreted for their application to actual complex cases. The case on a uniform slope ended by a horizontal bottom is analyzed. The run-up, $\overline{R}$, is then a function of the slope, S, (or tan α), the water depth over the horizontal bottom, h, and in the case of periodic waves, the wave period, τ (or the wave length, L) and the wave height, H. When $h \to \infty$, the only significant parameters are S, the deep water wave height, H_o, and the wave length, L.

Thus the relative run-up, $\overline{R}/H$, is given as function of dimensionless parameters, S, (or its inverse value, cot α), relative depth, h/L (or $\sigma = 2\pi h/L$), and wave steepness, H/L. The relative value, $\overline{R}/H$, can be schematically given by a surface for each value of H/L as a function of $2\pi h/L$ and cot α, as shown in Fig. V-1.

For a given H/L and h/L, the relative run-up has a tendency to increase as the slope decreases up to the point where the waves begin to break. Then the relative run-up of breaking waves decreases as the slope continues to decrease and becomes negligible as the slope tends to 1/100 as a result of dissipative processes. The relative run-up of nonbreaking waves also increases as the wave steepness increases (as a result of nonlinear effects) while the relative run-up of breaking waves decreases as the wave steepness increases (as a result of turbulent dissipation).

When the relative depth, h/L, decreases, the dependency of relative run-up upon H/L decreases. This is due to that fact that the relative importance of the wave length decreases.

The equation for wave run-up might be expressed more generally as follows:

$$\frac{\overline{R}}{H} = f\left(\alpha, \frac{2\pi h}{L}\right) + g\left(\frac{H}{L}, \frac{2\pi h}{L}\right) - K\left(\alpha, \frac{2\pi h}{L}, \frac{H}{L}\right) \qquad (V-1)$$

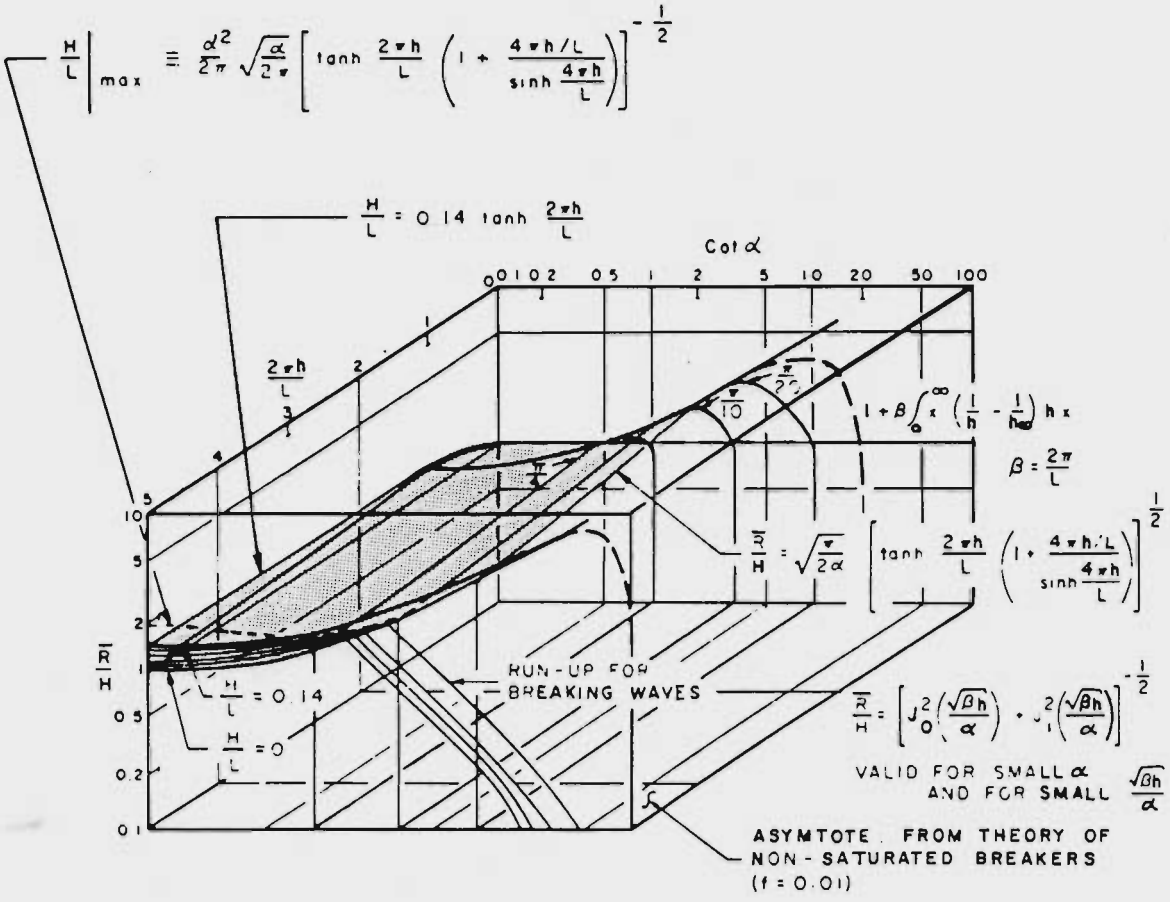

Figure V-1 Run-Up for Periodic Waves

in which the function $f(\alpha, 2\pi h/L)$ is the run-up contributed by linear approximations; i.e., when H/L tends to zero, $g(2\pi h/L, H/L)$ is the correction due to superelevation by nonlinear effects, and $K(\alpha, 2\pi h/L, H/L)$ is the reduction in relative run-up due to the loss of energy in breaking and bottom dissipation, as shown in Fig. V-2. The run-up of a wave with infinitesimal steepness is given on the surface covered with dotted points in Fig. V-1 and the run-up of waves with steepness greater than infinitesimal steepness is given on surface which lie successively above one another. Breaking will occur when these surfaces intersect the surface of breaking as denoted by the equation

$$\left.\frac{H}{L}\right|_{max} = \frac{\alpha^2}{2\pi}\sqrt{\frac{2\alpha}{\pi}}\left[\tanh\frac{2\pi h}{L}\left(1+\frac{\frac{4\pi h}{L}}{\sinh\frac{4\pi h}{L}}\right)\right]^{-\frac{1}{2}} \qquad \text{(V-2)}$$

When conditions are such that the wave breaks, the relative run-up will decrease as indicated by a few lines in the diagram. When the value $2\pi h/L$ reaches 5, the effect of water depth is practically negligible. Due to the difficulties in presenting three-dimensional graphs, details are not included in Fig. V-1. The reader should then refer to Figs. V-2 and V-3. Figures V-4 and V-5 show the experimental data summarized by the Beach Erosion Board (BEB, 1967). One finds that the results presented in Fig. V-3 are indeed a very good qualitative description.

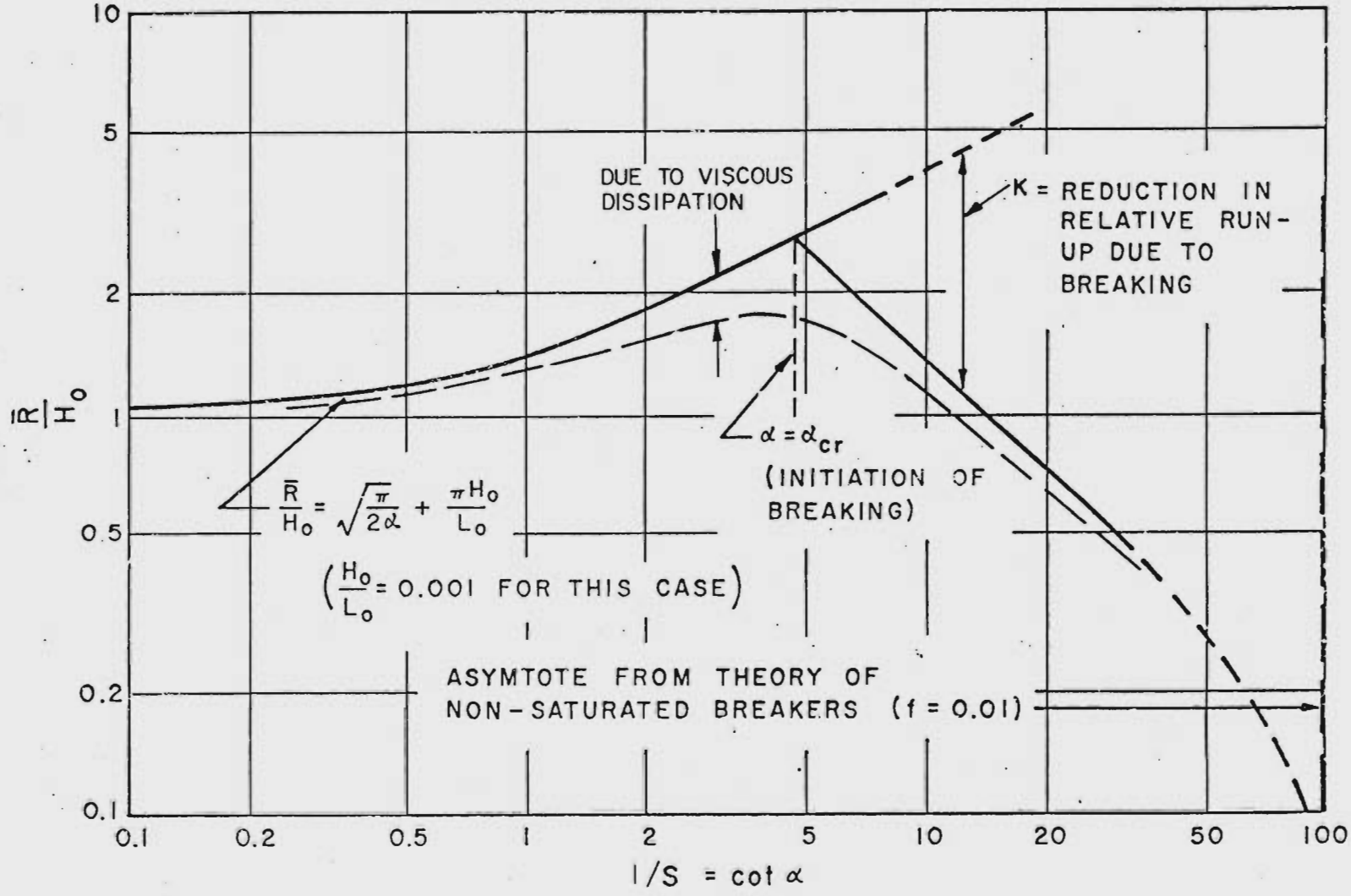

Figure V-2 Run-up on a Slope Deduced from Theory and Physical Reasoning $\left(\frac{H_o}{L_o} = 0.001\right)$

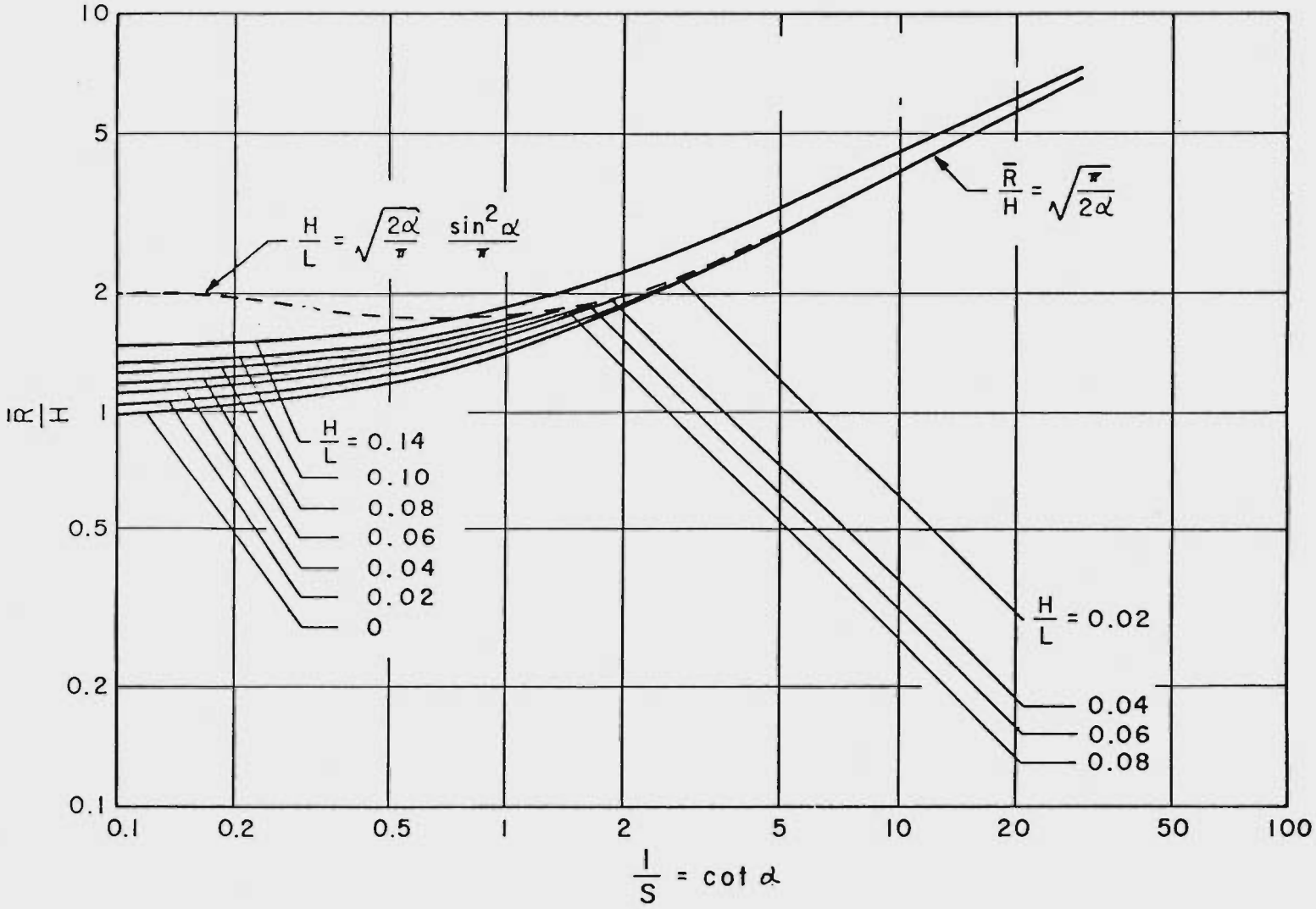

Figure V-3 Theoretically Deduced Nomograph for Run-Up of Waves on a Slope

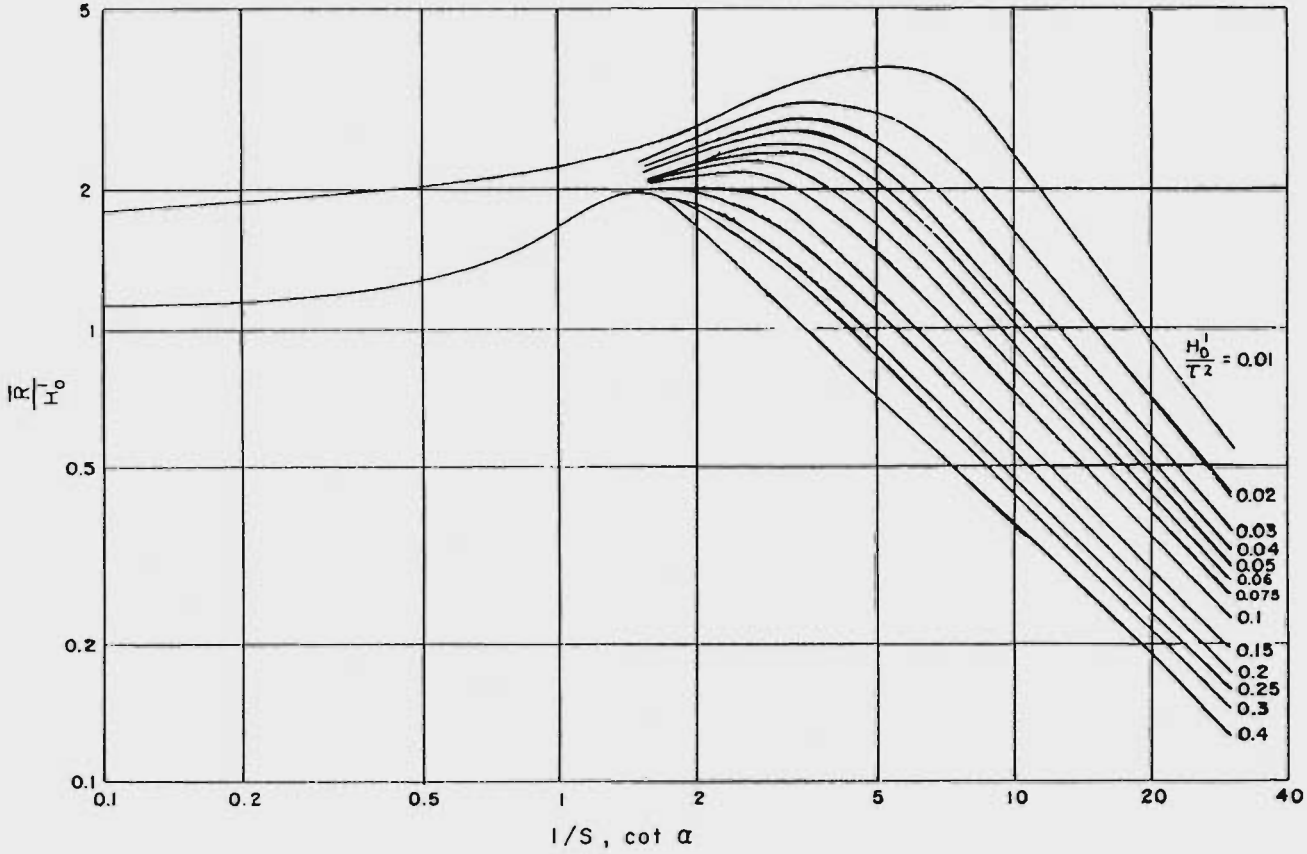

Figure V-4 Reproduction of BEB TM4 run-up nomograph (based on experiments) for $h/H'_o > 3$, where H'_o refers to deep water wave height obtained from back shoaling.

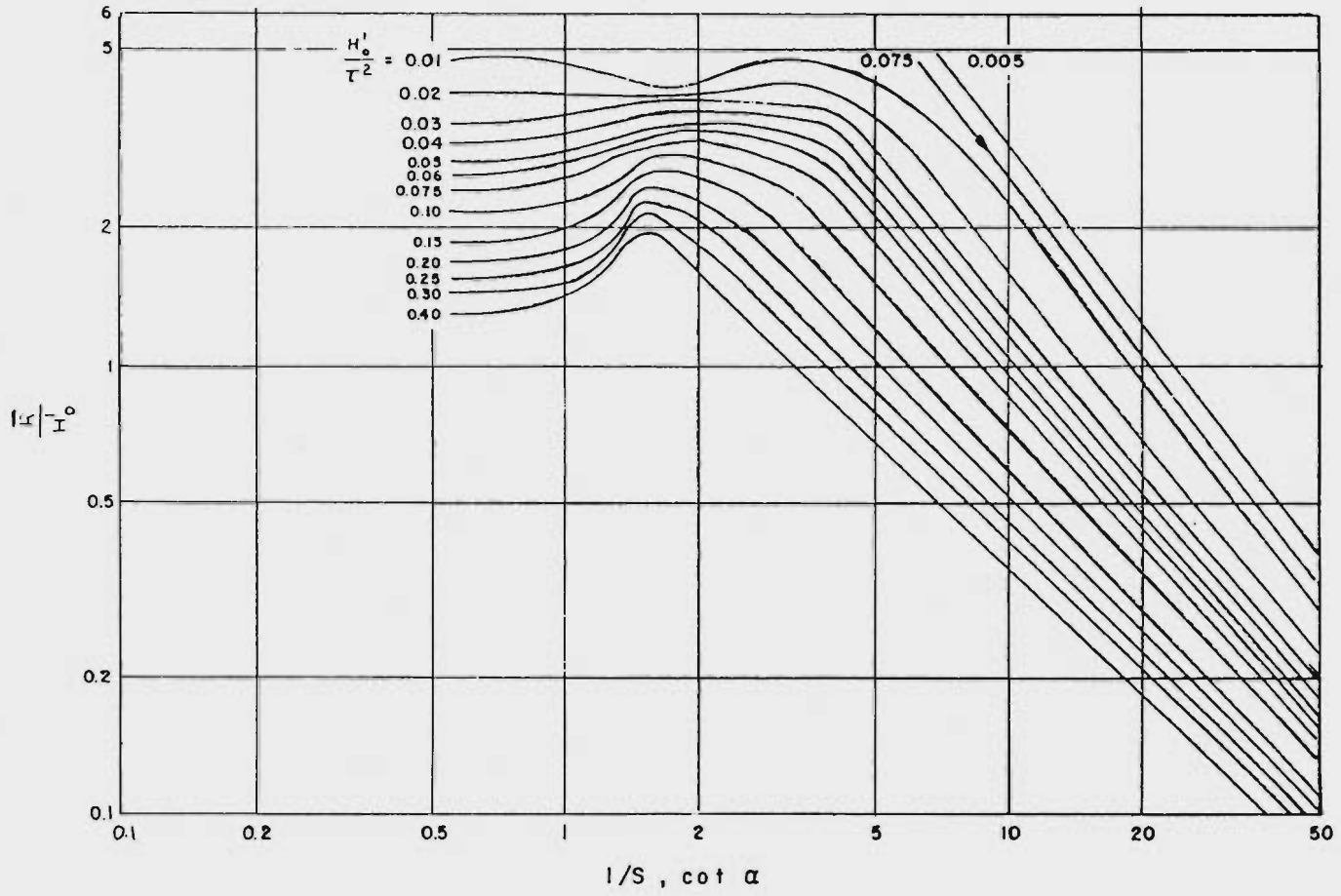

Figure V-5 Reproduction of BEB TM4 run-up nomograph (based on experiments) for $1 < h/H'_o < 3$

V-3 THEORIES FOR NONBREAKING WAVES

V-3.1 Periodic Waves

Under certain conditions, a wave may reach the beach without breaking. Such is the case when, for example, the beach is steep, the wave long, and the wave amplitude small.

Since the waves do not break, it is reasonable to assume that they are totally reflected by the beach, if one neglects bottom friction. This is the case of a standing wave or clapotis. The run-up is then directly related to the amplitude of the wave at the shore. In the extreme case of a vertical wall, the run-up is, in fact, equal to the amplitude of the wave at the wall, or twice that of the original progressive wave. Hence the run-up, $\overline{R}$, is equal to the wave height of the original wave, H, and $\overline{R}/H = 1$. For a beach that is not vertical but inclined at an angle, α, to the horizontal, Isaacson (1950) and Miche (1951), using linear theory, obtained the result

$$\overline{R}/H_o = \sqrt{\pi/2\alpha} \qquad \text{(V-3)}$$

By extending the analysis to include second order terms in the case of the vertical wall, Sainflou (1928) and Miche (1944) obtained correction terms to the above formula for a slightly more general geometry, where the wall is terminated at a finite depth. Both Miche's and Sainflou's results, however, are not complete because their solutions are given as power series and do not satisfy the continuity equation exactly. Miche's formula is

$$\frac{\overline{R}}{H} = 1 + \pi \frac{H}{L} \frac{1}{\tanh \frac{2\pi h}{L}} \left(1 + \frac{3}{4 \sinh^2 \frac{2\pi h}{L}} - \frac{1}{4 \cosh^2 \frac{2\pi h}{L}} \right) \qquad \text{(V-4)}$$

If h/L is small, this equation ceases to be useful. In fact, it formally predicts $\overline{R}/H \to \infty$ as $h/L \to 0$. A better approximation in this case can be obtained from the solitary wave theory.

For a sloping beach instead of a vertical wall, we may intuitively add the superelevation term obtained in front of a vertical wall to the formula $\bar{R}/H = \sqrt{\pi/2\alpha}$. This is a valid approximation provided the slope is not too gentle.

Linear small-amplitude solutions to the problem of progressive waves advancing from deep water to the shore over a uniformly sloping beach of arbitrary slope have been given by Isaacson, (1950) and Peters (1952). The same problem for beaches of special slopes was solved earlier by Bondi (1943), Miche (1944), Lewy (1946), and Stoker (1947). The case of three-dimensional waves on sloping beaches has been solved by Peters (1952) and Roseau (1952). Since progressive waves were assumed, energy is continuously flowing shoreward and reflection effects are ignored. Because the theory is linear, the waves cannot break. Thus, their solutions are not valid near shore because the wave amplitude tends to infinity. For the two-dimensional case, this singularity is found to be logarithmic.

To avoid the unrealistic assumption of no reflection, Keller (1961) has given several standing wave solutions by matching the solution obtained from the geometrical optics theory away from the shore to the linearized shallow water theory near the shore. For a bottom profile in which the depth, h(x), gradually increases monotonically with distance from shore to a constant value h_o at $x = \infty$, he obtains

$$\frac{\bar{R}}{H} = \sqrt{\frac{\pi}{2\alpha}} \cdot \frac{(k_o \sinh \bar{\beta} h k_o - \bar{\beta} h k_o)^{\frac{1}{2}}}{\cosh \bar{\beta} h k_o} \qquad (V-5)$$

in which α = slope angle of the beach at the shoreline, $\bar{\beta} = \frac{1}{g}\left(\frac{2\pi}{\tau}\right)^2$ and k_o is a root of

$$k_o \tanh \bar{\beta} h k_o = 1 \qquad (V-6)$$

By direct substitution of Eq. (V-6) into Eq. (V-5), it can be shown that the former is equivalent to

$$\frac{\bar{R}}{H} = \sqrt{\frac{\pi}{2\alpha}} \left\{ \tanh \frac{2\pi h}{L} \left(1 + \frac{4\pi h/L}{\sinh 4\pi h/L} \right) \right\}^{\frac{1}{2}} \qquad (V-7)$$

where the term in brackets is simply the linear shoaling coefficient (H/H_o). Thus Keller's solution is just the Miche formula (Eq. V-3) multiplied by the shoaling coefficient, showing that the linear run-up theory is relatively independent of the bottom profile, provided that it does not vary too rapidly.

Later, Keller and Keller (1964) applied the linear shallow water theory to a piecewise continuous bottom profile and obtained the result:

$$\frac{\bar{R}}{H} = \left[J_o^2(2\Omega/\alpha) + J_1^2(2\Omega/\alpha) \right]^{-\frac{1}{2}} \qquad (V-8)$$

where J_o and J_1 are Bessel functions.

This analytical result, for the case of small α, has been checked numerically by use of nonlinear shallow water theory and it appears to be satisfactory (Keller and Keller, 1965). However, for larger values of α, the result shows a considerable deviation from the values obtained by Keller's previous formula (1961).

V-3.2 Run-Up of Dispersive Waves

Carrier (1966), combining the Carrier and Greenspan transformation of the nonlinear shallow water wave theory on the sloping beach with linear dispersive wave theory in the deep water, obtained a solution which gives the maximum relative run-up in terms of distance from the bottom deformation and the angle of sloping beach. This method has been applied to calculate the time history of run-up of an explosion-generated wave train (Hwang and Fersht 1966, LeMéhauté and Hwang etc. 1967). It is found that the run-up, $\bar{R}$, is (see Fig. V-6)

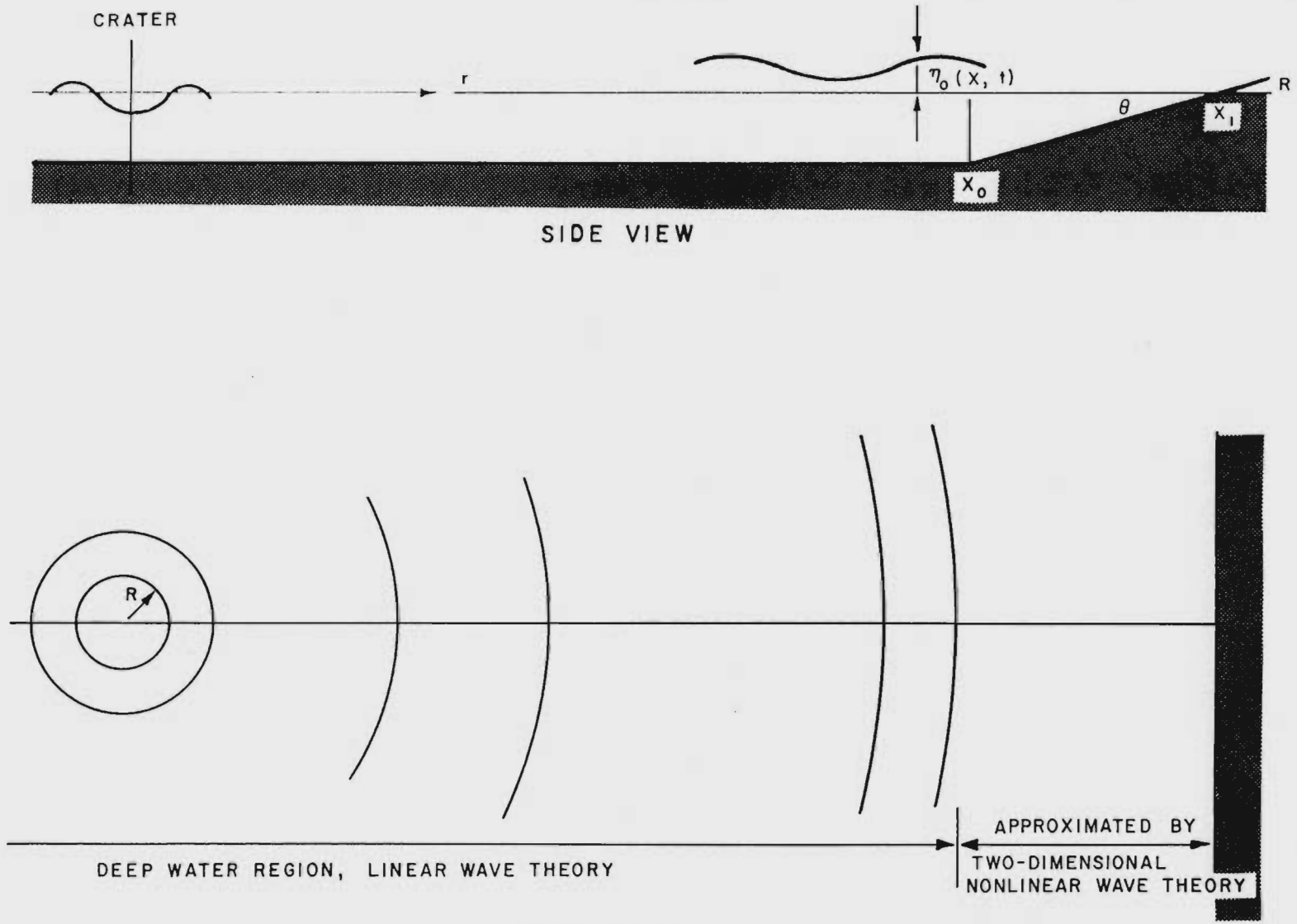

Figure V-6 Schematic Configuration for the Analysis of Run-up Explosion Waves

$$\bar{R} = \eta(0,\bar{\lambda}) = \frac{2}{D}\sum_{i=1}^{\infty}\frac{1}{J_1(\omega_i D)}\sin\omega_i\bar{\lambda}\int_o^{\bar{\lambda}}\eta_o\cos\omega_i\xi\,d\xi$$

$$-\cos\omega_i\bar{\lambda}\int_o^{\bar{\lambda}}\eta_o\sin\omega_i\xi d\xi - \frac{16}{D^2\theta}\left\{\sum_{i=1}^{\infty}\frac{1}{J_1(\omega_i D}\cdot\right.$$

$$\left.\left[\cos\omega_i\bar{\lambda}\int_o^{\bar{\lambda}}\eta_o\cos\omega_i\xi d\xi + \sin\omega_i\bar{\lambda}\int_o^{\bar{\lambda}}\eta_o\sin\omega_i\xi d\xi\right]\right\}^2 \qquad \text{(V-9)}$$

where $D = 4\sqrt{x_1 - x_o}$

$\bar{\lambda} = 2t\,\alpha^{\frac{1}{2}}$

$\eta_o(t)$ is the incoming wave train at the toe of the slope (Fig. V-7).

A sample of such calculation is shown in Fig. V-8, corresponding to the incoming wave train of Fig. V-7. The above run-up calculations have also been compared with those predicted for periodic waves over small slopes in Fig. V-7, the former being about 50% greater for the cases considered. The reason for this increase is not obvious because of the approximations involved in the calculations, but is possibly due to the interactions between consecutive waves that are ignored in the periodic solutions.

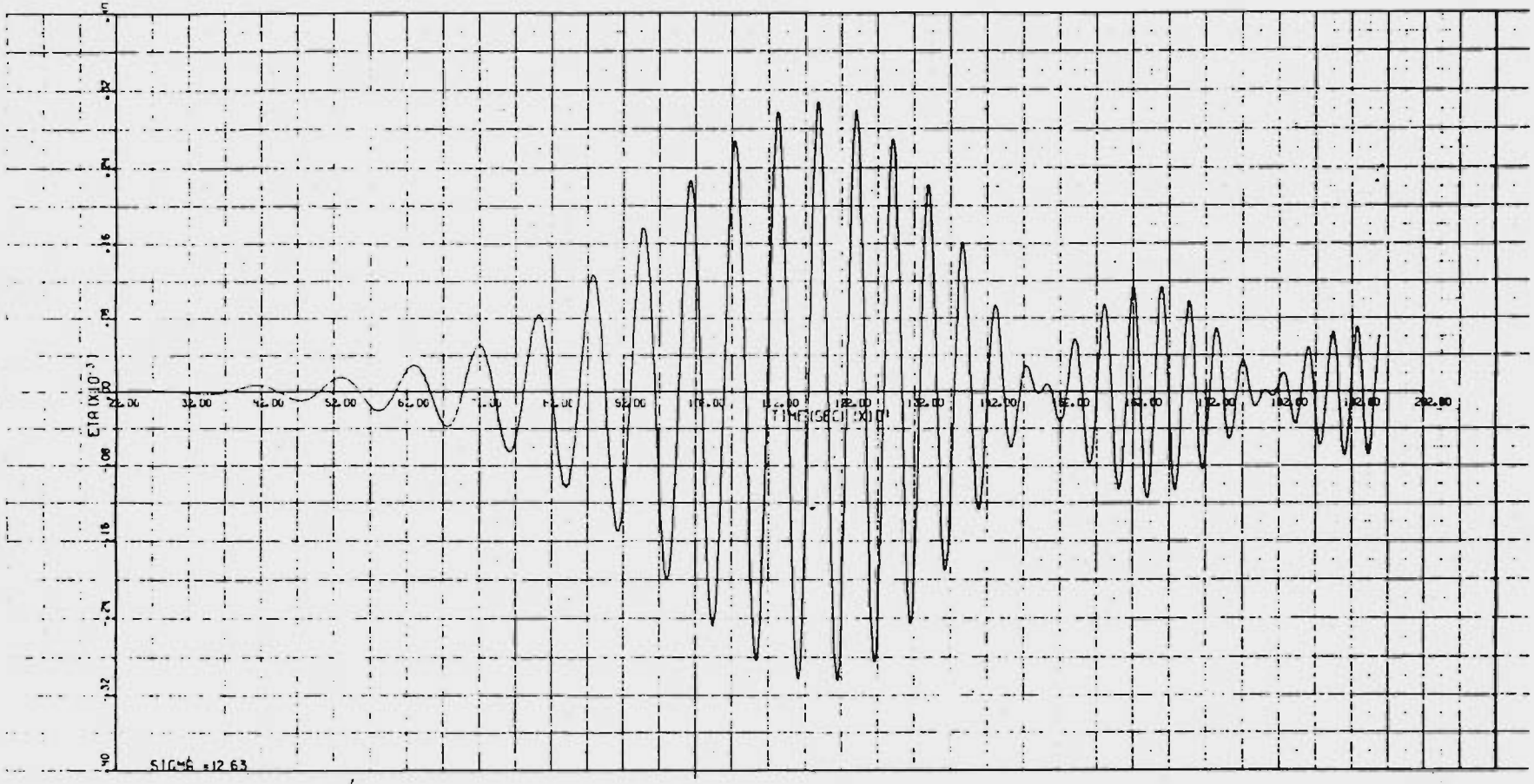

Figure V-7 Input Dispersive Wave Train at beach toe

Source Disturbance Radius = 3300 ft.
Source Disturbance Depth = 300 ft.
Source - 62 miles offshore
Deepwater Depth = 16400 ft. (see LeMehaute and Hwang, 1967)

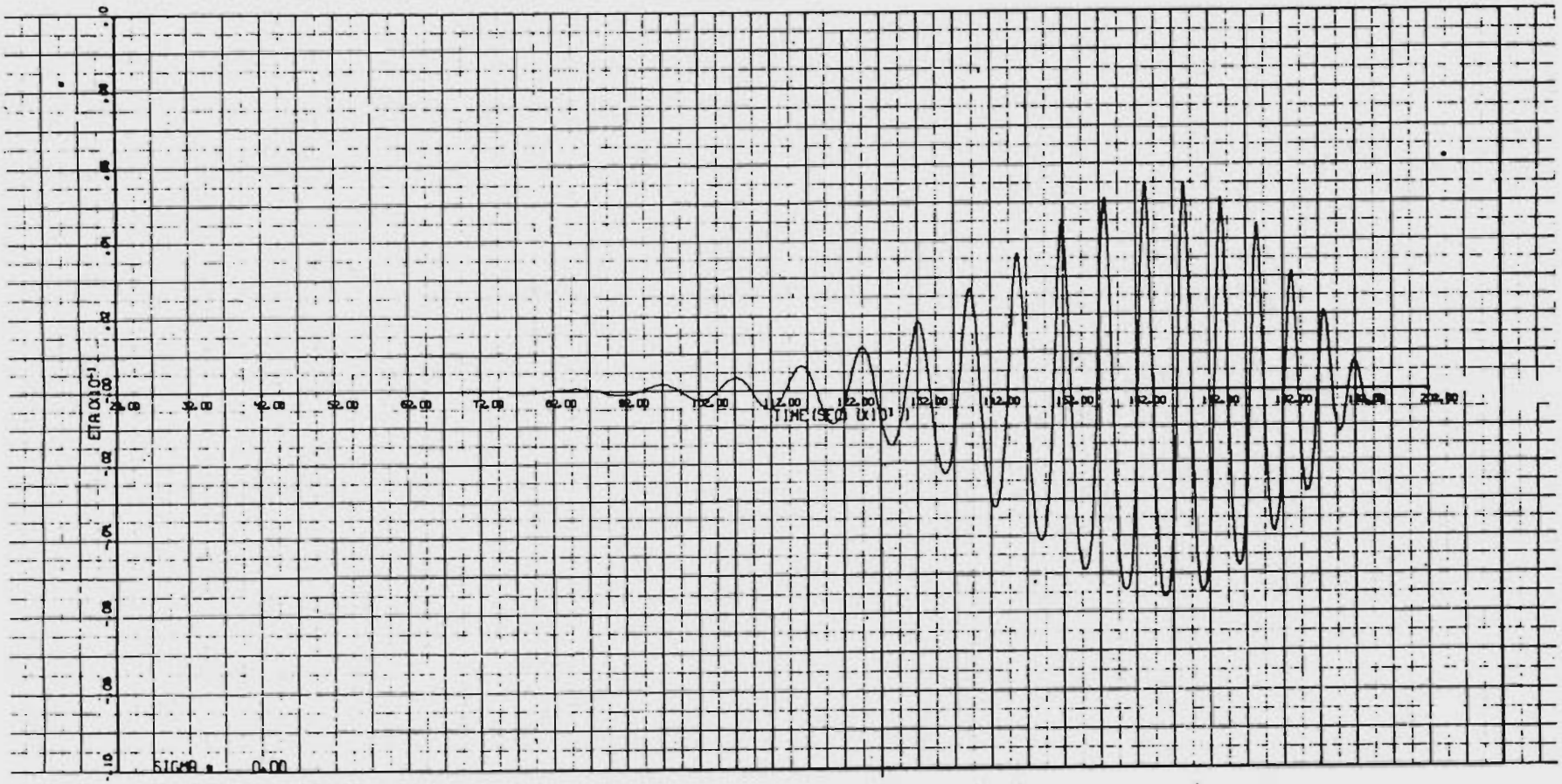

Figure V-8 Run-Up History at the Shoreline for the incoming wave train as shown in Fig. V-5

Beach Slope: 0. 1

V-4 RUN-UP OF BREAKING WAVES

V-4.1 Bore Run-Up Theory

In a sequence of papers [Ho and Meyer (1962); Shen and Meyer (1963 a, b); Ho, et al. (1963)], the problem of the climb of a bore on a beach is analyzed, based on the long wave equations. One of the conclusions reached for the case of long surf on a uniformly sloping beach is that the bore collapses when it reaches the shoreline and the run-up is given by $u_o^2/2g$, in which u_o = the horizontal velocity at the shoreline at the instant the bore reaches the shore, and g = the gravitational acceleration. The value of u_o depends on the initial bore characteristics and the characteristics of the beach. In these papers no simple method is given for the computation of this velocity. Whitham (1958) has proposed a simple approximation which can be used to calculate the bore behavior before it reaches the beach, by applying the equation for the forward moving bore characteristic line to the flow quantities just behind (i.e., on the seaward side of) the bore. Coupled with the bore equations (conservation of mass and momentum across the bore) this method yields a first-order ordinary differential equation for the bore strength as a function of depth. Thus, when the bore strength is known at one point, it can be determined at any other point. In particular, the bore strength (and hence the value of the velocity u_o at the moment the bore reaches the shoreline) may be determined. From this, the run-up, $\bar{R} = u_o^2/2g$ can be calculated.

Keller, Levine, and Whitham, (1960) checked the accuracy of Whitham's approximation by comparing certain cases with numerical solutions obtained by integrating the nonlinear shallow water equations by finite differences with good agreement.

It must be pointed out however, that this calculation is based on many assumptions, and cannot be applied in practice without substantial reservation. In particular, friction effects have been neglected, as well

as the vertical component of velocity at the free surface which tends to infinity. The Whitham approximation also ignores the slope of the wave behind the bore, which can substantially influence the run-up.

Lastly, the run-up is independent of the beach slope, which can be true only if the bore height decreases seaward from the bore front.

V-4.2 Run-Up of Nonsaturated Breakers

The nonsaturated breaker theory discussed in Section IV-4.2 provides an approximate means of determining whether or not run-up will be significant for breaking waves on a gentle slope. Reinterpreting the conclusions leading from Eq. IV-12,

1. If $S < 0.38\,f$, then the wave never breaks. All the energy is dissipated by bottom friction. No run-up is experienced. Actually, viscous dissipation should then be taken into account near the shore.
2. When $0.38f < S < 0.38\,f + 0.02$, the wave breaks as a spilling breaker and the rate of energy dissipated by the breaker increases as the bottom slope increases. All the wave energy is dissipated before reaching the shoreline. There is practically no run-up; however, a small rise of mean water level on the shore does exist as a result of mass transportation and the momentum of the breaker.
3. When $S > 0.01$ or thereabouts, the breaker becomes saturated and becomes a fully developed bore, and run-up is to be expected.

An interesting implication of this theory is that there is a maximum amount of energy which a solitary wave may carry towards the shore. If the depth decreases, the excess energy must be dissipated by breaking. The fact that the breaker may be saturated implies that there is also a maximum amount of energy which can be dissipated by breaking. If there is more energy available, it will be carried along (as a bore, instead of a spilling breaker) and the excess will cause run-up.

The theory of nonsaturated breakers has recently been extended to include mass transport and the wave set up, so that it satisfies the law of continuity and the momentum theorem (LeMéhauté, et al., 1968).

On a gentle slope ($S < 0.01$) which steepens near shore ($0.1 < S < 0.3$), the greatest run-up will be produced by a (solitary) wave which just exceeds the breaking criterion ($H = 0.78h$) at the point where $S \approx 0.01$. All larger waves will break earlier, dissipating their excess energy as spilling breakers, such that the same run-up will result. All smaller waves will break later on a steeper slope, and the run-up will be smaller.

V-4.3 Numerical Methods

When the method of characteristics is applied to the motion of a bore propagating to the shore, it is found that the bore height tends to zero on reaching the shoreline. This may be shown rigorously on the basis of the long wave equations (Keller, Levine, and Whitham, 1960). The run-up then consists of the further propagation of a sheet of water up the beach with zero thickness at the leading edge. From a physical point of view, this description implies very large frictional resistance at the leading edge. Hence friction cannot be neglected for evaluating the run-up. This theory also leads to the contradictory requirement that the bore collapses at the shoreline, as a result of neglecting the vertical component of velocity and vertical acceleration. It also requires that, in case of collapse, both should tend to infinity at zero depth. For these reasons, the theory appears to be invalid on purely physical premises.

LeMéhauté and Moore (1965) have also used the method of characteristics, where friction was included, but without resorting to the Whitham approximation. The particle velocity at the water's edge as it advances up the (dry) beach slope was assumed to be proportional to the bore propagation speed.

By this method the run-up, due to various kinds of solitary waves

travelling over several bottom slopes, was calculated, giving rise successively to spilling breakers and bores. Some of their results are shown in Fig. V-9, where the run-up is given as a function of the ratio $F = f/A^2$ of the assumed friction factor to the proportionality coefficient A relating particle velocity to bore speed.

It is concluded that the run-up of breaking waves has been determined by theory only for the case of solitary waves. The problem becomes increasingly difficult as the wave period decreases (or as the wave steepness increases) due to the influence of the backwash on the following wave. Because the backwash causes more energy dissipation in the bore, wave run-up decreases as the wave steepness increases. However, on the continental shelf, backwash is negligible and the solitary wave results should be adequate, although most of them have yet to be experimentally verified.

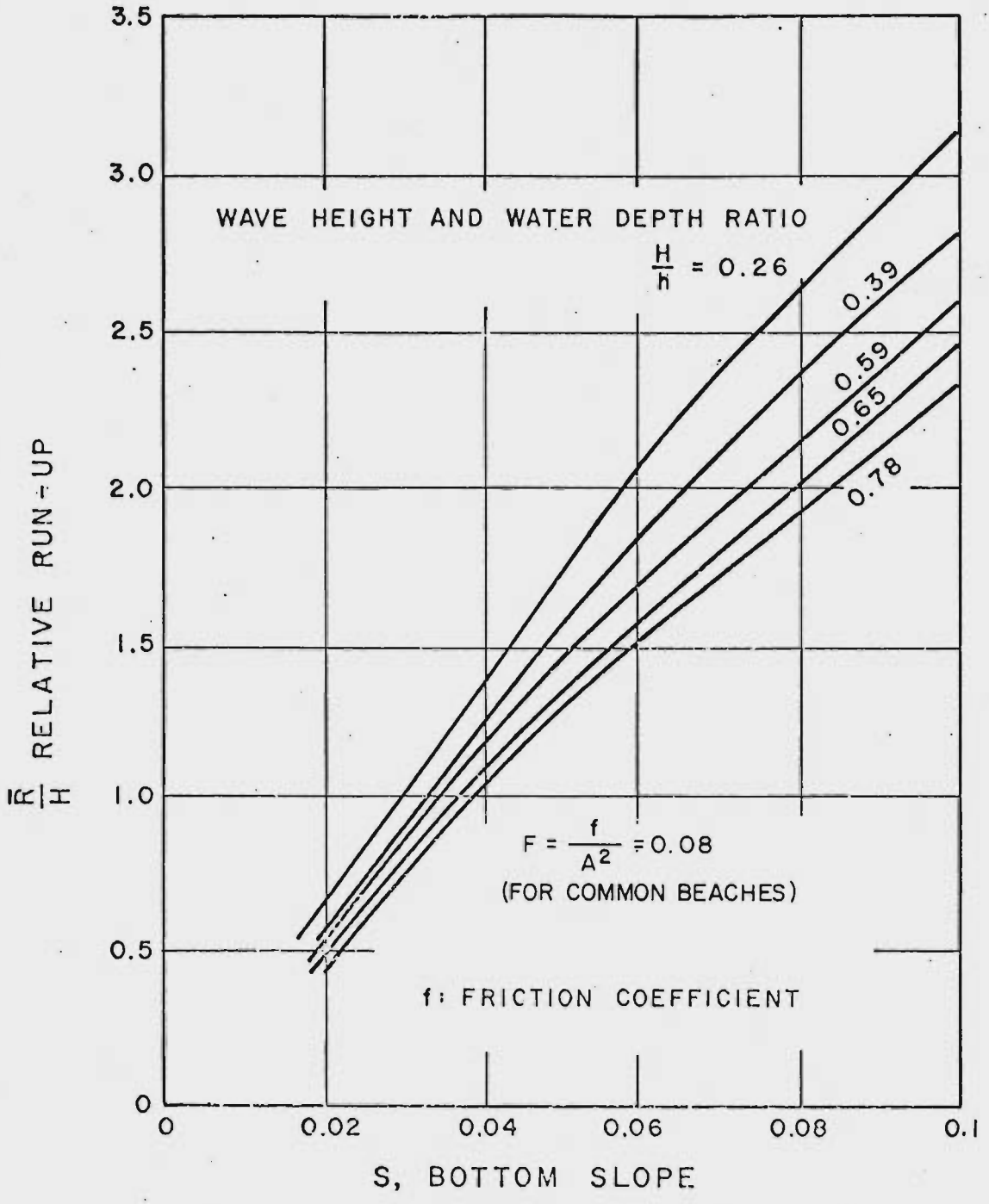

Figure V-9 The Run-up of Solitary Waves

V-5 EXPERIMENTAL INVESTIGATIONS

Relatively few experiments have been conducted on the run-up of breaking waves per se. Probably the most extensive study is that of Savage (1959) for periodic waves incident on relatively steep slopes ($0.03 < S < \infty$), and included both non-breaking and breaking waves, with no distinction between them. These results were later analyzed by Van Dorn (1966), who found that the data were clearly divisible according to whether or not they satisfied the breaking criterion of Hunt (Eq. IV-4), and that the run-up of breaking waves closely obeyed Hunt's empirical formula

$$\frac{\overline{R}}{H} = 2.3\, S\, (H/\tau^2)^{-\frac{1}{2}}$$

where H is the wave height in the uniform-depth section of the wave channel.

This relationship is compatible with the fact that the wave dissipation mechanism is fully turbulent, i. e., proportional to the square of velocity which is itself approximately proportional to the square of the wave height. Such a relationship should not hold when waves of small steepness break over very gentle slopes because the viscous dissipative mechanism has more relative importance. Thus this formula, based on experimental data, should not be extrapolated to waves of small steepness over very gentle slopes.

Additionally, there have been a number of run-up studies with leading waves of a wave train, of which the most extensive were those of Kaplan (1955) and Hall and Watts (1953). These results are presented as power functions of H/L and H/h, respectively, which make them difficult to interpret.

Van Dorn also found that the run-up of non-breaking waves reported by Savage was consistent with the small amplitude theory of Keller, provided

that the effect of finite height is included. Recently, experiments for wave run-up of dispersive wave trains were performed at NCEL (Jones, 1968). The results indicated that the relative run-up was smaller than the results calculated by Miche's formula.

Additional wave channel experiments with periodic non-breaking waves on small slopes ($0.1 < S < 0.03$) have been reported by Le Méhauté, et al. (1967), qualitatively verifying the theoretical curves given in Figs. V-1, V-2 and V-3, although for the smallest slopes the observed run-down exceeded the run-up, suggesting that frictional dissipation in the thin leading wave edge may be a limiting factor in such experiments. However, contradictory observations have been reported which indicate that the run-up is greater than the run-down (Wallace and Baird, 1968). The reason for this is not known.

Recently, experiments for measuring wave run-up in an idealized three-dimensional bay have been performed at Tetra Tech (Hwang, et al., 1968). As shown in Fig. V-10, the bay is S-shaped with a sloping beach; the beach slope is 1/5 and everywhere perpendicular to the local shoreline. This arrangement, with a convex shoreline at the entrance and a concave region at the rear of the bay, is adjacent to the tank wall and hence represents, by symmetry, half of a bay with general features similar to many natural bays. The results of experiments are shown in Fig. V-11.

As shown in that figure, the relative run-up at different locations with the same beach slope may vary from a value less than 0.7 to a value of 13. It is also shown that the relative run-up is strongly dependent on wave period. The run-up at locations 1, 10 and 17 on the same geometry has also been calculated from Miche's formula with refraction correction as shown in Fig. V-12. These values are considerably smaller than those obtained from the measurements. Thus, it demonstrates that when the shoreline includes bays one has to take into account the oscillation of the bay.

Experiments to measure wave run-up in the field were performed at

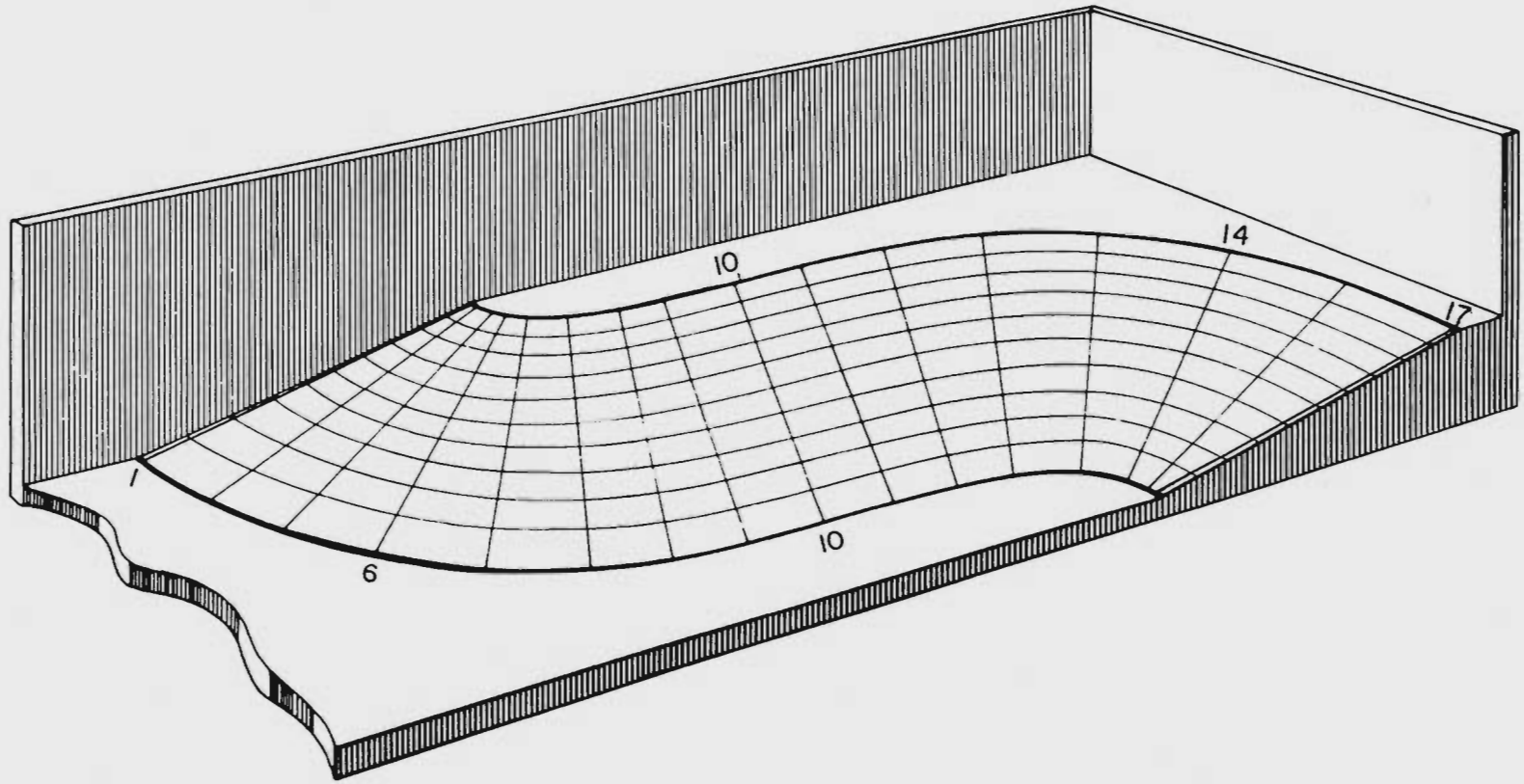

Figure V-10 An idealized three-dimensional bay used in the experiments for investigation of wave run-up due to bay oscillation

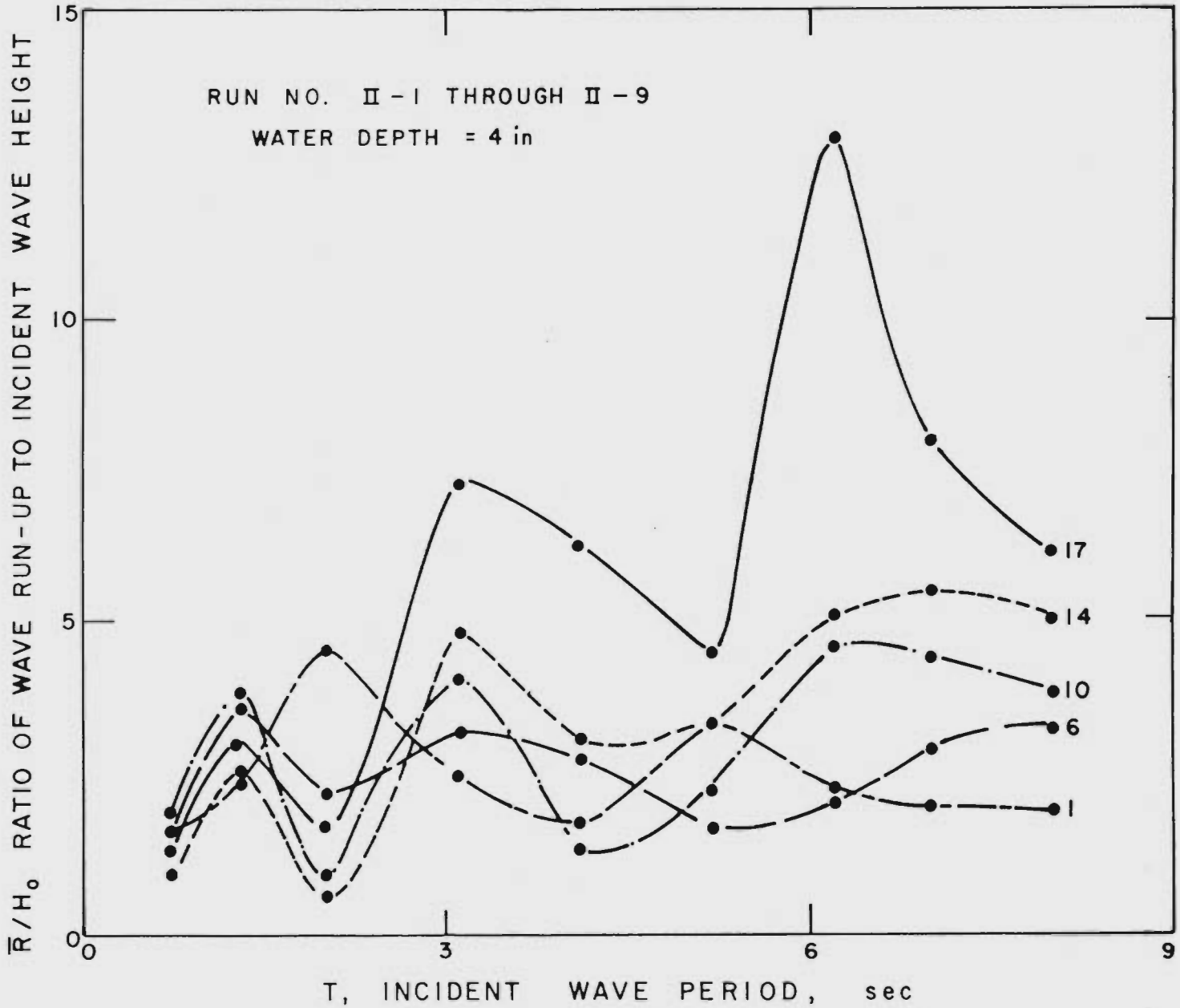

Figure V-11 The Effect of Wave Period on Wave Run-Up in a Three-Dimensional Bay (Numbers on the right indicate the location as shown in Fig. V-8)

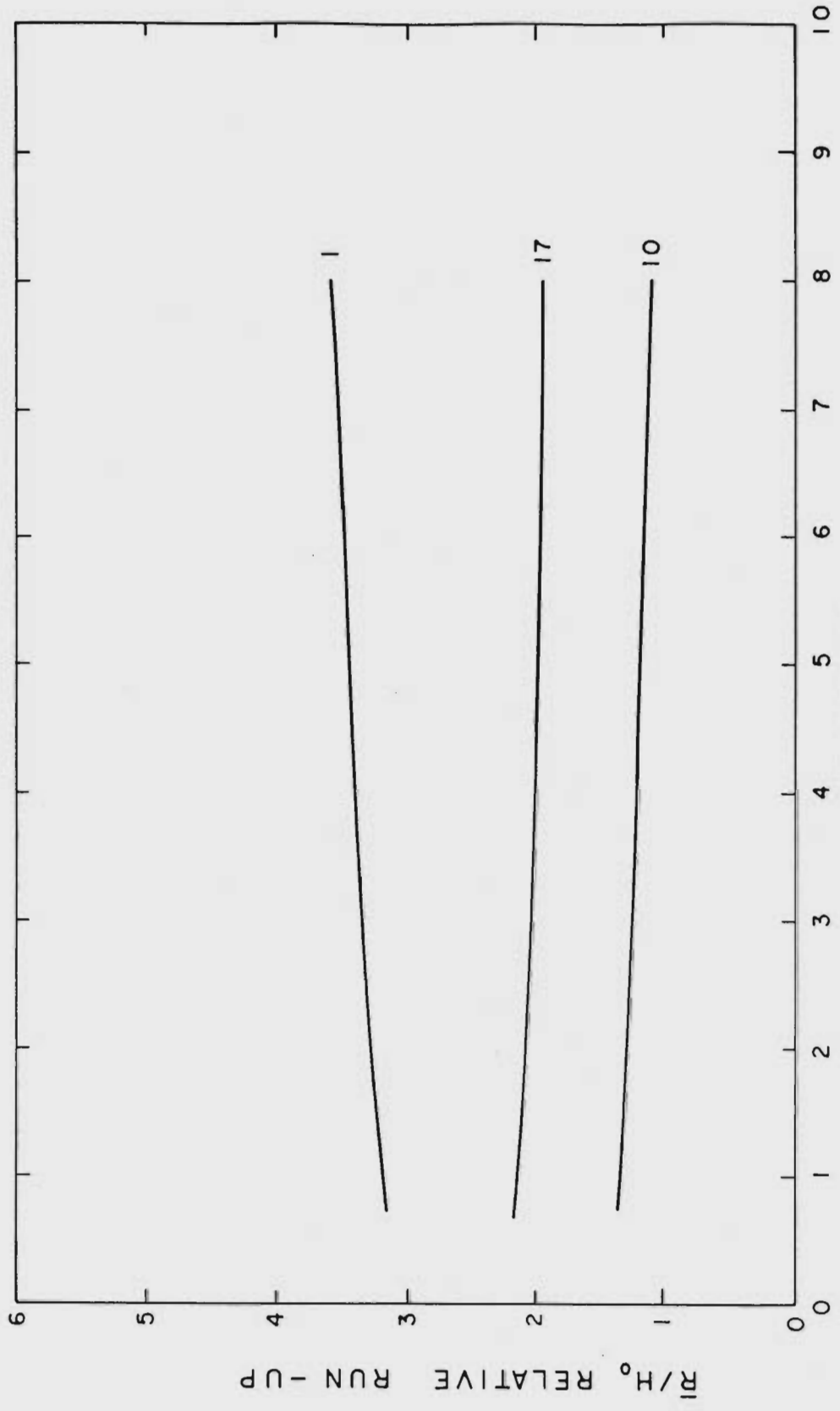

Figure V-12 Run-Up Calculated based on the Refraction Coefficients and Miche's Formula

A-2-738

Mono Lake in 1965 and 1966 (Rooke, et al, 1967, Wallace and Baird, 1968). In 1965 the run-up was measured on a relatively simple beach condition. These experiments indeed proved that the wave run-up obtained by extrapolation of what is obtained in tsunami waves cannot give a reliable estimate of the effect of explosion waves. As most of the energy is dissipated before the waves reach the shoreline, it is evident that no catastrophe of damage by flooding can result from explosion waves as was initially feared. These experiments proved that wave run-up due to explosion waves is much smaller as compared to relative run-up of tsunami waves.

A formal prediction based on these assumptions was made (LeMéhauté, et al., 1965) and, as a matter of fact, the maximum wave run-up prediction was even lower by 50% than that observed in the test. This discrepancy was largely due to the inaccuracy of the prediction in deep water wave trains. In 1966, experiments were performed in a complex geometry with shorelines containing large boulders and small bays. The experimental results, compared to the prediction, appear to be somewhat improved. However, the predicted results were, in general, larger than the observed results (LeMéhauté, et al., 1966, and Wallace and Baird, 1968).

The problem of prediction of leading wave run-up has been subjected to discussion due to the fact that the observed results do not fit the prediction. The difficulties in predicting the run-up of the leading wave are not only due to the difficulty in predicting the run-up of the leading wave itself, but also due to the fact that the scaling law for wave prediction, which is established for maximum wave amplitude, is not adequate for prediction of the leading wave.

CHAPTER VI

HARBOR OSCILLATION

VI-1 INTRODUCTION AND GENERAL REMARKS

Since harbor or bay oscillations may enhance the wave run-up and damage moored ships, it is well to consider in some detail the nature and practical importance of harbor resonance, and to recount some of the important progress made by earlier investigators.

The occurence of resonance in harbors is fundamentally due to the fact that waves arriving at a widening or narrowing (or at a depth increase or decrease) are partially reflected. Consider, for example, a rectangular harbor open to the sea. Waves arriving within the harbor are reflected seaward by the rear boundary; these outgoing waves upon reaching the harbor entrance are partially reflected by the sudden widening with the net result that part of the wave energy which got in does not get back out. This trapping of energy by the harbor leads to resonance if the phases of the various incident and reflected waves happen to be such that reinforcement occurs. In this case, the amplitude of oscillation may grow, within the harbor, to values far greater than those incident. At some stage of growth, however, energy dissipation equals energy trapping and the oscillation amplitude reaches its maximum. This stabilizing dissipation is of four main forms: wave radiation seaward (usually dominant); wave breaking within the harbor when the oscillation exceeds the breaking limit; frictional effects at the bottom; and wave absorption on the bounding beaches.

The problems of developing a practical calculation procedure applicable to these processes, already difficult, are compounded by the facts that harbors are usually of complex shape and that incident waves are never periodic. Irregularity of shape causes complicated reflections of the waves within the harbor so that even for periodic input the agitation may appear highly irregular. The response to random sea or swell or to a dispersive wave train generated by a localized disturbance is still worse. Furthermore, oscillations may be induced by other mechanisms

such as fluctuations in atmospheric conditions, currents moving past the entrance which generate a series of alternating vortices, and even ship transit in and out of the harbor. It is no wonder, then, that taken in its entirety the problem of harbor resonance is intimidating.

Yet, solutions must be found since the harbor resonance problem is of very great practical importance in coastal engineering. This is so since it is associated with the ship mooring problem. It is well known that harbor oscillations of only a few inches may excite large motions in ship-mooring systems causing mooring lines to break, and ships to collide with adjacent structures. To minimize such events is the goal of harbor and breakwater design and for that purpose one must be able to determine harbor response characteristics.

Analytical studies in this area are, for the most part, quite recent. McNown (1952) determined the resonant frequency of a circular harbor with a small opening under the assumption that the water surface remains essentially horizontal; a similar approach was applied by Kravtchenko and McNown (1955) to the rectangular harbor. Miles and Munk (1961) considered harbors of arbitrary shape and formulated an integral equation describing the agitation within the harbor by matching conditions inside and outside the harbor at the entrance. But they imposed the restrictions of narrow opening, and slim and rectangular harbor in order to obtain analytical expressions for the resonant condition and maximum amplification. Ippen and Goda (1963) applied Fourier transformation methods and obtained the solution of the rectangular harbor. The results were compared with a series of experiments. For long harbors, the agreement between theory and experiment was good except, of course, at the resonance point where viscous dissipation is important and the experiments become difficult. Biesel and LeMéhauté (1955, 1956) and LeMéhauté (1960, 1961, 1962) presented an interesting approach in the solution of rectangular harbor under various types of entrance conditions through the use of the theory of complex numbers. Through this method, the following results were found:

1. The smaller the harbor entrance width, the smaller the possibility of resonance. However, the resonance peak, if reached, is then very high, and its height increases as the width of the opening decreases.

2. Wide open bays and harbors always amplify the incoming wave agitation. However, the resonance peak is flatter.

3. Wave energy absorbers are efficient in cutting peak resonance in enclosed harbors. They are less efficient in wide open harbors.

Most recently, Leendertse (1967) has developed a numerical procedure to determine the response of basins to long waves, elevation at open boundaries being prescribed.

All of the foregoing studies suffer to some degree from various deficiencies; either they are applicable only to idealized shapes or matching conditions at the harbor entrance are required.

Advances have been made recently in the analysis of the harbor problem. Harbors of arbitrary shape with constant depth have been solved by Hwang and Le Méhauté (1968). The method they proposed has overcome the assumption of conditions at the entrance, which has been the major problem in previous analytical studies. Because of its importance to the mooring and run-up problems, this method is now summarized.

VI-2 THEORETICAL DEVELOPMENTS

VI-2.1 Formulation of the Problem

Assuming that the fluid is inviscid and incompressible, there exists a velocity potential $\Phi(x, y, z; t)$ which satisfies the Laplace equation

$$\nabla^2 \Phi = 0 \qquad \text{(VI-1)}$$

throughout the fluid contained within the boundary surfaces as shown in Fig. VI-1. If the wave is assumed to be of small amplitude, the velocity term in the Bernoulli equation may be neglected. Thus the governing dynamic boundary condition on the free surface becomes (see Stoker, 1965)

$$\eta = -\frac{1}{g}\frac{\partial \Phi}{\partial t} \qquad \text{at } z = 0 \qquad \text{(VI-2)}$$

where η is the wave elevation and g is gravitational acceleration.

The linearized kinematic condition at the free surface follows from the fact that surface water particles stay on the surface and is expressed in the form

$$\frac{\partial \eta}{\partial t} = \frac{\partial \Phi}{\partial z} \qquad \text{at } z = 0 \qquad \text{(VI-3)}$$

The condition on the fixed boundary surface is that the velocity normal to the surface equals zero; that is

$$\frac{\partial \Phi}{\partial n} = 0 \qquad \text{(VI-4)}$$

on the boundary $\overline{S}$.

Since we are dealing with uniform water depth, h, the condition at the bottom is simply

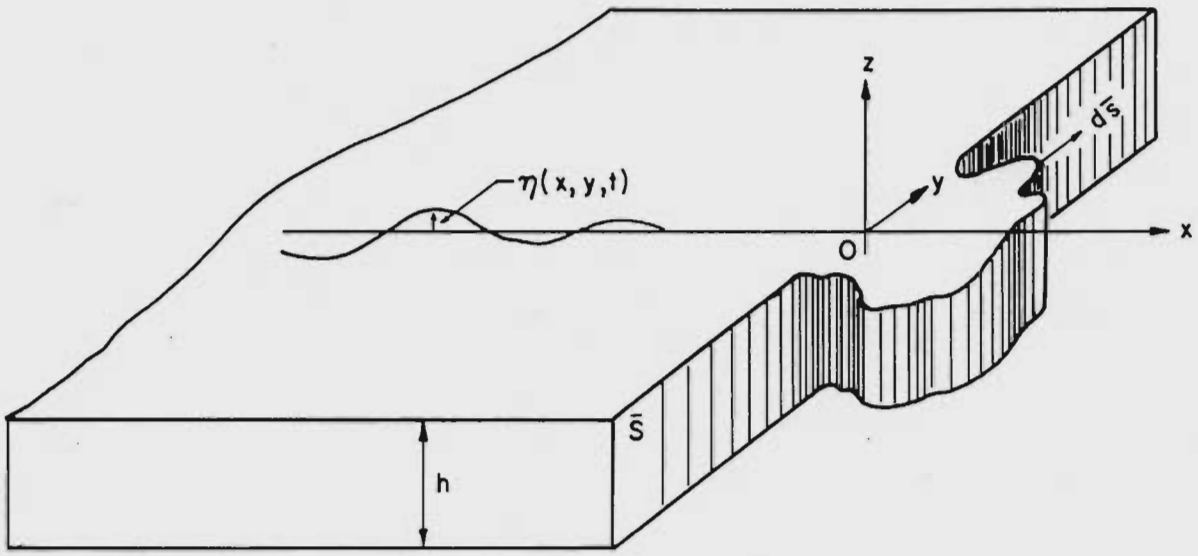

Figure VI-1 A Schematic Drawing of the Harbor

$$\frac{\partial \Phi}{\partial z} = 0 \qquad \text{at } z = -h \tag{VI-5}$$

Finally, the condition at infinity is that

$$\Phi = \Phi_o \tag{VI-6}$$

where Φ_o is prescribed (input).

The above equations complete the formulation of the problem of oscillation in harbors of arbitrary shape.

VI-2.2 Analytic Solution

Since the water depth is uniform, we may assume that the velocity potential is a product of functions of x and y, z, and t, such as

$$\Phi(x, y, z; t) = \frac{1}{\omega i} \varphi(x, y)\, Z(z)\, e^{i\omega t} \tag{VI-7}$$

where ω is the angular frequency.

Substituting the above expression into the Laplace equation, we have

$$\frac{1}{\varphi}\left(\frac{\partial^2 \varphi}{\partial x^2} + \frac{\partial^2 \varphi}{\partial y^2}\right) + \frac{1}{Z}\frac{d^2 Z}{dz} = 0 \tag{VI-8}$$

After separating the functions of x and y, and z in Eq. (VI-8), and equating them to a constant, say k^2, we have

$$\frac{\partial^2 \varphi}{\partial x^2} + \frac{\partial^2 \varphi}{\partial y^2} + k^2 \varphi = 0 \tag{VI-9}$$

and

$$\frac{\partial^2 Z}{\partial z^2} - k^2 Z = 0 \tag{VI-10}$$

where k is a constant which is related to the frequency ω.

The solution of Eq. (VI - 10) is simply

$$Z(z) = C_1 \cosh kz + C_2 \sinh kz \qquad \text{(VI-11)}$$

The constants C_1 and C_2 are related to each other by

$$C_2 = C_1 \frac{\sinh kh}{\cosh kh} \qquad \text{(VI-12)}$$

which is obtained from the bottom boundary condition

$$\frac{\partial Z}{\partial z} = 0 \qquad \text{at } z = -h \qquad \text{(VI-13)}$$

resulting from the substitution of Eq. (VI-7) into Eq. (VI-5).

After substituting Eq. (VI-12) into Eq. (VI-11), we have

$$Z(z) = \frac{C_1 \cosh k(z+h)}{\cosh kh} \qquad \text{(VI-14)}$$

The constant C_1 is determined from the free surface condition

$$\eta = -\frac{1}{g} \frac{\partial \Phi}{\partial t}\Big|_{z=0} = -\frac{C_1}{g} \varphi(x,y)\, e^{i\omega t} = A\varphi(x,y)\, e^{i\omega t} \qquad \text{(VI-15)}$$

where $A = -\frac{C_1}{g}$ is the wave amplitude. Thus we have

$$Z(z) = -\frac{A\, g \cosh k(z+h)}{\cosh kh} \qquad \text{(VI-16)}$$

The constant, k, is a wave number, and is related to the angular frequency, ω, and the water depth, h, through the kinematic boundary condition at the free surface (see Eq. VI-3).

Substituting Eqs. (VI-7), (VI-15) and (VI-16) into Eq. (VI-3) we obtain

$$\omega^2 = g k \tanh kh \qquad \text{(VI-17)}$$

The problem now is to obtain the solution of Eq. (VI-9) with the boundary condition

$$\frac{\partial \varphi}{\partial n} = 0 \qquad \text{on the solid boundary, } \overline{S} \qquad \text{(VI-18)}$$

which is obtained from the substitution of Eq. (VI-7) into Eq. (VI-4), and the prescribed condition,

$$\varphi = \varphi_o \qquad \text{at infinity,} \qquad \text{(VI-19)}$$

where φ_o represents the incoming wave.

For a straight-crested standing wave at infinity with the crest at the harbor at an angle β, as shown in Fig. VI-2, the wave form is simply

$$\eta = A\varphi_o e^{i\omega t} = A \cos kx' e^{i\omega t} \qquad \text{(VI-20)}$$

where x' is the coordinate measured perpendicular to the wave front, and is rotated an angle β from the x axis. Since

$$x' = x \cos\beta + y \sin\beta \qquad \text{(VI-21)}$$

we have

$$\varphi_o = \cos k(x \cos\beta + y \sin\beta) \qquad \text{(VI-22)}$$

If the wave front propagates directly toward the shore, β is equal to zero, so that

$$\varphi_o = \cos kx \qquad \text{(VI-23)}$$

For a standing wave of unit amplitude at infinity, the solution of Weber's equation, Eq. (VI-9), together with the boundary conditions, Eq. (VI-18) and (VI-19), can be found through the introduction of a source function $Q(\xi, \eta)$ along the boundary $\overline{S}$, where ξ and η refer to coordinates on the boundary.

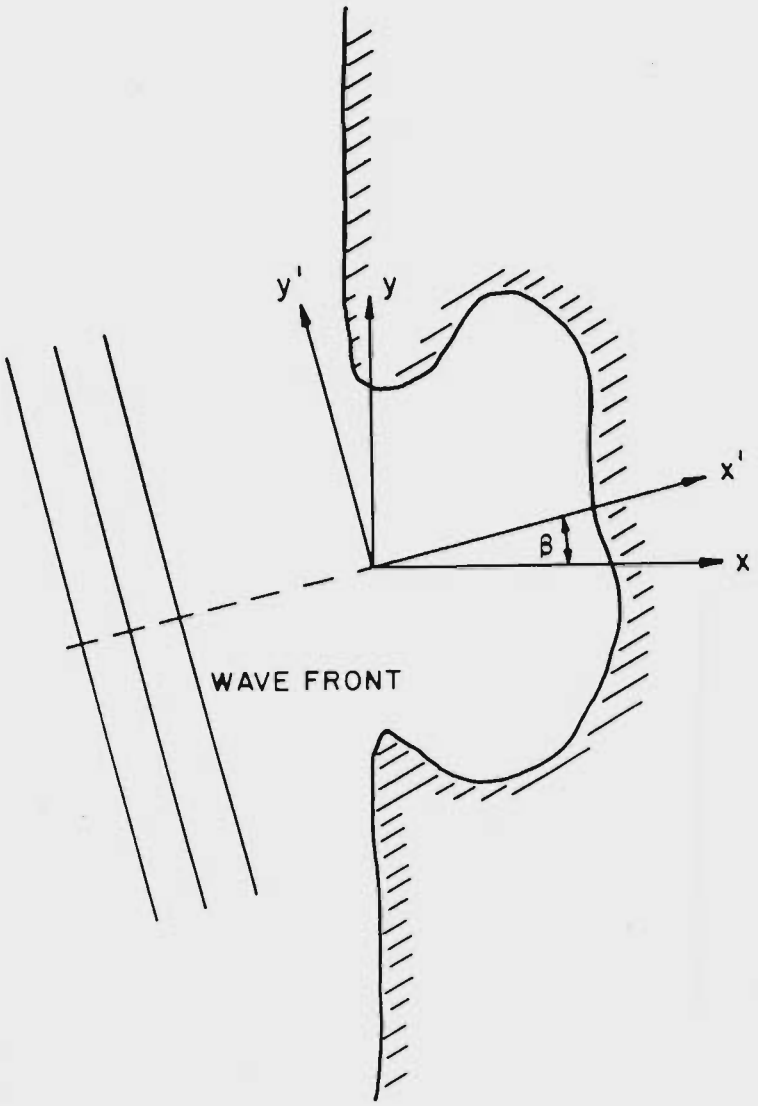

Figure VI-2 Determination of direction of the incoming waves

Thus the value of $\varphi(x, y)$ at any point $P(x, y)$ is equal to the sum of two parts; one is the influence from infinity, $\varphi_o(x, y)$, and the other is the contribution of the source distribution, that is, the scattered wave caused by the presence of the boundary

$$\int_{\bar{S}} d\bar{S}\, Q(\xi, \eta)\, G(x, y; \xi, \eta) \tag{VI-24}$$

where $G(x, y; \xi, \eta)$ is the Green's function and $Q(\xi, \eta)$ is the unknown source distribution which can be determined from the boundary conditions.

The Green's function has to be chosen so that it is the solution of Weber's equation, satsifies the radiation condition at infinity, and has a singularity at the source point. The Green's function may be determined easily from Weber's equation in cylindrical coordinates, that is

$$\frac{1}{R}\ \frac{d}{dR}\left(R\,\frac{d\varphi}{dR}\right) + k^2\varphi = 0 \tag{VI-25}$$

The solution of this equation involves Bessel functions or Hankel functions. Since the Hankel function of zero order and first kind has the following properties

$$-\frac{i}{4} H_o^{(1)}(kR) \rightarrow \frac{1}{2\pi} \ell n\,(kR) \qquad \text{as } R \rightarrow 0$$

and

$$\rightarrow -\frac{1}{4\pi}\sqrt{\frac{2\pi}{kR}}\, e^{i(kR + \frac{1}{4}\pi)} \qquad \text{as } R \rightarrow \infty$$

it satisfies the requirements prescribed previously. Therefore, we choose the Green's function to be

$$G(x, y; \xi, \eta) = -\frac{i}{4} H_o^{(1)}(kR) \tag{VI-26}$$

where

$$R = \sqrt{(x-\xi)^2 + (y-\eta)^2}$$

so that the value of $\varphi(x, y)$, at any point, $P(x, y)$, is

$$\varphi(x, y) = \varphi_o(x, y) + \int_{\bar{S}} d\bar{S}\, Q(\xi, \eta)\, G(x, y; \xi, \eta) \qquad \text{(VI-27)}$$

The problem now is to determine the strength of the source distribution, $Q(\xi, \eta)$. This can be accomplished by applying the boundary condition of Eq. (VI-18) which gives

$$\lim_{x, y \to \xi, \eta} \left[\frac{\partial \varphi_o}{\partial n} + \frac{\partial}{\partial n} \int_{\bar{S}} d\bar{S}\, Q(\xi, \eta)\, G(x, y; \xi, \eta) \right] = 0 \qquad \text{(VI-28)}$$

Since the limit is singular inside the integral, it has to be treated with care.

Considering the contour of integration, as shown in Fig. (VI-3)

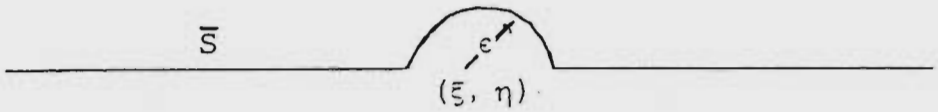

Figure VI-3 Contour of Integration

we evaluate the integral in Eq. (VI-28) as follows

$$\lim_{x, y \to \xi, \eta} \frac{\partial}{\partial n} \int_{\bar{S}} d\bar{S}\, Q(\xi, \eta)\, G(x, y; \xi, \eta)$$

$$= \oint_{\bar{S}} d\bar{S}\, Q(\xi, \eta)\, G_n(x, y; \xi, \eta) + \lim_{x, y \to \xi, \eta} \int_{\varepsilon} d\bar{S}\, Q(\xi, \eta)\, G_n(x, y; \xi, \eta) \qquad \text{(VI-29)}$$

where the sign, $\oint_{\bar{S}}$ refers to the principal value. Since the Hankel function can be approximated by

$$-\frac{i}{4} H_o^{(1)}(kR) \to \frac{1}{2\pi} \ell n\,(kR), \qquad \text{as } R \to 0 \tag{VI-30}$$

the second integral of the right hand side of (VI-29) may be integrated analytically. We have

$$\lim_{x,y \to \xi,\eta} \frac{\partial}{\partial n} \int_{\varepsilon} d\bar{S}\, Q(\xi,\eta)\, G(x,y;\xi,\eta)$$

$$= \lim_{R\to 0} \frac{1}{2\pi} Q(\xi,\eta) \int_{-\pi}^{0} \left(\frac{\partial}{\partial R} \ell n\, kR\right) R d\theta = \frac{Q(\xi,\eta)}{2} \tag{VI-31}$$

Thus the integral equation becomes

$$\frac{1}{2} Q(\xi,\eta) + \int_{\bar{S}} d\bar{S}\, Q(\xi,\eta)\, G_n(kR) = -\frac{\partial}{\partial n} \varphi_o(x,y) \tag{VI-32}$$

where

$$G_n(kR) = -\frac{i}{4} \frac{\partial}{\partial n} H_o^{(1)}(kR)$$

The above equation can not be evaluated analytically. A numerical method for evaluating the source distribution $Q(\xi,\eta)$ has been developed by Hwang and Le Méhauté (1968).

VI-3 CALCULATION OF VELOCITY AND AMPLIFICATION FACTOR

Once the source strength Q has been calculated the value of $\varphi(x, y)$ can be evaluated by substituting values of Q into Eq. (VI-27). Thus the velocity potential can be calculated from Eq. (VI-7).

$$\Phi(x, y, z; t) = -\frac{Ag}{i\omega} \varphi(x, y) \frac{\cosh k(z+h)}{\cosh kh} e^{i\omega t} \qquad \text{(VI-33)}$$

The velocity components at any location, $P(x, y, z)$, can be calculated as

$$u = -\frac{\partial \Phi_r}{\partial x} = -\frac{Ag}{\omega}\left[\frac{\partial \varphi_i}{\partial x} \cos \omega t - \frac{\partial \varphi_r}{\partial x} \sin \omega t\right]\frac{\cosh k(z+h)}{\cosh k h} \qquad \text{(VI-34)}$$

$$v = -\frac{\partial \Phi_r}{\partial y} = -\frac{Ag}{\omega}\left[\frac{\partial \varphi_i}{\partial v} \cos \omega t - \frac{\partial \varphi_r}{\partial y} \sin \omega t\right]\frac{\cosh k(z+h)}{\cosh k h} \qquad \text{(VI-35)}$$

where the subscripts i and r refer to the imaginary and real parts of the complex values and u, v are horizontal and vertical velocity components.

The velocity field corresponding to $\omega t = 90^\circ$ for the harbor of Port Hueneme is calculated by use of this method and is plotted in Fig. VI-4.

The amplification factor at any point $P(x, y)$ is equal to the ratio of maximum wave height obtained at point $P(x, y)$ to the wave height at infinity. The maximum wave height at infinity is A. However, the maximum wave amplitude at point $P(x, y)$ is

$$\eta = \left| -\frac{1}{g} \frac{\partial \Phi}{\partial t}\Big|_{z=0} \right| = A \left|\varphi(x, y)\right|$$

Thus the amplification factor at any point $P(x, y)$ is simply

$$A_p = \frac{\eta}{A} = \left|\varphi(x, y)\right| \qquad \text{(VI-36)}$$

and the result of this calculation is shown in Fig. VI-5.

Figures VI-6 through VI-8 are results extracted from a study made by

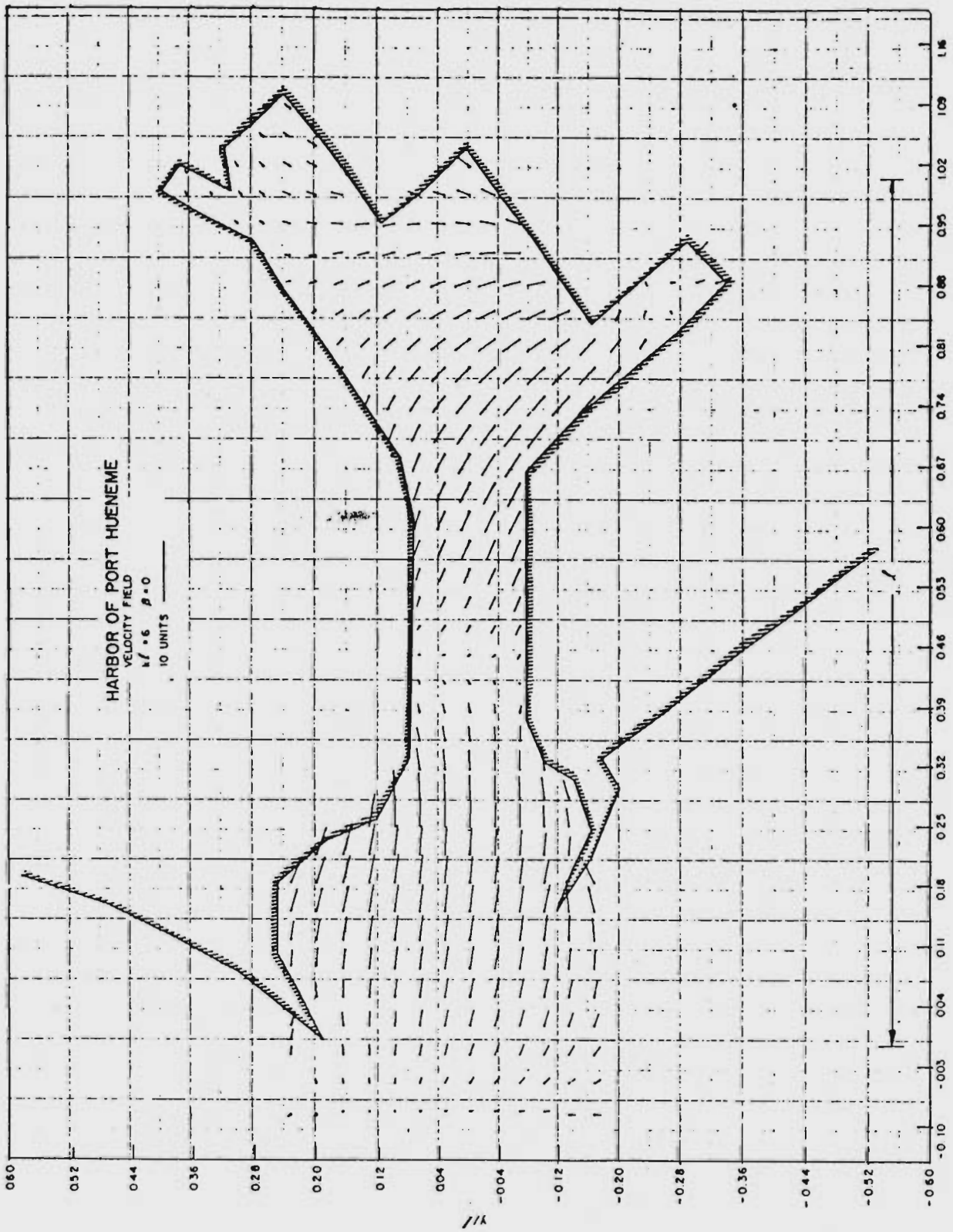

Figure VI-4 Instantaneous Velocity Field at Harbor of Port Hueneme

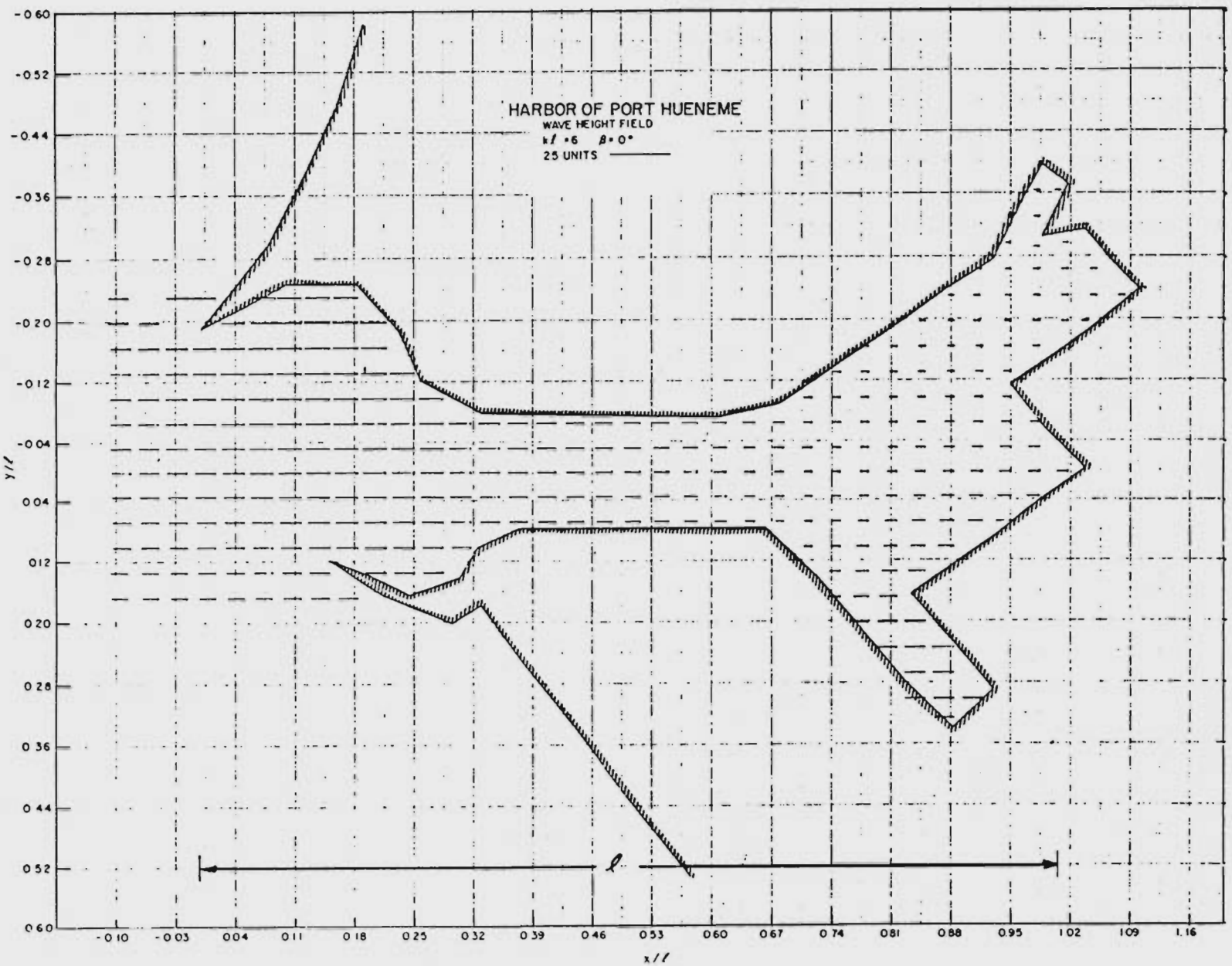

Figure VI-5 Wave Height Field at Harbor of Port Hueneme

Figure VI-6 Barbers Point Harbor

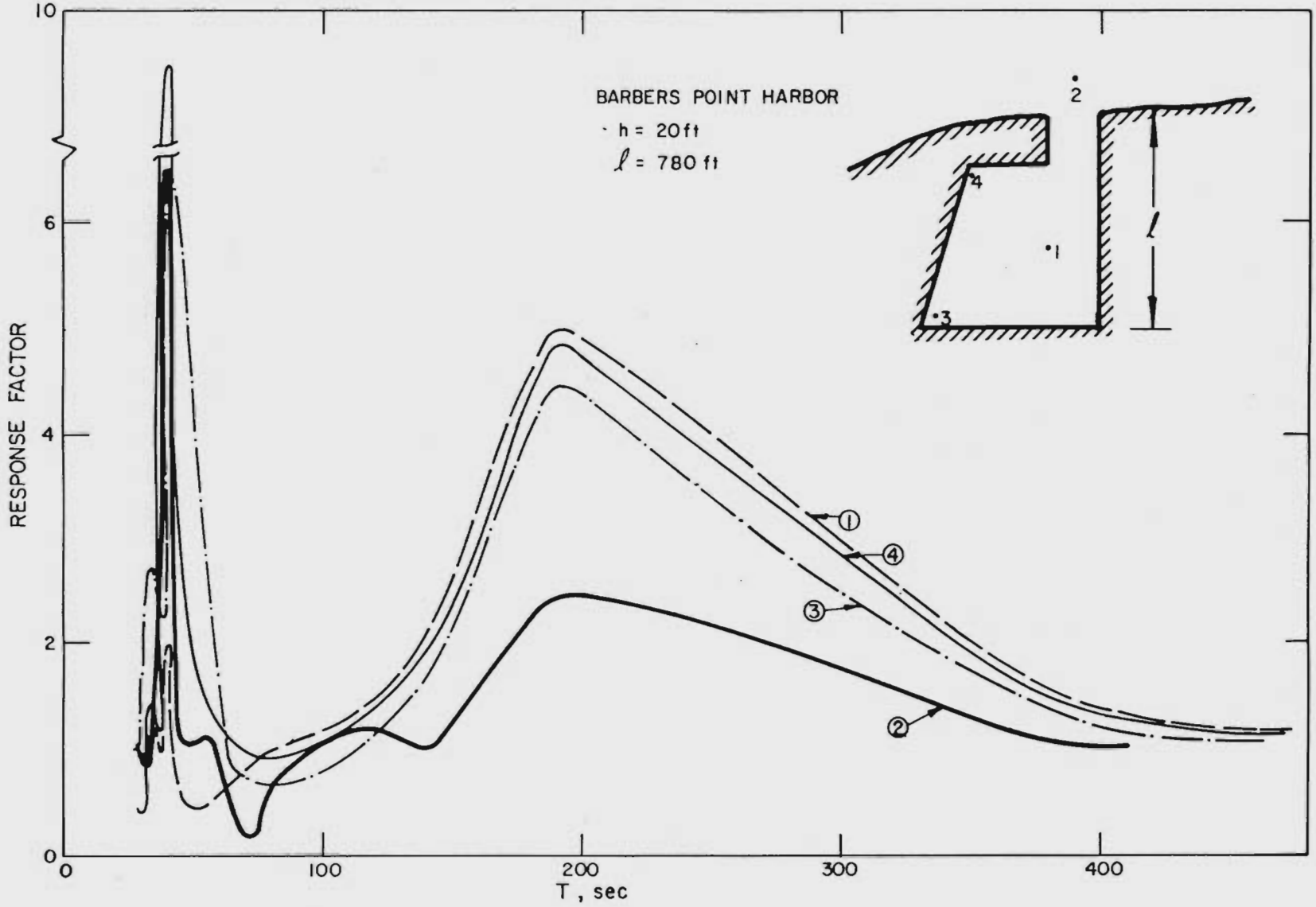

Figure VI-7 Response Function at Barbers Point Harbor

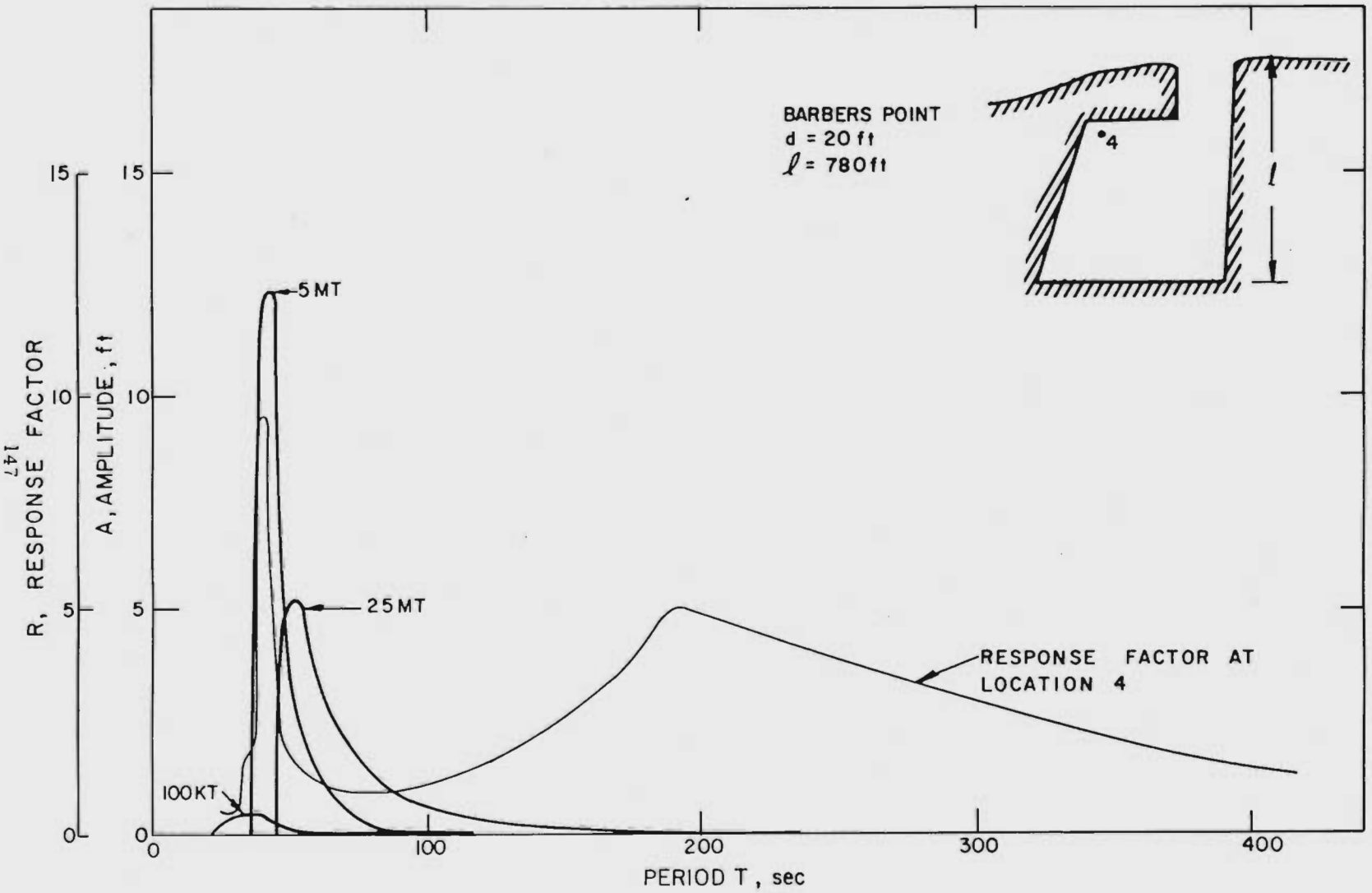

Figure VI-8 Wave amplitude inside Barbers Point Harbor resulting from explosion at Johnston Island

A-2-581

Tetra Tech for the Atomic Energy Commission (Hwang, et al., 1968). Figure VI-6 shows Barbers Point Harbor, Hawaii, while Fig. VI-7 indicates the response to periodic waves by the harbor at locations 1, 2, 3 and 4 as indicated in the figure. Figure VI-8 shows the response curve at location 4 together with the first amplitude envelopes resulting from 100 KT, 5 MT and 25 MT nuclear explosions near Johnston Island. The method of calculation has been outlined in several reports (Hwang, et al., 1968, Hwang and LeMéhauté, 1968).

It is necessary to point out that viscous dissipation and the effects of water depth and large wave amplitude are not considered in this calculation and will certainly tend to decrease the peak resonance amplitude. Further research on these effects is necessary in order to obtain more accurate predictions.

CHAPTER VII

A SUMMARY FOR MAKING ROUGH ESTIMATES OF WAVE CHARACTERISTICS

VII. A SUMMARY FOR MAKING ROUGH ESTIMATES OF WAVE CHARACTERISTICS

Chart VII-1, presented on the following page, summarizes the calculation procedures for explosion-generated waves and their propagation and transformation. These calculations are quite time consuming, and necessary only when detailed information is required. In some cases, a quick estimation is required for operational purposes. For this reason a simplified method which gives only the properties of the maximum waves is given.

As shown in Fig. VII-1, a nuclear explosion of yield Y is assumed to occur in deep water off the continential slope. The explosion generates a wave train propagating in all directions. The maximum wave amplitude η_{max} of the wave train in deep water is related to the distance from the explosion, r, and the yield, Y, as follows (see Eq. II-23):

$$\eta_{max} = \left(18\ Y^{0.54}/r\right) \text{ft.}, \quad [r] = \text{ft}, \quad [Y] = \text{lbs. TNT} \tag{VII-1}$$

assuming that the detonation occurs at the upper critical depth. The wave period, τ, of this maximum wave is (see Eq. II-25)

$$\tau = 1.63\ Y^{0.15} \text{ sec.} \quad [Y] = \text{lbs. TNT} \tag{VII-2}$$

As the maximum wave propagates towards the continential shelf, its amplitude decreases as a result of radial spreading, until shoaling and refraction effects become important. The calculation of wave amplitude including these effects is rather complicated as discussed in section III-3.2. Here, for simplicity, we assume that the explosion is rather far away from shallow water so that the waves are almost two-dimensional when they arrive. Thus we may calculate the maximum wave amplitude η_{max} by use of Eq. VII-1, until the water depth, h, is equal to one quarter of the wave length, $\frac{1}{4}L_{max}$ (we assume that shoaling becomes important when $h = \frac{1}{4}L_{max}$). From there on, the maximum wave height may be calculated by simply multiplying by the shoaling coefficient

CHART VII-1

SUMMARY CHART

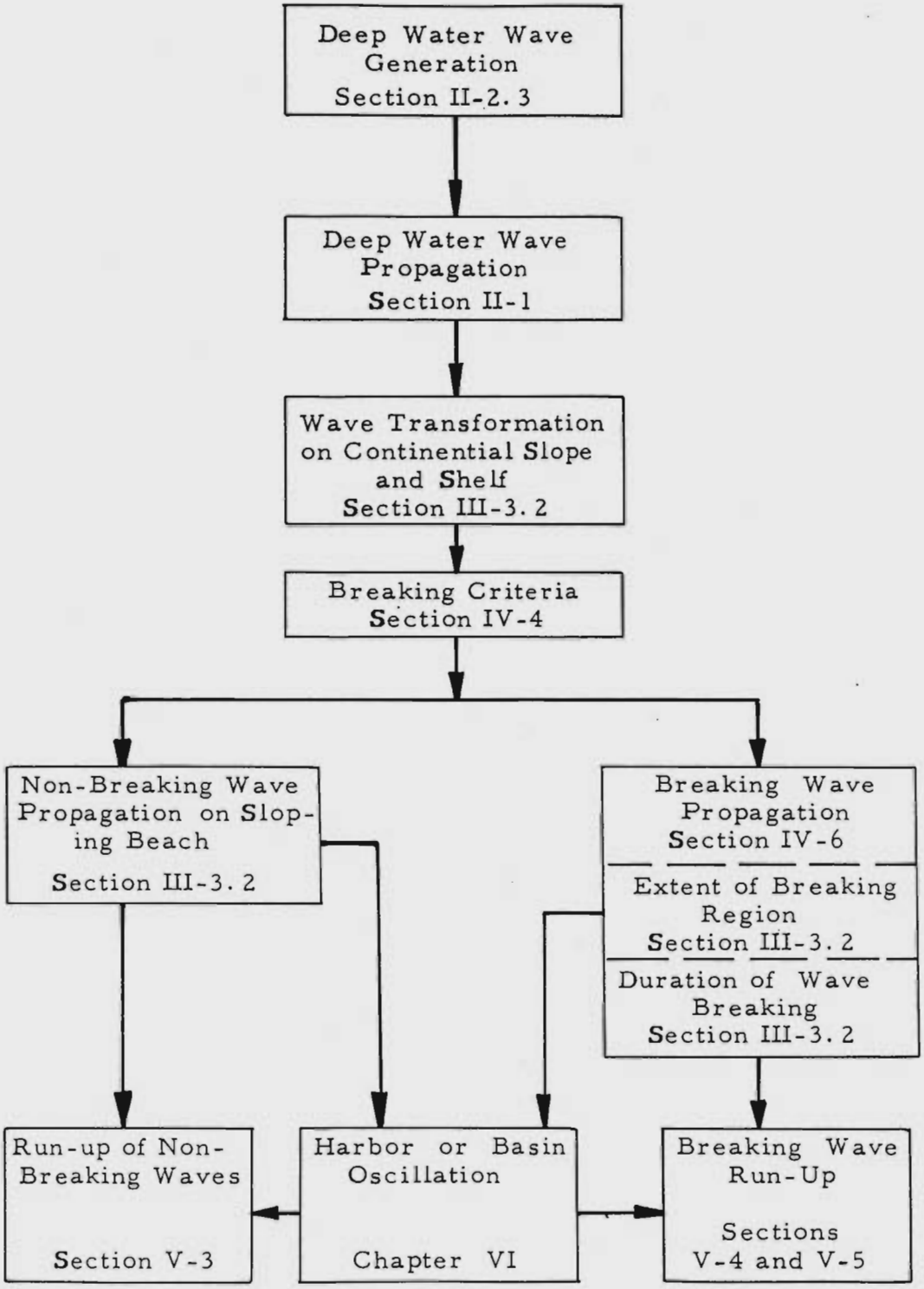

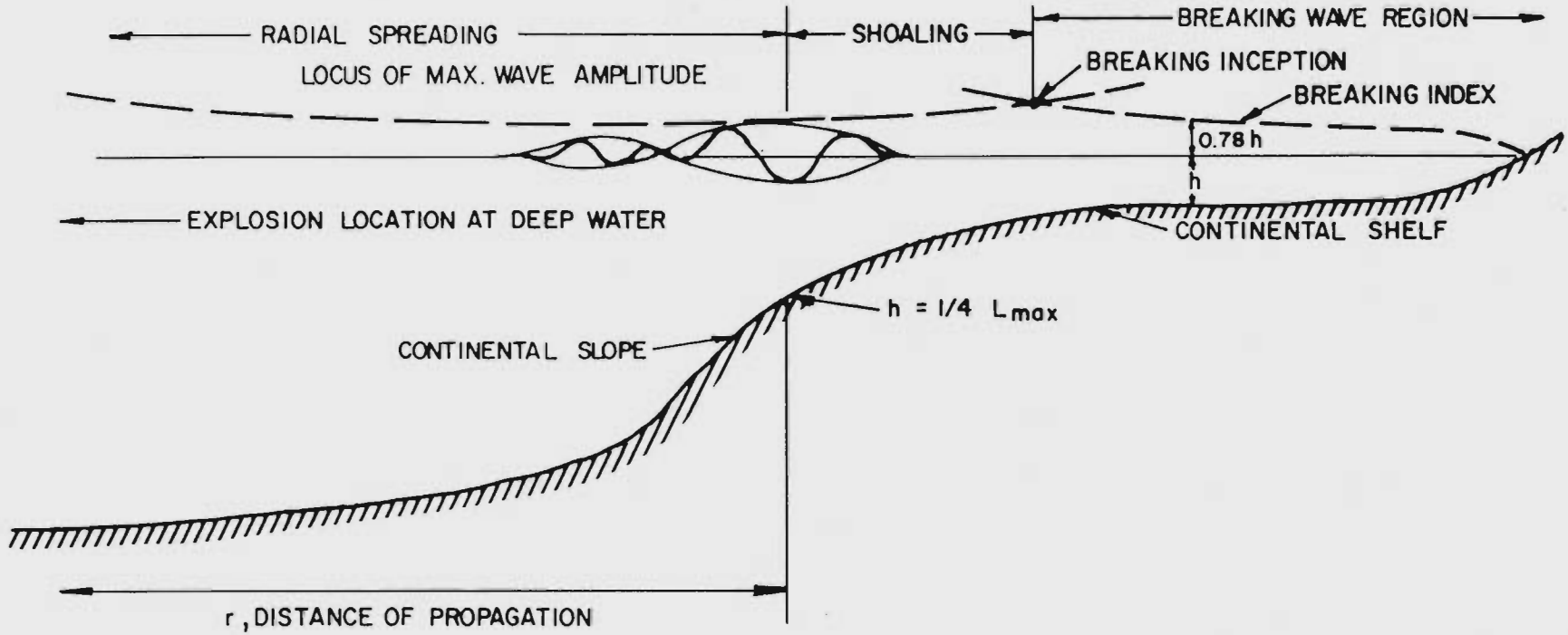

Figure VII-1 Schematic Drawing of the Maximum Wave Transformation as it Propagates Towards the Shore

$S_c = \frac{H_1}{H_o}$ as given in Fig. III-1. Refraction must also be accounted for, and may be determined from linear theory to a good approximation.

As the wave increases its amplitude by shoaling to the point that the water depth is insufficient to transmit the wave energy, the wave will break; this occurs at the intersection of the curve of wave height and the line of breaking index as shown in Fig. VII-1. After the wave breaks, it propagates towards the shore, as described by the non-saturated breaker theory.

There is no simple formula to estimate the lateral extent of the breaking region. However, previous calculations (Le Méhauté, et al., 1967) indicate that it is typically approximately equal to two times the distance between shore and the point of breaking inception.

The estimation of wave run-up is extremely difficult because of the usually complicated shore geometry. However, if the shoreline is assumed locally straight one may estimate the run-up according to the flow chart (VII-2) on the following page. It is based on available theories and empirical results discussed previously, and is drawn in such a way that it is reasonably simple to use and covers a wide class of possible situations. As such it cannot always be expected to give as reliable a result as the best that can be done by an experienced person analyzing a particular problem. It is only intended to be a guide for a reasonable estimate of the run-up.

The basic problem involves the following:

Given:
- H_i, the incident wave height,
- L_i, the incident wave length,
- τ, the incident wave period obtained from Eq. II-31, and
- h, depth of bottom profile at which the above values are given

To find: The run-up, $\bar{R}$.

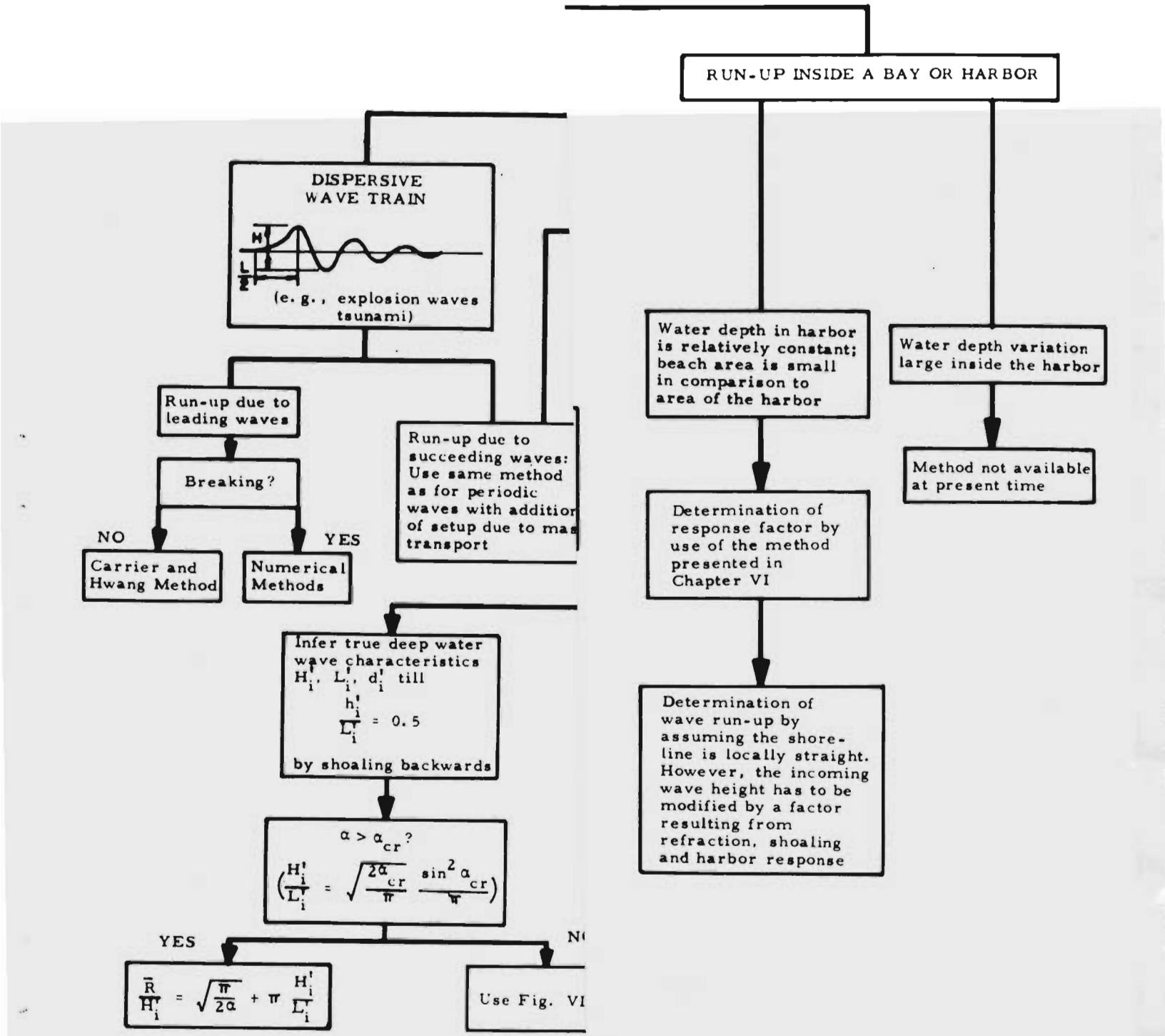
RUN-UP INSIDE A BAY OR HARBOR
DISPERSIVE WAVE TRAIN
(e.g., explosion waves tsunami)
Run-up due to leading waves
Breaking?
NO
YES
Carrier and Hwang Method
Numerical Methods
Run-up due to succeeding waves: Use same method as for periodic waves with addition of setup due to mas transport
Infer true deep water wave characteristics H_i', L_i', d_i' till $\frac{h_i'}{L_i'} = 0.5$ by shoaling backwards
$\alpha > \alpha_{cr}$?
$\left(\frac{H_i'}{L_i'} = \sqrt{\frac{2\alpha_{cr}}{\pi}} \frac{\sin^2 \alpha_{cr}}{\pi}\right)$
YES
N
$\frac{\bar{R}}{H_i'} = \sqrt{\frac{\pi}{2\alpha}} + \pi \frac{H_i'}{L_i'}$
Use Fig. VI
Water depth in harbor is relatively constant; beach area is small in comparison to area of the harbor
Water depth variation large inside the harbor
Method not available at present time
Determination of response factor by use of the method presented in Chapter VI
Determination of wave run-up by assuming the shoreline is locally straight. However, the incoming wave height has to be modified by a factor resulting from refraction, shoaling and harbor response

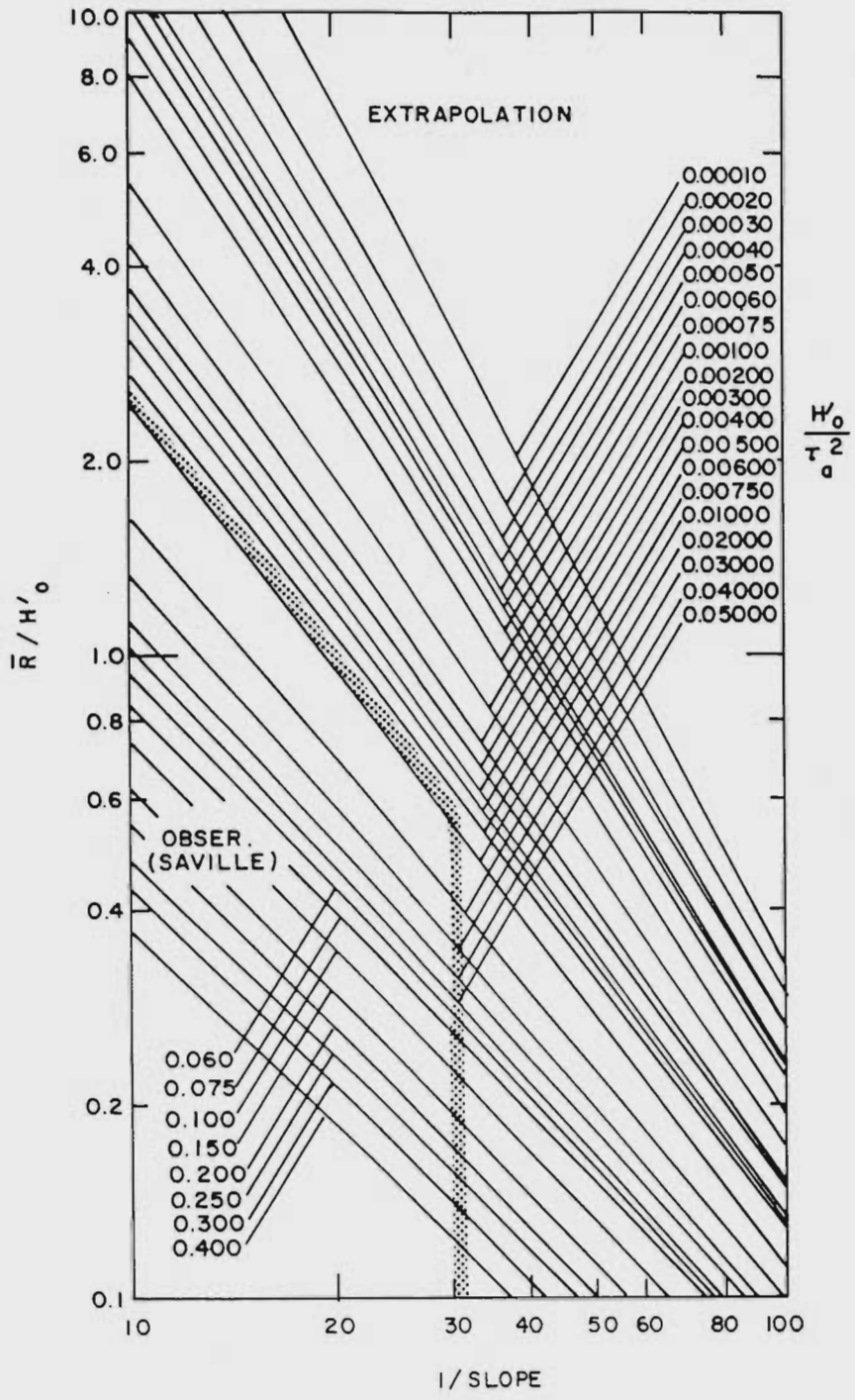

Figure VII-2 Run-up on a Uniform Slope Showing Regions of Observation and Extrapolation (adapted from Beach Erosion Board TR-4)

The first question that must be answered is whether the wave is preceded and followed by more waves with the same properties. If it is, the wave may be classified as purely periodic, to which most of the theories and experiments apply. If, however, it is a member of a wave package, the theories and experiments described before cannot, strictly speaking, be applied. Nevertheless, in view of the fact that in most cases the properties of the waves vary only slowly from one to the next within the wave train, one may apply them even in this case provided the wave under consideration is not very near the front or tail of the wave package. For the leading wave of such a wave package, either the Carrier and Hwang theory (if it does not break) or Kaplan's experimental results may be applied. One must be careful, however, of the definition of wave length in such a case. For purposes of estimating the run-up, the succeeding waves in such a wave train may be considered as periodic in character. If the succeeding wave breaks, the run-up may be calculated by use of Fig. VII-2, which is obtained from extrapolation of Saville's observations (BEB TR-4).

For evaluation of wave run-up inside a bay, the procedure is also outlined in the flow chart. However, the method involved is rather complex, so that no straightforward formulas can be given to obtain the wave run-up. Estimates of run-up in such conditions require considerable understanding of the nature of the harbor or bay response.

Finally, it is important to point out here that no beaches are perfectly straight and uniform in bottom slope, and no waves are perfectly two-dimensional. Thus the run-up observed may exhibit a large variation from time to time and from location to location for relatively uniform incoming waves. Such random behavior has not yet been tackled with an analytical approach. Observations at Hawaii and Mono Lake indicate that the distribution of all run-up data about the average run-up appears to follow a log normal distribution.

REFERENCES

Ash, J.E. and Eichler, T.V. (1964) "Water Waves from Surface and Shallow Underwater Bursts", Illinois Inst. Tech. Res. Inst. Report No. T 6038.

Beach Erosion Board (1967) "Shore Protection Planning and Design", Office of the Chief of Engineers, Department of the Army, T.R. 4.

Biesel, F. (1952) "Equations generales au second ordre de la houle irregulier", La Houille Blanche, May.

Biesel, F. and Le Méhauté, B. (1955) "Notes on the Similitude of Small Scale Models for Studying Seiches in Harbors", La Houille Blanche, V. 10(3), pp. 392-407.

Biesel, F. and Le Méhauté, B. (1956) "Etude théorique de la réflexion de la houle sur certains obstacles", La Houille Blanche, pp. 130-140, March-April.

Bondi, H. (1943) "On the Problem of Breakers", Admiralty Computing Service, WA-2304-13, Great Britain.

Bowen, A.J.; Inman, D.L.; and Simmons, V.P. (1968) "Wave Set-Down and Set-Up", Journal of Geophysical Research.

Caldwell, J.M. (1949) "Reflection of Solitary Waves", Beach Erosion Board, T.M. 11.

Carrier, G.F. (1966) "Gravity Waves on Water of Variable Depth", Journal of Fluid Mechanics.

Dean, R.G. (1965) "Stream Function Wave Theory; Validity and Application", Specialty Conference on Coastal Engineering, American Society of Civil Engineers.

Freeman, J.C. and Le Méhauté, B. (1964) "Wave Breakers on a Beach and Surge on a Dry Bed", Journal of Hydraulics Division, ASCE, Paper No. 3834, Vol. 90, No. HY2.

Goda, Y. (1964) "Wave Forces on a Vertical Circular Cylinder", Report No. 8, Port and Harbour Technical Research Inst., Japan.

Hall, J. V. and Watts, G. M. (1953) "Laboratory Investigation of the Vertical Rise of Solitary Waves on Impermeable Slopes", Beach Erosion Board, T. M. No. 33.

Ho, D. V. and Meyer, R. E. (1962) "Climb of a Bore on a Sloping Beach, Part 1," Journal of Fluid Mechanics, Vol. 14, pp. 305-318.

Ho, D. V.; Meyer, R. E.; and Shen, M. C. (1963) "Long Surf," Journal of Marine Research, Vol. 21, No. 3, pp. 219-230.

Hunt, I. A. (1959) "Design of Seawalls and Breakwaters", Journal of the Waterways and Harbors Division, ASCE, Vol. 85, No. WW3, Proc. Paper 2172.

Hwang, Li-San and Fersht, Samuel (1966) "On the Run-up of Non-breaking Dispersive Waves", Explosion Waves and Run-up, DASA Report, Vol. 5, Part 1.

Hwang, Li-San and Divoky, D. (1967) "Summary of Techniques of Explosion Wave Predictions", Tetra Tech Report No. TC-103, Vol. 2, Pasadena, California.

Hwang, Li-San; Lin, A.; and LeMéhauté, B (1967) "Wave Set-up and Shelf Oscillation", Defense Atomic Support Agency, DASA No. 2032.

Hwang, Li-San; Lin, A.; and LeMéhauté, B. (1968) "Experimental Studies on Wave Run-up under the Influence of Harbor Oscillations", Tetra Tech Report No. TC-123.

Hwang, Li-San and Le Méhauté, B. (1968) "On the Oscillations of Harbors of Arbitrary Shape", Tetra Tech, Inc., Report No. TC-123.

Hwang, Li-San; Le Méhauté, B.; Divoky, D.; and Lin, A. (1968) "A Study of Five Harbors under the Effect of the Explosion-Generated Waves", Tetra Tech, Inc. Report No. TC-137.

Ippen, A. T. and Goda, Y. (1963) "Wave Induced Oscillations in Harbors: The Solution for a Rectangular Harbor Connected to the Open-Sea", Hydrodynamics Lab., Report No. 59, Office of Naval Research, Washington, D. C.

Isaacson, E. (1950) "Water Waves on a Sloping Bottom", Communications on Pure and Applied Mathematics, Vol. 3, pp. 1-52.

Jones, Don (1968) "Wave-Basin Study of Run-Up on Beaches from Simulated Underwater Explosions Near Shore", Naval Civil Engineering Laboratory, publication pending.

Kajiura, Kinjiro (1963) "The Leading Waves of Tsunami", Bulletin of the Earthquake Research Institute, Vol. 41, pp. 535-571.

Kaplan, K. (1955) "Generalized Laboratory Study of Tsunami Run-up", Beach Erosion Board, T. M. No. 60.

Kaplan, K. and Goodale, Thomas (1962) "Study of Explosion-Generated Surface Water Waves", United Research Services Report No. 162-4, DASA 2013-6.

Keller, H. B.; Levine, D. A.; and Whitham, G. B. (1960) "Motion of a Bore over a Sloping Beach", Journal of Fluid Mechanics, Vol. 7, pp. 302-316.

Keller, J. B. (1961) "Tsunamis - Water Waves Produced by Earthquakes", Tsunami Hydrodynamics Conference, Honolulu, Hawaii.

Keller, J. B. and Keller, H. B. (1964, 1965) "Water Wave Run-Up on a Beach", Service Bureau Corporation Research Report, Contract No. Nonr 3828(00), prepared for Office of Naval Research, Washington, D. C.

Keulegan, G.H. and Patterson, G.W. (1940) "Theory of Irrotational Translation Waves", J. Res., National Bureau of Standards, 24, 1, pp. 47-101.

Kinsman, B. (1965) Wind Waves, Prentice-Hall, Inc., Englewood Cliffs, New Jersey.

Koh, R.C.Y. and Le Méhauté, B. (1966) "Wave Shoaling", Journal of Geophysical Research, Vol. 71, No. 8, pp. 2005-2012.

Korteweg, D.J. and de Vries, G. (1895) "On the Change of Form of Long Waves Advancing in a Rectangular Canal and on a New Type of Long Stationary Waves", Philosophical Magazine, Series 5, Vol. 39.

Kot, C.A. (1964) "Theoretical Study of Bubble Behavior in Underwater Explosions", U.S. N.R.D.L. Tech. Report No. 747.

Kranzer, H.C. and Keller, J.B. (1959) "Water Waves Produced by Explosions", Journal of Applied Physics, Vol. 30, No. 3.

Kravtchenko, J. and McNown, J.S. (1955) "Seiche in Rectangular Ports", Quarterly of Applied Mathematics, Vol. XII, pp. 19-26.

Kriebel, A.R. (1968) "Analysis of Water Waves Generated Explosively at the Upper Critical Depth", United Research Services Report URS-679-1, NR 089-053.

Laitone, E.V. (1961) "Higher Approximation to Nonlinear Water Waves and the Limiting Heights of Cnoidal, Solitary, and Stokes' Waves", Inst. of Eng. Res., Tech. Report Series 89, Issue 6, University of California.

Leendertse, Jan J. (1967) "Aspects of a Computational Model for Long-Period Water-Wave Propagation", Rand Co. Report No. RM-5294-PR.

Le Méhauté, B. (1960) "Periodical Gravity Wave on a Discontinuity", Journal of the Hydraulics Division, ASCE, pp. 11-41.

Le Méhauté, B. (1961) "Theory of Wave Agitation in a Harbor", ASCE Journal of the Hydraulics Division, No. 2765.

Le Méhauté, B. (1962) "Theory of Wave Agitation in a Harbor", Transactions, ASCE, Vol. 127, Part I, Paper No. 3313, pp. 364-383.

Le Méhauté, B. (1962) "On the Non-Saturated Breaker Theory and Wave Run-Up", Proc. VIIIth Conf. on Coastal Engineering, Mexico City, pp. 77-92.

Le Méhauté, B. and Webb, L. M. (1964) "Periodic Gravity Waves over a Gentle Slope at a Third Order of Approximation", Proceedings, IXth Conference on Coastal Engineering, Lisbon, Portugal.

Le Méhauté, B. and Moore, M. (1965) "On the Wave Run-up of Solitary Waves", United States-Japan Cooperative Scientific Research Seminars on Tsunami Run-Up, Sapporo, Japan.

Le Méhauté, B. (1965) "Wave Absorbers in Harbors", Contract Report No. 2-112, prepared for U.S. Army Engineer Waterways Experiment Station under Contract No. DA-22-079-civeng-64-81.

Le Méhauté, B.; Whalin, R.; Webb, L.; and Divoky, D. (1965) "Contribution to the Mono Lake Experiment, Volume I: Predictions of Water Waves Produced by 10,000 lb. TNT Explosions in Mono Lake", NESCO Report No. S256-1, 2 and 3.

Le Méhauté, B.; Whalin, R. W.; and Divoky D. J. (1966) "Explosion Waves and Run-up", Vol. III, Mono Lake Experiments, NESCO Report No. SN 300.

Le Méhauté, B.; Snow, G.; and Webb, L. M. (1966) "Gravity Waves on Bottom Slopes", NESCO Report No. S245A; Defense Atomic Support Agency Report No. DASA-1671-1.

Le Méhauté, B. (1966) "Hydrodynamic Effects of Nuclear Explosions, Vol. I: State of the Art", NESCO Report S244-1.

Le Méhauté, B.; Hwang, Li-San; Divoky, D.; and Butler, L. (1967) "Explosion-Generated Wave Environment in Shallow Water", Defense Atomic Support Agency, Report No. DASA 1963.

Le Méhauté, B. and Hwang, Li-San (1967) "Run-Up of Non-Breaking Waves", Tetra Tech Report No. TC-103, Tetra Tech, Inc., Pasadena, California.

Le Méhauté, B.; Divoky, D.; and Lin, A. (1968) "Internal Characteristics of Explosion-Generated Waves on the Continental Shelf", Tetra Tech Report No. TC-116, Tetra Tech, Inc., Pasadena, California.

Le Méhauté, B.; Koh, R. C. Y.; and Hwang, Li-San (1968) "A Synthesis on Wave Run-Up", ASCE Journal of the Waterways and Harbors Division.

Lewy, H. (1946) "Water Waves on Sloping Beaches", Bulletin of the American Mathematical Society, Vol. 52.

Londgren, H. (1963) "Wave Thrust and Energy Level", IAHR Congress, London, pp. 147-151.

Longuet-Higgins, M.S. and Stewart, R.W. (1960) "Changes in the Form of Short-Gravity Waves on Long Waves and Tidal Currents", Journal of Fluid Mechanics, No. 8, pp. 565-583.

Longuet-Higgins, M.S. and Stewart, R.W. (1962) "Radiation Stress and Mass Transport in Gravity Waves and Application to Surf Beats", Journal of Fluid Mechanics, No. 13, pp. 481-504.

Longuet-Higgins, M.S. and Stewart, R.W. (1963) "A Note on Wave Set-Up", Journal of Marine Research, No. 21, pp. 4-10.

Longuet-Higgins, M.S. and Stewart, R.W. (1964) "Radiation Stress in Water Waves, a Physical Discussion, with Applications", Deep Sea Research, Vol. II, pp. 529-563.

McNown, J.S. (1952) "Waves and Seiche in Idealized Ports", Gravity Waves Symposium, National Bureau of Standards, Circular 521.

Miche, M. (1944) "Mouvements ondulatoires de la mer en profondeur constante au décroissante", Annals des ponts et chaussées.

Miche, M. (1951) "Le pouvoir reflechissant des ouvrages maritimes", Annals des ponts et chaussées, Ministere des Traveus Publics et des Transports, Paris.

Miles, J. and Munk, W. (1961) "Harbor Paradox", ASCE Journal of Waterways And Harbors Division, No. 2888.

Miller, G.R.; Munk, W.H.; and Snodgrass, F.E. (1962) "Long-Period Waves over California's Continental Borderland, Part II: Tsunamis", Sears Foundation: Journal of Marine Research, Vol. 20, No. 1, pp. 31-41.

Miller, R.L. and Zeigler, J.M. (1964) "The Internal Velocity Field in Breaking Waves", IXth Conference on Coastal Engineering.

Munk, W.H. (1949) "The Solitary Wave Theory and its Application to Surf Problems", in "Ocean Surface Waves", Annals of the N.Y. Academy of Sciences, Vol. 51, Art. 3.

Nordyke, M.D. (1962) "An Analysis of Cratering Data from Desert Alluvium", Journal of Geophysical Research, Vol. 67, p. 1965.

Penney, W.G. (1945) "Gravity Waves Produced by Surface and Underwater Explosions", British contribution to "Underwater Explosion Research", 1950, Office of Naval Research, Washington, D.C.

Peters, A.S. (1952) "Water Waves over Sloping Beaches and the Solution of a Mixed Boundary Value Problem for $\Delta\Phi - k^2\Phi = 0$ in a Sector", Comm. Pure and Appl. Math., Vol. 5, pp. 87-108.

Pollard, Dwight D. and Wallace, N.R. (1967) "Water Surface Wave Measurement Experiment - Mono Lake", OSI Report NVO-266-1, prepared for the U.S. Atomic Energy Commission by Oceanographic Services, Inc., Santa Barbara, California.

Rooke, A. D.; Davis, L. K.; and Strange, J. N. (1967) "Mono Lake Explosion Test Series: 1965 Results of the Wave Run-Up Experiments", U.S. Army Engineer Waterways Experiment Station, Misc. Paper No. 1-947.

Roseau, M. (1952) "Contributions a la theorie des ondes liquides de gravite en profondeur variable", Publications scientifiques et techniques du Ministere de l'áir, No. 275.

Sainflou, M. (1928) "Essai sur les digues maritime verticales", Annals des Ponts et Chaussées, Ministére des traveus Publics et des Transports, Paris, p. 5.

Savage, R. P. (1959) "Wave Run-Up on Roughened and Permeable Slopes", Transactions, ASCE, Vol. 124, Paper No. 3003, pp. 852-870.

Saville, T. (1961) "Experimental Determination of Wave Set-Up", IAHR, Second Tech. Conf. on Hurricanes, pp. 242-252.

Shen, M. C. and Meyer, R. E. (1963a, b) "Climb of a Bore on a Sloping Beach, Parts 2 and 3", Journal of Fluid Mechanics, Vol. 16, pp. 108-112 and 113-125.

Skjelbreia, L. (1959) "Gravity Waves, Stokes' Third Order Approximation: Tables of Functions", Council on Wave Research, The Engineering Foundation.

Skjelbreia, L. and Hendrickson, J. A. (1962) "Fifth Order Gravity Wave Theory", National Engineering Science Company.

Stoker, J. J. (1947) "Surface Waves in Waters of Variable Depth", Quarterly Applied Math., Vol. 5, pp. 1-54.

Stoker, J. J. (1965) Water Waves, Interscience Publishers, Inc., New York.

Street, R. L. and Camfield, F. E. (1966) "Observations and Experiments on Solitary Wave Deformation", Xth Conference on Coastal Engineering.

Synge, J. L. (1962) "Water Waves and Hydrons", Science, Vol. 138, pp. 13-16.

Van Dorn, W. G. and Montgomery, W. S. (1963) "Water Waves from 10,000 lb High-Explosive Charges", SIO Report No. 63-20.

Van Dorn, W.G. (1964) "Explosion-Generated Waves in Water of Variable Depth", Journal of Marine Research, Vol. 22, No. 2.

Van Dorn, W. G. (1965) "Tsunamis", Advances in Hydroscience, Vol. III, Academic Press, New York.

Van Dorn, W. G. (1966) "Theoretical and Experimental Study of Wave Enhancement and Run-Up on Uniformly Sloping Impermeable Beaches", SIO 66-11, Scripps Institution of Oceanography, University of California.

Wallace, N. R. (1967) "Explosion-Generated Shallow Water Waves, Mono Lake", Oceanographic Services, Inc., CONFIDENTIAL.

Wallace, N. R. and Baird, C. W. (1968) "Run-Up on an Irregular Shoreline - Mono Lake Tests", Oceanographic Services, Inc., U.S. Atomic Energy Commission Report NVO-297-2.

Webb, L. M., LeMéhauté, B. (1966) "Explosion Waves and Run-Up, Vol. II, Wave Set-Up and the Mass Transport of Cnoidal Waves, NESCO Contract No. SN-300.

Whalin, R. W. (1965) "Research on the Generation and Propagation of Water Waves Produced by Underwater Explosions, Part II: A Prediction Method", NMC-IEC Report.

Whalin, R. W. (1965) "Water Waves Generated by Explosions: Propagation Theory for the Area Near the Explosion", Journal of Geophysical Research, Vol. 70, No. 22, November 15.

Whitham, G. B. (1958) "On the Propagation of Shock Waves through Regions of Non-Uniform Areas of Flow", Journal of Fluid Mechanics, Vol. 4, pp. 337-360.

Whitham, G. B. (1962) "Mass, Momentum, and Energy Flux in Water Waves", Journal of Fluid Mechanics, Vol. 12, pp. 135-147.

Wiegel, R. L. (1964) Oceanographical Engineering, Prentice Hall, Inc. Englewood Cliffs, New Jersey.

DISTRIBUTION LIST

Addressee	No. of Copies
Defense Documentation Center (DDC) Cameron Station Alexandria, Virginia 22314 ATTN: TISIA-21	20
Chief of Research and Development Department of the Army Washington, D. C. 20310 ATTN: Atomic Division	1
Chief of Engineers Department of the Army Washington, D. C. 20310 ATTN: ENGTE-E	2
Commanding General U. S. Army Material Command Washington, D. C. 20310 ATTN: AMCRD-DE-N	2
Director of Civil Defense Department of the Army Washington, D. C. 20310 ATTN: Mr. J. W. Kerr Support Systems Research	2
Commanding Officer U. S. Army Combat Development Command Institute of Nuclear Studies Fort Bliss, Texas 79906 ATTN: Effects Division	2
Director U. S. Army Ballistic Research Laboratories Aberdeen Proving Ground Maryland 21005 ATTN: Technical Library	4
Commanding General The Engineer Center Fort Belvoir, Virginia 22060 ATTN: Commandant, Engineer School	1
Director U. S. Army Research and Development Laboratory Fort Belvoir Virginia 22060 ATTN: Chief, Technical Support Branch	1

Addressee	No. of Copies
Commanding Officer Picatinny Arsenal Dover, New Jersey 07801 ATTN: ORDBB-TK	1
Commanding General U.S. Army Electronic R&D Laboratory Fort Monmouth, New Jersey 07703 ATTN: Technical Documents Center	1
Commanding General U.S. Army Missile Command Redstone Arsenal Huntsville, Alabama 35808	1
Commanding Officer U.S. Army Corps of Engineers Coastal Engineering Research Center Washington, D.C. 20315	1
Commanding Officer U.S. Army Nuclear Defense Laboratory Edgewood Arsenal Edgewood, Maryland 21040 ATTN: Technical Library	1
Director Waterways Experiment Station U.S. Army Corps of Engineers Vicksburg, Mississippi 29181 ATTN: Mr. F. Brown Mr. J. Strange	2
Director U.S. Army Corps of Engineers Nuclear Cratering Group Livermore, California 94551	1
Chief of Naval Operations Navy Department Washington, D.C. 20350 ATTN: OP-75	2
Chief of Naval Material Navy Department Washington, D.C. 20360 ATTN: Code 03L	1
Director of Naval Intelligence Navy Department Washington, D.C. 20350 ATTN: OP-922V	1

Addressee	No. of Copies
Director Special Projects Navy Department Washington, D. C. 20360 ATTN: Sp-272	1
Commander Naval Air Systems Command Navy Department Washington, D. C. 20360 ATTN: Code AIR-350	1
Commander Naval Ordnance Systems Command Navy Department Washington, D. C. 20360 ATTN: Code ORD-0352	1
Commander Naval Ship Systems Command Technical Library Navy Department Washington, D. C. 20360 ATTN: Code 035	2
Commander Naval Ship Engineering Center Navy Department Washington, D. C. 20360 ATTN: Code 6115	2
Commander Naval Facilities Engineering Command Navy Department Washington, D. C. 20370 ATTN: Code 032A	1
Chief of Naval Research Navy Department Washington, D. C. 20360 ATTN: Code 418	2
Commandant of the Marine Corps Navy Department Washington, D. C. 20380 ATTN: Code A03H	4
Commanding Officer Nuclear Weapons Training Center Atlantic, Naval Base Norfolk, Virginia 23711 ATTN: Nuclear Warfare Department	1

Addressee	No. of Copies
Commanding Officer U.S. Naval Weapons Evaluation Facility Code WEVS Kirtland Air Force Base New Mexico 87117	1
Superintendent U.S. Naval Academy Annapolis, Maryland 21402	1
Superintendent U.S. Naval Postgraduate School Monterey, California 93940	1
Commanding Officer Nuclear Weapons Training Center Pacific, Naval Station North Island, San Diego, California 92109	2
Commander U.S. Naval Ordnance Laboratory White Oak, Silver Spring, Maryland 20910 ATTN: EA, EU, and E	3
Commander U.S. Naval Ordnance Test Station China Lake, California 93556	1
Commanding Officer and Director U.S. Naval Civil Engineering Laboratory Port Hueneme, California 93041 ATTN: Mr. T. O'Brien	1
Director U.S. Naval Research Laboratory Washington, D.C. 20390	1
Commanding Officer and Director U.S. Naval Electronics Laboratory San Diego, California 92152	1
Commanding Officer and Director U.S. Naval Radiation Defense Laboratory San Francisco, California 94129 ATTN: Technical Information Division	1
Commander Test Command DASA, Sandia Base Albuquerque, New Mexico 87115 ATTN: FCTG	3

Addressee	No. of Copies
Commander Joint Task Force EIGHT Sandia Base Albuquerque, New Mexico 87115	1
Commandant Army War College Carlisle Barracks, Pennsylvania 17013 ATTN: Library	1
Officer-in-Charge U.S. Naval School Civil Engineering Corps Officers U.S. Naval Construction Battalion Center Port Hueneme, California 93041	1
University of California Lawrence Radiation Laboratory P. O. Box 803 Livermore, California 94551 ATTN: Tech Information Division	2
Los Alamos Scientific Laboratory P. O. Box 1663 Los Alamos, New Mexico 87554 ATTN: Report Librarian	1
Director Advanced Research Projects Agency Washington, D.C. 20301 ATTN: Mr. D. Clements	1
Director Defense Intelligence Agency Washington, D.C. 20301 ATTN: DIAAP-1K2	1
Chief, Classified Technical Library Technical Information Service U.S. Atomic Energy Commission Washington, D.C. 20545	1
Sandia Corporation P. O. Box 5800 Albuquerque, New Mexico 87115 ATTN: Classified Document Division (M. L. Merrit)	1
ASD Wright-Patterson Air Force Base Ohio 45433	1

Addressee	No. of Copies
AFFDL Wright-Patterson Air Force Base Ohio 45433	1
AFSC Andrews Air Force Base Washington, D. C. 20331 ATTN: RDRWA	1
AFWL Kirtland Air Force Base New Mexico 87117 ATTN: WLRS	1
Commandant Institute of Technology Wright-Patterson Air Force Base Ohio 45433 ATTN: MCLI-ITRIDL	1
BSD Norton Air Force Base California 92409	1
Director of Civil Engineering HQ U.S. Air Force Washington, D. C. 20330 ATTN: AFOCE	1
Director of Defense Research and Engineering Washington, D. C. 20330 ATTN: Technical Library	1
Assistant to the Secretary of Defense (Atomic Energy) Washington D. C. 20330	1
Director Weapons Systems Evaluation Group OSD, The Pentagon Washington, D. C. 20301	1
Commander Field Command DASA, Sandia Base Albuquerque, New Mexico 87115 ATTN: FCTG	3
Director, DASA Washington, D. C. 20301 ATTN: Document Library	3

Addressee	No. of Copies
University of California Scripps Institution of Oceanography LaJolla, California 92037 ATTN: Dr. W. Van Dorn	1
University of Chicago Department of Geophysical Sciences 1101 East 58th Street Chicago, Illinois 60637	1
Department of Civil Engineering Stanford University Stanford, California 94305 ATTN: Dr. R. L. Street	1
URS Corporation 1700 South El Camino Real San Mateo, California 94402	1
Oceanographic Services, Inc. 5375 Overpass Road Santa Barbara, California 93105	1
Tetra Tech, Inc. 630 North Rosemead Blvd Pasadena, California 91107	1
University of Illinois Urbana Campus Urbana, Illinois 61803 ATTN: Civil Engineering Department Dr. N. M. Newmark	1
Massachusetts Institute of Technology Division of Sponsored Research 77 Massachusetts Avenue Cambridge, Massachusetts 02115 ATTN: Professor Robert V. Whitman	1
The RAND Corporation 1700 Main Street Santa Monica, California 90401 ATTN: Dr. H. L. Brode Dr. O. Nance Dr. Harry Mow	3
Stanford Research Institute 333 Ravenswood Avenue Menlo Park, California 94025 ATTN: Mr. Fred Sauer	1

Addressee	No. of Copies
The Boeing Company 7755 E. Marginal Way Seattle, Washington 98101	1
GE TEMPO 816 State Street Santa Barbara, California 93102 ATTN: DASIAC	2
Commanding Officer and Director Naval Ship Research and Development Center Washington, D. C. 20007 ATTN: Code 700	2
Underwater Explosions Research Division Naval Ship Research and Development Center Norfolk Naval Shipyard Portsmouth, Virginia 23709 ATTN: Document Control	1
Institute of Naval Studies Center of Naval Analyses 1401 Wilson Blvd Arlington, Virginia 22209 ATTN: Library	1
HQ USAF (AFRSTG) Washington, D. C. 20330	2
Deputy Chief of Staff Plans and Programs HQ, USAF Washington, D. C. 20330 ATTN: War Plans Division	1
Director of Research and Development DCS/D, HQ, USAF Washington, D. C. 20330 ATTN: Guidance and Weapons Division	1
Air Force Intelligence Center HQ, USAF, ACS/I(AFCIN-3K2) Washington, D. C. 22212	1
Commander-in-Chief Strategic Air Command Offutt AFB, Nebraska 68113 ATTN: OAWS	1
Commander, Tactical Air Command Langley AFB, Virginia 23365 ATTN: Document Security Branch	1

UNCLASSIFIED

Security Classification

DOCUMENT CONTROL DATA - R&D

(Security classification of title, body of abstract and indexing annotation must be entered when the overall report is classified)

1. ORIGINATING ACTIVITY (Corporate author)
Tetra Tech, Incorporated
630 North Rosemead Boulevard
Pasadena, California 91107

2a. REPORT SECURITY CLASSIFICATION

2b GROUP

3. REPORT TITLE
"Handbook of Explosion-Generated Waves"
Volume I - State of the Art

4. DESCRIPTIVE NOTES (Type of report and inclusive dates)
Technical Report

5. AUTHOR(S) (Last name, first name, initial)
Van Dorn, William, G.
LeMéhauté, Bernard
Hwang, Li-San

6. REPORT DATE	7a. TOTAL NO. OF PAGES	7b. NO. OF REFS
October, 1968	188	97

8a. CONTRACT OR GRANT NO.	9a. ORIGINATOR'S REPORT NUMBER(S)
N00014-68-C-0227	TC-130
b. PROJECT NO.	
c.	9b. OTHER REPORT NO(S) (Any other numbers that may be assigned this report)
d.	[redacted]

10. AVAILABILITY/LIMITATION NOTICES
"Each transmittal of this document outside the agencies of the U.S. Government must have prior approval of the Office of Naval Research, Field Projects Programs, Washington, D. C. 20360."

11. SUPPLEMENTARY NOTES	12. SPONSORING MILITARY ACTIVITY
	Office of Naval Research Washington, D. C. 20360

13 ABSTRACT

This report summarizes the state of the art in the field of explosion-generated waves, their generation, propagation and their effects on coastal environment.

DD FORM 1 JAN 64 1473

UNCLASSIFIED

Security Classification

14. KEY WORDS	LINK A		LINK B		LINK C	
	ROLE	WT	ROLE	WT	ROLE	WT
Characteristics of explosion-generated waves breaking waves wave run-up harbor oscillations						

INSTRUCTIONS

1. ORIGINATING ACTIVITY: Enter the name and address of the contractor, subcontractor, grantee, Department of Defense activity or other organization *(corporate author)* issuing the report.

2a. REPORT SECURITY CLASSIFICATION: Enter the overall security classification of the report. Indicate whether "Restricted Data" is included. Marking is to be in accordance with appropriate security regulations.

2b. GROUP: Automatic downgrading is specified in DoD Directive 5200.10 and Armed Forces Industrial Manual. Enter the group number. Also, when applicable, show that optional markings have been used for Group 3 and Group 4 as authorized.

3. REPORT TITLE: Enter the complete report title in all capital letters. Titles in all cases should be unclassified. If a meaningful title cannot be selected without classification, show title classification in all capitals in parenthesis immediately following the title.

4. DESCRIPTIVE NOTES: If appropriate, enter the type of report, e.g., interim, progress, summary, annual, or final. Give the inclusive dates when a specific reporting period is covered.

5. AUTHOR(S): Enter the name(s) of author(s) as shown on or in the report. Enter last name, first name, middle initial. If military, show rank and branch of service. The name of the principal author is an absolute minimum requirement.

6. REPORT DATE: Enter the date of the report as day, month, year; or month, year. If more than one date appears on the report, use date of publication.

7a. TOTAL NUMBER OF PAGES: The total page count should follow normal pagination procedures, i.e., enter the number of pages containing information.

7b. NUMBER OF REFERENCES: Enter the total number of references cited in the report.

8a. CONTRACT OR GRANT NUMBER: If appropriate, enter the applicable number of the contract or grant under which the report was written.

8b, 8c, & 8d. PROJECT NUMBER: Enter the appropriate military department identification, such as project number, subproject number, system numbers, task number, etc.

9a. ORIGINATOR'S REPORT NUMBER(S): Enter the official report number by which the document will be identified and controlled by the originating activity. This number must be unique to this report.

9b. OTHER REPORT NUMBER(S): If the report has been assigned any other report numbers *(either by the originator or by the sponsor)*, also enter this number(s).

10. AVAILABILITY/LIMITATION NOTICES: Enter any limitations on further dissemination of the report, other than those imposed by security classification, using standard statements such as:

(1) "Qualified requesters may obtain copies of this report from DDC."

(2) "Foreign announcement and dissemination of this report by DDC is not authorized."

(3) "U. S. Government agencies may obtain copies of this report directly from DDC. Other qualified DDC users shall request through

_____."

(4) "U. S. military agencies may obtain copies of this report directly from DDC. Other qualified users shall request through

_____."

(5) "All distribution of this report is controlled. Qualified DDC users shall request through

_____."

If the report has been furnished to the Office of Technical Services, Department of Commerce, for sale to the public, indicate this fact and enter the price, if known.

11. SUPPLEMENTARY NOTES: Use for additional explanatory notes.

12. SPONSORING MILITARY ACTIVITY: Enter the name of the departmental project office or laboratory sponsoring *(paying for)* the research and development. Include address.

13. ABSTRACT: Enter an abstract giving a brief and factual summary of the document indicative of the report, even though it may also appear elsewhere in the body of the technical report. If additional space is required, a continuation sheet shall be attached.

It is highly desirable that the abstract of classified reports be unclassified. Each paragraph of the abstract shall end with an indication of the military security classification of the information in the paragraph, represented as *(TS)*, *(S)*, *(C)*, or *(U)*.

There is no limitation on the length of the abstract. However, the suggested length is from 150 to 225 words.

14. KEY WORDS: Key words are technically meaningful terms or short phrases that characterize a report and may be used as index entries for cataloging the report. Key words must be selected so that no security classification is required. Identifiers, such as equipment model designation, trade name, military project code name, geographic location, may be used as key words but will be followed by an indication of technical context. The assignment of links, rules, and weights is optional.